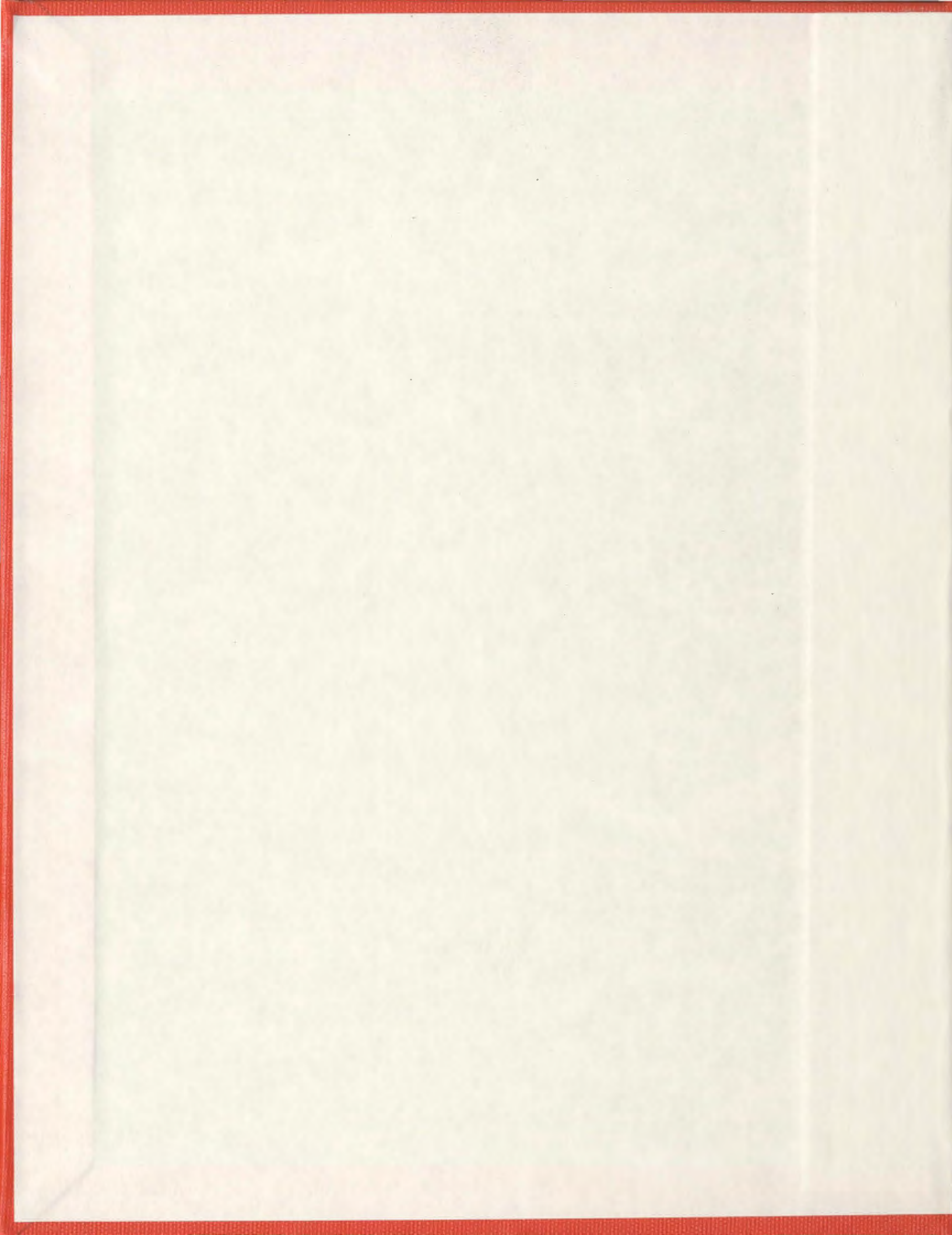


FINITE ELEMENT ANALYSES OF SOIL/PIPELINE  
INTERACTIONS IN SAND WITH AN ADVANCED  
SOIL CONSTITUTIVE MODEL

KSHAMA SUNDAR ROY







**FINITE ELEMENT ANALYSES OF SOIL/PIPELINE INTERACTIONS IN SAND  
WITH AN ADVANCED SOIL CONSTITUTIVE MODEL**

by

© KSHAMA SUNDAR ROY

B. Sc. (Eng.), Bangladesh University of Engineering and Technology

A Thesis submitted to the

School of Graduate Studies

in partial fulfillment of the requirements for the degree of

**Master of Engineering (Civil Engineering)**

**FACULTY OF ENGINEERING AND APPLIED SCIENCES**

Memorial University of Newfoundland

**September 2012**

St. John's

Newfoundland

## ABSTRACT

Inexorable demand of energy intensified the search for oil and gas in remote and harsh regions. The operations related to exploration and production of oil and gas has been increased significantly over the last 30 years. The liquid hydrocarbon and natural gas products are usually transported through pipelines, which traverse large distances through a variety of soils. Failure of such pipelines could cause a significant economic loss and environmental damage. Geohazards and the associated ground movement represent a significant threat to pipeline integrity that may result in pipeline damage and potential failure. Safe, economic and reliable operation of pipeline transportation systems is the primary goal of the pipeline operators and regulatory agencies. Pipelines are usually buried or partially embedded into the seabed. To develop a reliable pipelines design method the complex behaviour of seabed sediment (soil) and soil/pipeline interaction should be properly modeled and analyzed.

Finite element (FE) modeling has been widely used for predicting the response of buried pipelines. One of the main challenges in FE modeling of buried pipelines is to use appropriate soil constitutive model. Most of the FE analyses used built-in soil constitutive models in available commercial FE software. However, their prediction might be better if an advanced soil constitutive model is used.

The main objective of this research is to perform finite element modeling for analyzing the response of pipelines buried in sand. The primary focus of this research is to adopt an

advanced soil constitutive model which might have a significant impact on pipeline response due to soil movement and to implement it in the commercial finite element software package ABAQUS with a user defined subroutine UMAT. All the analyses presented are in drained condition.

In this study numerical analyses of soil/pipeline interaction are performed using the built-in Mohr-Coulomb soil constitutive model in ABAQUS FE program. This study shows the limitations and advantages of this constitutive model. Reviewing available soil constitutive models in the literature, it is identified that NorSand soil model proposed by Jefferies (1993) could better simulate the behaviour of sand particularly the dilation under monotonic loading. NorSand soil constitutive model implemented in ABAQUS FE software using user defined subroutine UMAT is used for modeling the response of pipelines under lateral, vertical (upward) and oblique loading events. Finite element analyses are also performed with built-in Mohr-Coulomb model. It is shown that the NorSand UMAT can simulate better the force displacement behaviour including the post-peak softening, which cannot be done with Mohr-Coulomb model with a constant dilation angle. The failure envelope obtained with NorSand UMAT for combined lateral and vertical (upward) oblique loading for a deep burial pipeline in dense sand is comparable with the analytical solution and previous numerical analyses.

**This thesis is dedicated to my late father, who was always encouraging me to increase my knowledge and was a driving force in my decision to pursue a graduate degree; who always had confidence in me and is ever so perpetually present in spirit to light my life's path.**

## ACKNOWLEDGEMENTS

The two years of my masters was an incredible journey in which I have learned so many things and I have been matured in so many ways. I have come in touch with so many brilliant and excellent people.

First and foremost, I would like to offer my sincere gratitude to my supervisor, Dr. Bipul Hawlader who is an extraordinary academic supervisor as well as an ideal person to follow for all aspects of life. He was not only my supervisor but also my mentor, my guide and my friend. I feel a deep sense of pride and satisfaction to get the opportunity to work so closely with him.

I am also grateful to Drs. Kenichi Soga, Tzi Piau Cheong, Dilan Jeyachandran Robert of the University of Cambridge, Dr. Ganesh Dasari of ExxonMobil and John Barrett of C-CORE for providing me consultation and suggestion at different stages of my research. Thanks to my friends in the Faculty of Engineering - Rajib, Sujan, Anup, John, Kenton, Chris, Waqas and many others who helped me several times in my numerical analyses and with whom I have had very good times.

I am thankful to the funding agencies – Memorial University of Newfoundland, and Research and Development Corporation (RDC) of Newfoundland for supporting my research. Special thanks to RDC for offering me ‘RDC Ocean Industries Students Research Award’, which was truly inspirational.

Last, but not least I would like to thank my mother and my sweet sister for their unconditional love and support throughout my life.

## Table of Contents

ABSTRACT .....	ii
ACKNOWLEDGEMENTS .....	v
Table of Contents .....	vi
List of Tables .....	x
List of Figures .....	xi
List of Symbols .....	xv
Chapter 1 INTRODUCTION.....	1
1.1 General .....	1
1.2 Scope of the Work.....	2
1.3 Objectives.....	2
1.4 Organization of Thesis .....	3
1.5 Original Contributions.....	5
Chapter 2 LITERATURE REVIEW .....	6
2.1 Introduction .....	6
2.2 Soil/Pipeline Interaction .....	7
2.3 Effects of Soil Constitutive Model.....	14
2.4 Summary .....	15
Chapter 3 CONSTITUTIVE MODELING OF SAND.....	17

3.1	General .....	17
3.2	Stress-Strain Behaviour of Sand .....	17
3.3	Typical Response of Sand in Triaxial Test .....	22
3.4	Mohr-Coulomb Model .....	25
3.5	NorSand Model .....	29
3.6	Advantages of NorSand in Modeling Soil/Pipeline Interaction.....	36
Chapter 4 FINITE ELEMENT ANALYSES WITH MOHR-COULOMB SOIL		
CONSTITUTIVE MODEL .....		
		39
4.1	General .....	39
4.2	Model Tests at Cornell University .....	39
4.3	Finite Element Modeling.....	49
4.3.1	Pipe/soil Interface .....	50
4.3.2	Loading .....	51
4.3.3	Soil Properties .....	51
4.4	Mesh Sensitivity and Boundary Effects .....	53
4.4.1	Mesh sensitivity .....	54
4.4.2	Boundary Effect .....	55
4.5	Geostatic Loading Step .....	57
4.6	Pure Lateral Loading .....	59

4.7	Pure Vertical (Upward) Loading.....	63
4.8	Three-Dimensional Analyses .....	66
4.8.1	Pure Lateral Loading.....	68
4.9	Summary .....	72
Chapter 5 FINITE ELEMENT ANALYSES WITH NORSAND SOIL CONSTITUTIVE		
	MODEL .....	73
5.1	General .....	73
5.2	Implementation of NorSand Model into ABAQUS.....	74
5.3	NorSand Model Parameters .....	76
5.3.1	Modulus of Elasticity .....	76
5.3.2	Critical Stress Ratio in three-dimensional stress space.....	77
5.4	Simulation of Triaxial Tests using NorSand UMAT .....	79
5.5	Modeling of soil/pipeline interaction using NorSand UMAT .....	89
5.5.1	Input Parameter for NorSand Model.....	89
5.5.2	Input parameters for Mohr-Coulomb model.....	91
5.6	Pure Lateral Loading.....	94
5.7	Pure Vertical (Upward) Loading.....	96
5.8	Oblique Loading.....	99
5.8.1	Force-Displacement Curves.....	101

5.8.2	Peak Forces Caused by Oblique Soil Movement.....	105
5.8.3	Failure envelopes under oblique loading .....	108
Chapter 6 CONCLUSIONS AND FUTURE RECOMMENDATIONS .....		114
6.1	Conclusions .....	114
6.2	Recommendations for Future Work.....	116
Bibliography .....		118

## List of Tables

Table 3-1: Typical range of NorSand model parameters (Shuttle and Jefferies, 2010).....	36
Table 4-1: Geometry and Parameters used in the finite element analyses.....	53
Table 5-1: Input parameters required for UMAT .....	75
Table 5-2: Triaxial test data on Erksak sand (Regenerated from Been et al., 1991).....	79
Table 5-3: Model parameters of NorSand for simulating triaxial tests.....	80
Table 5-4: Parameters used for soil/pipeline interaction analyses with NorSand UMAT.....	90
Table 5-5: Parameters used for soil/pipeline interaction analyses with Mohr-Coulomb Model.....	93

## List of Figures

Figure 2-1: (a) Schematic illustration of continuum soil/pipe interaction, (b) Idealization of pipe/soil interaction based on structural model (ALA, 2002) .....	8
Figure 2-2: ASCE horizontal bearing capacity factor: adapted from Hansen (1961).....	11
Figure 2-3: ASCE horizontal bearing capacity factor: after Trautmann and O'Rourke (1983).....	12
Figure 3-1: Contributions to the shear strength of granular soils (Mitchell, 1993). .....	21
Figure 3-2: Definition of the state parameter.....	22
Figure 3-3: Schematic of typical results of a drained triaxial test on loose and dense sand (a) Deviator stress vs Axial strain (b) Volumetric strain vs Axial strain.....	24
Figure 3-4: Mohr-Coulomb failure criteria.....	26
Figure 3-5: (a) Mohr-Coulomb failure criterion in deviatoric plane, (b) Mohr-Coulomb flow potential in deviatoric plane and (c) Mohr-Coulomb flow potential in meridional plane.....	28
Figure 3-6: Typical CSL and NCL in $e-\ln p'$ plot.....	31
Figure 3-7: Yield surfaces in triaxial stress state (Jefferies, 1993).....	34
Figure 4-1: Two-dimensional view of experimental setup (Trautmann and O'Rourke, 1983) .....	40
Figure 4-2: Relationship between normal stress and shear stress at the peak of Cornell University (CU) filter sand (Trautmann, 1983) .....	41
Figure 4-3: Force-displacement curve of lateral pipe tests in loose sand (Trautmann, 1983) .....	43

Figure 4-4: Force-displacement curve of lateral pipe tests in medium sand (Trautmann, 1983).....	44
Figure 4-5: Force-displacement curve of lateral pipe tests in dense sand (Trautmann, 1983).....	45
Figure 4-6: Force-displacement curves for uplift tests on buried pipe in loose sand.....	46
Figure 4-7: Force-displacement curves for uplift tests on buried pipe in medium sand....	47
Figure 4-8: Force-displacement curves for uplift tests on buried pipe in dense sand.....	48
Figure 4-9: Structured meshing in ABAQUS.....	49
Figure 4-10: Default meshing in ABAQUS.....	55
Figure 4-11: Location of right and bottom boundaries.....	56
Figure 4-12: Bottom and right boundary effects in 2D analysis.....	56
Figure 4-13: Geostatic loading (a) for analysis with medium dense sand for $H/D = 2$ (b) for analysis with dense sand for $H/D = 11.5$ .....	58
Figure 4-14: Normalized Force-Displacement curve for lateral loading in (a) Medium dense sand with $H_b/D = 2$ and (b) Dense sand with $H_b/D = 2$ .....	61
Figure 4-15: Normalized Force-Displacement curve for lateral loading in (a) Medium dense sand with $H_b/D = 11.5$ and (b) Dense sand with $H_b/D = 11.5$ .....	62
Figure 4-16: Normalized Force-Displacement curve for upward loading in (a) Medium dense sand with $H_c/D = 4$ and (b) Dense sand with $H_c/D = 4$ .....	64
Figure 4-17: Normalized Force-Displacement curve for upward loading in (a) Medium dense sand with $H_c/D = 11.5$ and (b) Dense sand with $H_c/D = 11.5$ .....	65
Figure 4-18: Typical meshing for lateral 3-D pipe-soil interaction analysis.....	67
Figure 4-19: Typical geostatic loading for lateral 3-D pipe-soil interaction analysis.....	68

Figure 4-20: Normalized Force-displacements curves from Lateral-3D analysis for dense sand (a) $H_b/D = 2$ (b) $H_b/D = 11$ .....	69
Figure 4-21: Shear failure pattern under lateral loading (a) $H_b/D = 2$ (b) $H_b/D = 11.5$ ....	71
Figure 5-1: Variation of $M$ in $\pi$ -plane used in UMAT .....	78
Figure 5-2: Axisymmetric 4-noded element CAX4 for FE simulation of triaxial tests.....	81
Figure 5-3: Finite element simulation (Very Dense Sand) .....	82
Figure 5-4: Finite element simulation (Dense Sand) .....	83
Figure 5-5: Finite element simulation (Loose Sand) .....	84
Figure 5-6: Finite element simulation (Very Loose Sand) .....	85
Figure 5-7: Void ratio in $e$ - $\ln p'$ plot for different density.....	87
Figure 5-8: Deviatoric stress vs axial strain plot .....	87
Figure 5-9: Volumetric strain vs axial strain plot for different void ratios.....	88
Figure 5-10: Deviatoric stress vs mean effective stress plot for over-consolidated sand.....	88
Figure 5-11: Normalized force-displacement curve with (a) $H_b/D = 2$ (b) $H_b/D = 11.5$ .....	95
Figure 5-12: Vertical Force vs vertical displacement curve for $H_c/D=4$ .....	97
Figure 5-13: Displacement and plastic strain for pure upward loading.....	97
Figure 5-14: Vertical Force vs vertical displacement curve for $H_c/D=13$ .....	99
Figure 5-15: Definition of oblique angle in 2-D oblique loading .....	101
Figure 5-16: Force-displacement curves for horizontal component in oblique loading ..	102
Figure 5-17: Force-displacement curves for vertical component in oblique loading .....	103

Figure 5-18: Force–displacement responses for oblique loading for $H/D=3.03$ : (a) total, (b) horizontal, and (c) vertical forces (Guo, 2005).....	104
Fig. 5-19: Force–displacement responses for oblique loading: (a) $H/D = 2$ and (b) $H/D = 4$ (Daiyan, 2009).....	105
Figure 5-20: Variation of horizontal and vertical interaction factors with oblique angles.....	107
Figure 5-21: Normalized lateral and vertical components of peak oblique load on the pipeline in clay (Daiyan et. al, 2009).....	108
Figure 5-22: Lateral-vertical bearing factor interaction diagram as a function of the oblique angle.....	110
Figure 5-23: Comparison of different representations of failure envelope.....	111
Figure 5-24: Oblique load capacity (a) Meyerhof model for inclined anchor, (b) anchor-buried pipe analogy (Nyman 1984).....	112
Figure 5-25: Typical Plastic shear strain in oblique loading.....	113

## List of Symbols

$c'$	cohesion in Mohr-Coulomb strength parameter
CSL	critical state line
$D$	dilatancy
$D_r$	relative density
$e$	void ratio
$\nu$	Poisson's ratio
$E$	Young's modulus
$G$	shear modulus
$H$	hardening/softening modulus in loading, a NorSand model input parameter
$K$	bulk modulus
$M$	critical state stress ratio ( $q/p'$ at critical state), a NorSand model input parameter
$M_c$	value of $M$ in triaxial compression
$M_e$	value of $M$ in triaxial extension
$M_i$	stress ratio at image state
$N$	volumetric coupling coefficient, a NorSand model input parameter
NC	normally consolidated
NCL	normally consolidated line
OCR	overconsolidation ratio
$p$	mean effective stress, for triaxial condition $p = (\sigma_1 + 2\sigma_3)/3$
$\phi'$	angle of internal friction
$\phi'_p$	peak friction angle

$\phi'_c$	critical state friction angle
$\phi'_m$	mobilised friction angle
$\phi'_u$	true friction angle
$\psi_m$	dilatancy angle
$\psi$	state parameter of NorSand
$\tau_f$	shear stress at failure on the failure plane
$\sigma'_1$	effective major principal stress
$\sigma'_3$	effective minor principal stress
$\delta \dot{\epsilon}_1$	principal major strain increment
$\delta \dot{\epsilon}_3$	principal minor strain increment
$\eta$	stress ratio ( $= q/p'$ )
$q$	deviator stress in triaxial condition
$\lambda$	slope of CSL in $e-\ln p$ or $v-\ln p$ plot
$\Gamma$	critical void ratio at $p'=1$ kPa
$I_r$	shear rigidity
$F$	lateral or upward pipe force
$F_{oh}$	horizontal component of oblique pipe force
$F_{ov}$	vertical component of oblique pipe force
$\gamma$	unit weight of soil
$H_c$	depth from the top of the soil to the center of the pipe for upward movement
$H_b$	depth from the top of the soil to the base of the pipe for lateral movement
$L$	length of the pipe involved in the test

$\delta_l$	lateral displacement of the pipe
$\delta_u$	vertical (upward) displacement of the pipe
$\delta_{oh}$	horizontal component of pipe displacement in oblique loading
$\delta_{ov}$	vertical component of pipe displacement in oblique loading
$t$	thickness of the pipe
$\rho_s$	density of steel
$g$	gravitational acceleration
$K_0$	earth pressure coefficient at rest

# **Chapter 1**

## **INTRODUCTION**

### **1.1 General**

Pipelines are extensively used for transporting water and hydrocarbons. The vital role that they play in our present economy is reflected in the many kilometers of pipelines laid in onshore and offshore locations worldwide. Arctic and offshore Newfoundland and Labrador have been considered to be the major sources of oil and gas reserves in Canada. In recent years, oil and gas industries are moving into these areas for exploration. They are also planning for development and transportation of oil and gas to the markets. The liquid hydrocarbon and natural gas products are usually transported through buried pipelines, which traverse large distances through a variety of soils. Geohazards and the associated ground movement represent a significant threat to pipeline integrity that may result in pipeline damage and potential failure. In certain situations, pipelines can be exposed to potential ground failures such as surface faulting, liquefaction-induced soil movements, and landslide induced permanent ground deformation (PGD). These ground movements might cause excessive stresses in pipelines that may impact serviceability or trigger failure such as buckling or wrinkling and pipeline damage in some cases. Therefore, safe, economic and reliable operation of pipeline transportation systems is the primary goal of the pipeline operators and regulatory agencies.

## **1.2 Scope of the Work**

Finite element (FE) modeling has been widely used for predicting the response of buried pipelines to lateral, upward (vertical) and oblique loading conditions. Most of the FE analyses used built-in soil constitutive model in commercially available FE software. However, their prediction might be better if an advanced soil constitutive model is used.

A number of researchers including the researchers at Memorial University and C-CORE studied soil/pipeline interaction behaviour of onshore and offshore buried pipelines. Finite Element modeling has been considered one of the successful and efficient modeling techniques to analyze the response of buried pipeline to lateral, upward (vertical) and oblique loading conditions and also for varying soil conditions. Commercially available software packages such as ABAQUS have been used for modeling the behaviour. Previous researchers also recognized that advanced soil constitutive model is required for better prediction of the response as the built-in soil constitutive models in software packages have significant deficiencies.

## **1.3 Objectives**

The main objective of the present study is to develop a finite element modeling technique using ABAQUS FE software for analyzing the response of buried pipelines in sand subjected to ground movement using an advanced soil constitutive model. The following steps are taken to achieve this objective.

- i) Conduct FE analyses using available constitutive model in ABAQUS;
- ii) Identify an advanced soil constitutive model that better simulates the stress-strain behaviour of sand;
- iii) Implement the soil model in ABAQUS FE software using UMAT;
- iv) Calibrate the FE model including the UMAT using triaxial test results; and
- iv) Conduct soil/pipeline interaction analyses for different loading conditions and compare with previous studies.

#### **1.4 Organization of Thesis**

The thesis is organized into six chapters that cover the literature review and developments carried out during the research. The manuscript starts with this chapter dedicated to the background and objectives of the study followed by a chapter on literature review of soil/pipeline interaction problems. The main contributions towards the advancement of modeling soil/pipeline interaction are presented in the subsequent chapters.

Constitutive models for sand available in the literature have been reviewed. An advanced soil constitutive model NorSand which is not very complex yet can simulate most of the features observed in laboratory tests is selected. In Chapter 3 the various aspects of this model is discussed. The limitations of Mohr-Coulomb model which is typically used are also discussed. The details and comparison of these two soil constitutive models are described. The possible advantages of NorSand model to simulate soil/pipeline interaction problems are also discussed in this chapter.

Chapter 4 describes the FE analyses that were conducted to simulate the behaviour of pipelines in sand for pure lateral, pure upward and oblique loading with Mohr-Coulomb soil model. It presents the results of the 2-D and 3-D FE analyses conducted to simulate the large scale tank test performed by Trautmann and O'Rourke (1983). Results from FE analyses are presented with particular attention to the load-displacement plots.

Chapter 5 describes the implementation and validation of the NorSand soil constitutive model. The implemented NorSand UMAT is first validated with available triaxial test results for varying soil conditions. The implemented NorSand model was also compared for soil/pipeline interaction events for pure lateral and pure upward loading with the FE analyses using Mohr-Coulomb model. Finally, FE analyses were conducted to simulate the behaviour of soil/pipeline interaction for a deep burial pipeline in dense sand for oblique (lateral-vertical) loading. The effects of oblique angle on soil-pipeline interaction are examined and a diagram of variation of horizontal and vertical interaction factors with oblique angles is developed. The failure envelope is also obtained with NorSand UMAT for combined lateral and vertical (upward) oblique loading and compared with analytical solutions and previous numerical analyses.

Chapter 6 presents the summary of the analyses and the conclusions that are drawn from this research. Some recommendations for the future work are also provided in this chapter.

## **1.5 Original Contributions**

In this research, an advanced soil constitutive model for simulating the response of buried pipelines is identified first. Reviewing the available soil constitutive models, it is identified that NorSand soil constitutive model proposed by Jefferies and his co-workers could better model sand behaviour. NorSand model implemented in ABAQUS FE software using user defined subroutines UMAT is used for numerical analyses. The numerical model is used for simulating the response of pipelines to lateral, upward (vertical) and oblique loading conditions subjected to ground movement.

ABAQUS is a general purpose finite element software which is very powerful in analysis of boundary value problems and has been considered as a numerical tool for analyzing different types of problems in civil and mechanical engineering. This is not a pure geotechnical software with built-in advanced soil constitutive models. However, a number of researchers in geotechnical and pipeline engineering used ABAQUS as it is very efficient. In the present study, one of the main limitations is addressed for analysis of pipelines and other infrastructures by implementing NorSand soil constitutive model in ABAQUS FE software.

## Chapter 2

### LITERATURE REVIEW

#### 2.1 Introduction

Buried pipelines are extensively used for transporting water and hydrocarbons. In the oil and gas industries, energy pipeline systems are critical transportation elements for transmission of hydrocarbon products over long distances. Over 97% of Canadian natural gas and crude oil production is transported by transmission pipelines and the estimate of Canada's underground natural gas and liquids pipeline network (gathering, transmission and delivery lines) is approximately 825,000 km ([www.cepa.com](http://www.cepa.com)). One of the challenges in buried pipeline design is the effect of geohazards on the mechanical response and integrity of pipelines. In certain situations, pipelines can be exposed to potential ground failures, such as surface faulting, liquefaction-induced soil movements, and landslide induced permanent ground deformation (PGD). Ground deformation often causes the most serious local damage in buried pipeline networks (Hamada and O'Rourke, 1992; O'Rourke, 1998; O'Rourke, 2010). Permanent ground deformation effects not only apply to earthquakes, but also occur in response to floods, tunneling, deep excavations, and subsidence caused by dewatering or the withdrawal of minerals and fluids during mining and oil production. Such loading conditions are becoming increasingly more important as technologies are developed to cope with natural hazards, human threats, construction in congested urban environments, and offshore structures. Many previous studies (e.g.

Trautmann, 1983; ALA, 2002; O'Rourke, 1998; Paulin, 1998; Conte et al., 2002; Anderson et al., 2004; Yeh et al. 2006; Giovanazi and Cubrinovski, 2007; O'Rourke and Bonneau, 2007; Ha et al., 2008a and b; O'Rourke, M.J. et al., 2008; O'Rourke, T.D. et al., 2008; and Oliveira et al., 2010) have addressed the effects of PGD, including soil liquefaction, landslides, surface faulting, and tunneling and urban excavations, on critical underground infrastructure. These ground movements might cause excessive stresses in pipelines and might cause the damage in some cases. Therefore, the advancement of the understanding of pipe/soil interaction will not only lead to improved engineering designs but also to reduced uncertainty, improved economy, and greater safety for the oil and gas pipeline industries.

## **2.2 Soil/Pipeline Interaction**

In the current state-of-practice (e.g., Committee on Gas and Liquid Fuel Lifelines of ALA 2002), the pipeline is generally modeled by a simplified beam, while the soil/pipeline interaction is modeled by three soil springs in the axial (or longitudinal), transverse horizontal, and transverse vertical directions using Winkler type model (Winkler, 1867) as shown in Figure 2-1.

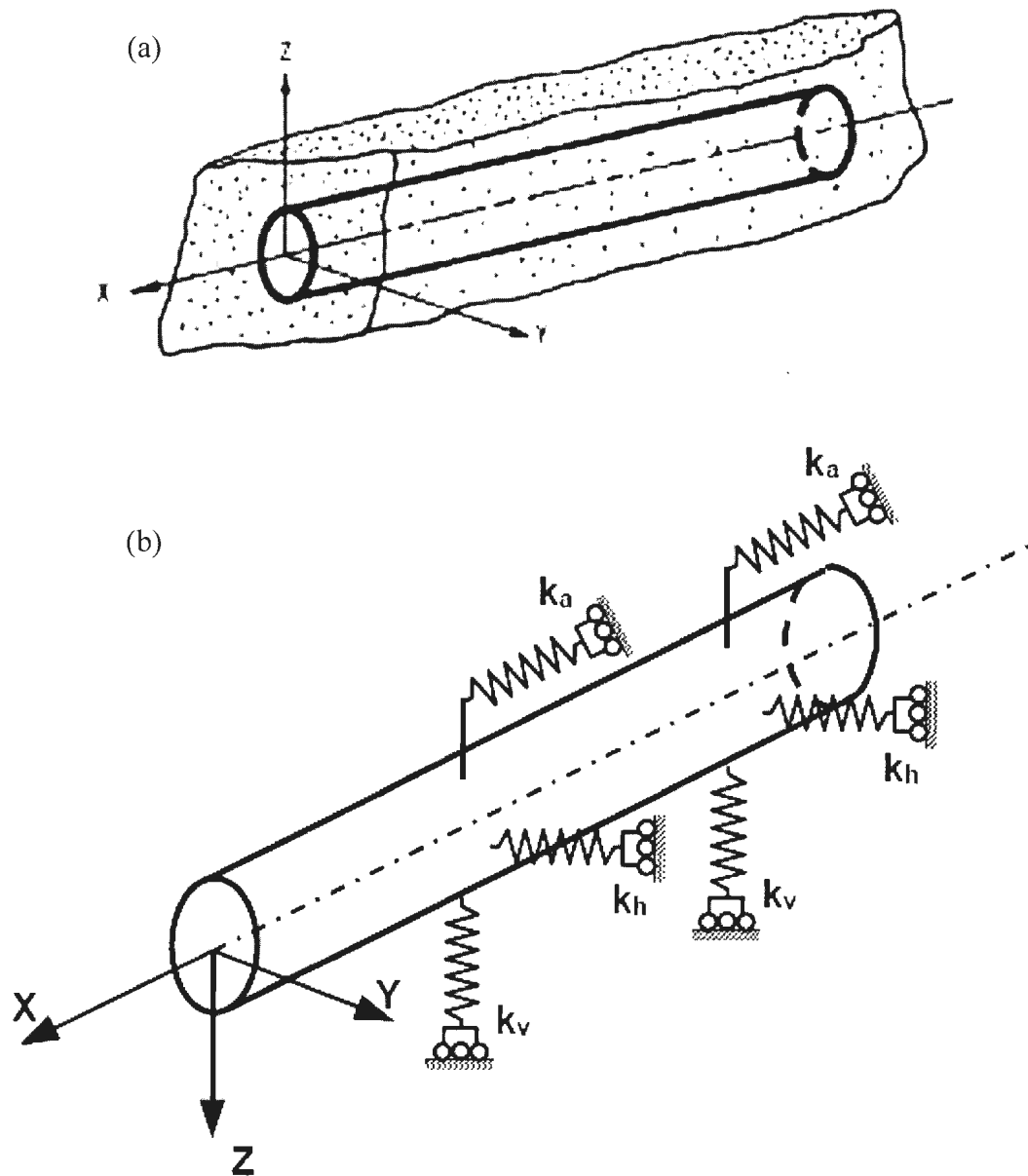


Figure 2-1: (a) Schematic illustration of continuum soil/pipeline interaction, (b) Idealization of pipe/soil interaction based on structural model (ALA, 2002)

The properties of soil springs in three orthogonal directions are independent which means that the deformation of soil in one direction has no effect on pipe/soil interactions in other

directions. The general form of the load-displacement relations for these springs can be expressed as:

$$T = f(x); P = f(y); Q = f(z) \quad (2.1)$$

Where  $T$ ,  $P$  and  $Q$  are the soil loads applied to unit length of the pipeline and  $x$ ,  $y$  and  $z$  are the relative displacements between pipe and soil in longitudinal, lateral and vertical directions, respectively. This approach benefits from ease of application and its incorporation in available finite element (FE) codes (ALA, 2002), but suffers from the uncoupled representation of soil as a series of spring-slider reactions (Honegger and Nyman, 2004). Whereas simplified models for pipeline response to abrupt soil movement (Kennedy et al., 1977; O'Rourke and Trautmann, 1981) provide guidance for design, numerical simulations of the nonlinear and post-yield performance of pipelines (O'Rourke and Liu, 1999; Eidinger et al, 2002) are also being considered nowadays. Numerical modeling methods have been validated through large-scale tests or physical tests that simulate soil-structure interaction, which are essential for reliable model development and acceptance in practice (O'Rourke and Liu, 1999; O'Rourke, 2010). Continuum models are now being developed for replicating soil-pipeline interaction in a realistic way (O'Rourke, 2010).

The soil reaction that develops as the pipe moves relative to the ground is of key importance in the response of underground lifelines to PGD. Theoretical and experimental studies were conducted in the past to determine the forces on pipelines due

to the relative movement of the soil in a specific direction, namely longitudinal, transverse horizontal, or transverse vertical (e.g. Hansen, 1961; Ovesen, 1964; Vesic, 1971; Audibert and Nyman, 1977; Ranjan and Aurora, 1980; Trautmann *et al*, 1985; Paulin, 1998; Scarpelli et al., 1999; and Rizkalla et al., 1992; Guo, 2005; Wijewickreme et al., 2009).

ALA (2002) provides two models to calculate the horizontal bearing factor for sand,  $N_{qh}$ , (Figure 2-2 and Figure 2-3). The first one is based on the work of Audibert and Nyman (1977). They adapted Hansen (1961) model for vertical piles subjected to lateral loading and a good agreement with experimental data was found. The value of  $N_{qh}$  increases with soil friction angle and burial depth-diameter ratio,  $H/D$  (PRCI, 2003). The second model for the bearing factor,  $N_{qhs}$ , is based on the work of Trautmann (1983). They found good agreement between experimental results and the theory for vertical plate anchors subjected to horizontal loading (Ovesen and Stromann, 1972). ALA (2002) has pointed out that for the same burial geometry and soil properties, the factor  $N_{qh}$  obtained from the model of Hansen (1961) is 50 to 100% greater than that obtained from the Ovesen and Stromann (1972) based model (PRCI, 2003). Guo and Stolle (2005) reconciled the difference between Hansen (1961) and Ovesen and Stromann (1972) based on the size effect, stress level and soil weight.

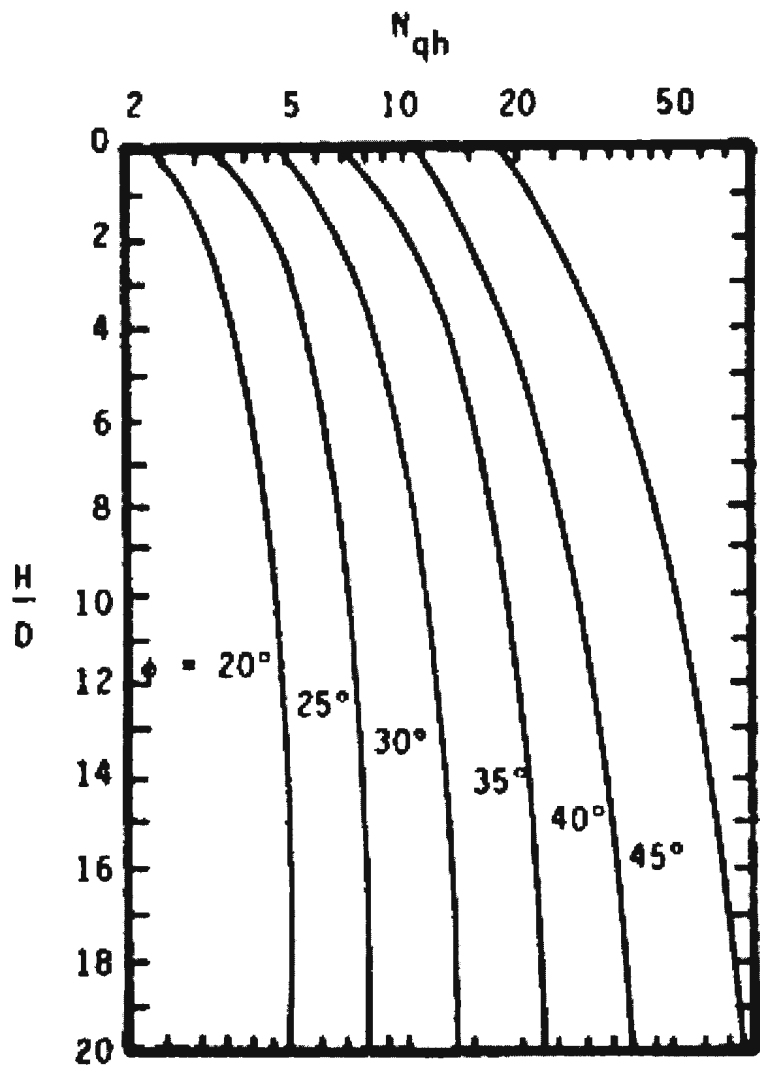


Figure 2-2: ASCE horizontal bearing capacity factor: adapted from Hansen (1961)

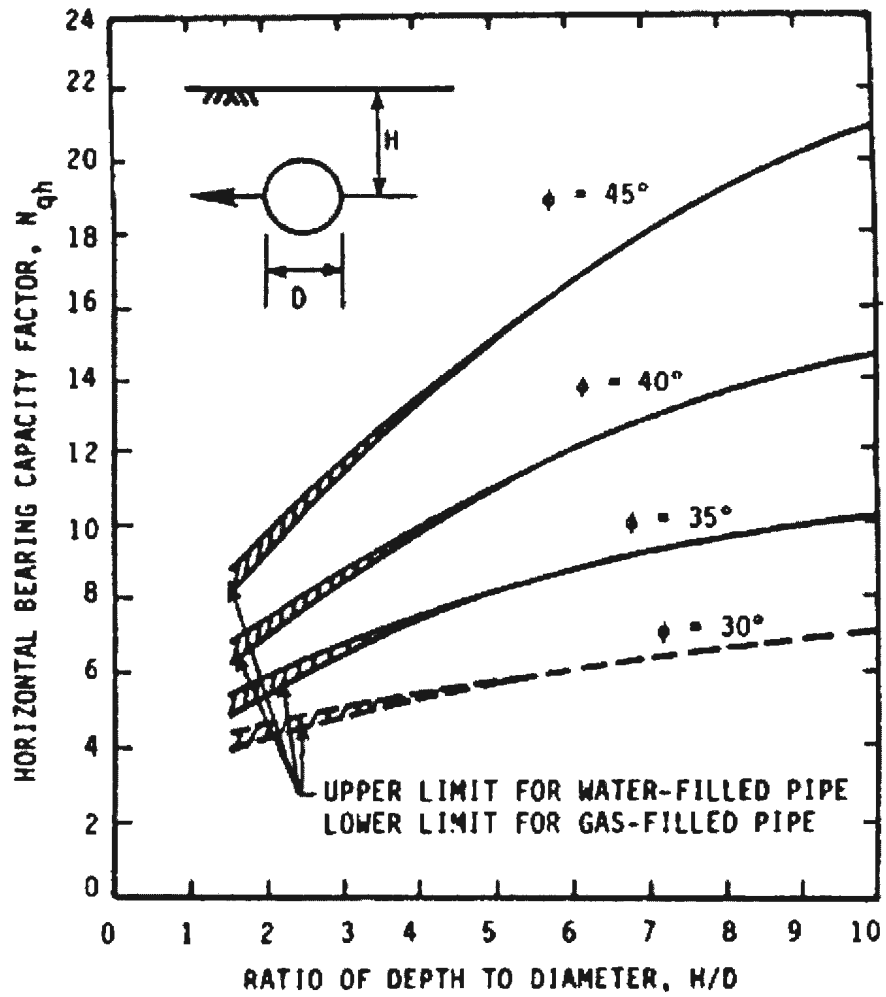


Figure 2-3: ASCE horizontal bearing capacity factor: after Trautmann and O'Rourke (1983)

Several theoretical, numerical and experimental analyses have been conducted on load-displacement behaviour of piles and anchor plates that can be also used to define the pipe/soil load-displacement behaviour for each of the three perpendicular (axial or longitudinal, lateral horizontal and vertical) directions. Although the available guidelines (e.g., ALA, 2002) provide procedures for characterizing the force-displacement relationships for vertical uplift, settlement, and lateral displacement of buried pipelines in

soil using spring models, these springs are usually independent and during a 3D pipe/soil relative displacement they cannot account for cross effects due to the shear interaction between different soil zones along the pipe. A number of studies have been conducted in the past to investigate the pipe/soil interaction during an oblique or three-dimensional pipe/soil relative movement, which includes experimental (e.g. Daiyan et al., 2010a and b, Hsu et al., 2006), theoretical (e.g. Cocchetti et al., 2009a) and numerical (e.g. Cocchetti et al., 2009b, Phillips et al., 2004) investigations. It is also to be noted here that the response of a pipeline under combined loading in centrifuge (Daiyan et al., 2010a & b) is slightly different from the model test results conducted by Hsu et al., (2006), which also need to be resolved. Previous researchers (e.g. Daiyan et al., 2010a and b, Phillips et al., 2004) show that there is a considerable increase in the axial soil restraint on the pipeline when a lateral relative displacement occurs between pipe and soil. Therefore, more investigations on complex loading conditions are needed to enhance the numerical tools and to develop engineering guidelines to assess pipeline's response in a 3D pipeline/soil interaction event.

Although there are several experimental, theoretical and numerical studies, the number of numerical studies for oblique especially for lateral-vertical loading using advanced soil constitutive model is limited. As continuum finite element models can provide the means of simulating buried pipeline behaviour in a more reliable way than finite element modeling with spring-slider elements that is often performed in current practice, finite element modeling of oblique loading events of pipe-soil interaction both in plane strain and three-dimensional conditions are equally important.

### **2.3 Effects of Soil Constitutive Model**

While previous numerical studies available in the literature show the similar trend as observed in model tests, for successful quantification of the response of pipeline to lateral, upward (vertical) and oblique loading conditions, the soil behavior should be modeled properly. Fortunately, a large number of research works in geotechnical engineering are devoted to the development of better constitutive model for sand which can capture most of the salient features of stress-strain behaviour. Unfortunately, these advanced soil constitutive models are not implemented in most of the commercially available software such as ABAQUS. Therefore, most of the research works on buried pipelines are based on simple built-in model such as Mohr-Coulomb plasticity model. The Mohr-Coulomb plasticity model has a number of limitations including the modeling of dilation and could be questionable at low stress level. For pipeline-soil interaction analyses in sand, the peak forces from Mohr-Coulomb model also overestimate the model test results (Yimsiri et al., 2004). In this research, an advanced soil constitutive model for simulating the response of buried pipelines was identified first. Reviewing available soil constitutive models, it was identified that NorSand soil constitutive model proposed by Jefferies (1993) could better model the soil behaviour particularly in sand. NorSand soil constitutive model implemented in ABAQUS FE software using user defined subroutines UMAT is used for numerical analyses in the current study.

The research described in this thesis is undertaken to improve the analysis of buried pipelines under the effects of PGD by simulating soil-pipeline interaction by continuum

finite element models and with an advanced soil constitutive model, NorSand. First, several finite element models in plane strain condition were developed with built-in Mohr-Coulomb model and also with implemented NorSand soil constitutive model in ABAQUS to analyze the pipe/soil interaction event for pure horizontal and pure upward loading. The results of large-scale tests are used to compare with numerical results with built-in Mohr-Coulomb model to either validate the finite element models or generate improvements in the modeling process, resulting in more effective simulation techniques. The developed finite element tools with the implemented NorSand model are used for further soil-pipeline interaction analyses on oblique loading event in plane strain condition.

## **2.4 Summary**

The current state of practice for pipeline design is fully reflected in the ALA (2002) guidelines, and more recently, C-CORE Report (2003). In general, pipeline is represented as an elastic beam, while the soil along the pipeline is modelled by a series of discrete nonlinear springs (i.e. elasto-plastic, multi-linear). Using different equations corresponding to assumed conditions, the maximum soil spring forces and associated relative displacement necessary to mobilize these forces are computed. Even though the above mentioned guidelines follow the same basic principles, the calculations of soil forces are very different, since they are based on different considerations and assumptions. However, for accurate simulation of load transfer to the pipeline, proper

modelling of the soil-structure interaction is very important taking into account relative movements between the pipeline and soil.

The response of pipelines is very much dependent upon the properties of the surrounding soil. For a pipeline buried in loose sand, the measured force-displacement curves are almost hyperbolic. However, a peak point followed by a decrease in force is observed in dense sand which is termed as strain softening. The built-in Mohr-Coulomb model in ABAQUS cannot simulate this behaviour. So implementation of an advanced soil constitutive model that can capture different features of sand in ABAQUS has become a prime concern for the researchers in geotechnical engineering.

## Chapter 3

### CONSTITUTIVE MODELING OF SAND

#### 3.1 General

Soil constitutive modeling describes qualitative and quantitative understanding of soil behaviour. Soil behaviour depends on many factors including stress level and void ratio. A good constitutive model should be able to predict the stress-strain response of soil for the range of applicable stress level and void ratio. Constitutive modeling is also important as geotechnical engineers depend to a large extent on *in situ* tests to determine sand or silt properties but *in situ* tests do not really measure soil properties; rather they measure the response to the loading. An inverse boundary value problem needs to be solved for obtaining soil properties from the *in situ* tests, and a constitutive model is required for this. Constitutive modeling is also an excellent way to simulate full-scale experience. A sound framework is needed to understand the full-scale experience and this framework necessarily comes from the mechanics. Mechanics, in turns, is based upon understanding soil constitutive behaviour. The need for ‘good’ constitutive models is ever increasing because, with the advance in computers, more complex numerical analyses are becoming a routine practice.

#### 3.2 Stress-Strain Behaviour of Sand

The mechanical behaviour of reconstituted sands is governed by a number of material properties such as mineralogy, grain size distribution, grain shape, specific gravity and

friction angle. Been et al. (1991) grouped these as intrinsic material properties as they can be uniquely defined and are independent of the state of the sands. The strength of sand is usually characterized by the angle of internal friction  $\phi'$ , angle of dilation,  $\psi_m$  and critical state friction angle,  $\phi'_c$ . As there is no bond between the grains, the shear strength of sand can be defined by the Mohr-Coulomb failure criterion with zero cohesive intercept:

$$\tau_f = \sigma'_f \tan \phi'_m \quad (3.1)$$

where  $\tau_f$  is the shear stress at failure on the failure plane,  $\sigma'_f$  is the normal stress on the failure plane and  $\phi'_m$  is the mobilised friction angle. In triaxial condition, the mobilized angle of internal friction and dilation can be written in terms of the effective principal stresses and strains as:

$$\sin \phi'_m = \frac{\frac{\sigma'_1}{\sigma'_3} - 1}{\frac{\sigma'_1}{\sigma'_3} + 1} \quad (3.2)$$

$$\sin \psi_m = \frac{\delta \epsilon_1 + 2\delta \epsilon_3}{\delta \epsilon_1 - \delta \epsilon_3} \quad (3.3)$$

where  $\sigma'_1$  and  $\sigma'_3$  denote the major and minor effective principal stresses, respectively, and  $\delta \epsilon_1$  and  $\delta \epsilon_3$  are the major and minor principal strain increments, respectively in triaxial condition.

The relationship between  $\phi'_m$  and  $\psi_m$  has been the focus of many geotechnical researchers (e.g. Rowe, 1962; Bolton, 1986; Wood, 1990; Been et al., 1991) in the past. Rowe (1962) developed the well-known stress-dilatancy theory, which defined the relationship between stress ratio  $\eta$  and dilatancy rate  $D^p$  as:

$$D^p = \frac{\delta \varepsilon_p^p}{\delta \varepsilon_q^p} = \frac{9(M-\eta)}{9+3M-2M\eta} \quad (3.4)$$

where  $\eta = q/p'$  and  $M$  is the slope of the Critical State Line (CSL) in the  $p'$ - $q$  stress space which can be related to the critical state friction angle  $\phi'_c$  by:

$$M_c = \frac{6 \sin \phi'_c}{3 - \sin \phi'_c} \quad (3.5)$$

$$M_e = \frac{6 \sin \phi'_c}{3 + \sin \phi'_c} \quad (3.6)$$

where  $M_c$  and  $M_e$  are the slopes of CSL in triaxial compression and extension, respectively. From the Eqs. 3.5 and 3.6, it is clear that  $M_c > M_e$  if the critical state friction angle is constant in both compression and extension spaces. Rowe (1962) proposed that for dense sands, the mobilised friction angle  $\phi'_m$  could be interpreted as the sum of the sliding resistance at the contact (i.e. the true friction angle  $\phi'_u$ ), particle rearrangement and dilation. The component of crushing has some role at high stress level, but for typical

stress range in geotechnical practice may not be very significant. As shown in Figure 3-1 the dilatation plays a significant role on internal friction and thereby shear resistance. From experimental results on various sands, Bolton (1986) proposed a simple correlation between the mobilized friction angle  $\phi'_m$ , critical state friction angle  $\phi'_c$  and mobilized dilatancy angle  $\psi_m$ , as:

$$\phi'_m = \phi'_c + 0.8\psi_m \quad (3.7)$$

It has been also shown that the dilatancy rate depends on relative density of the soil.

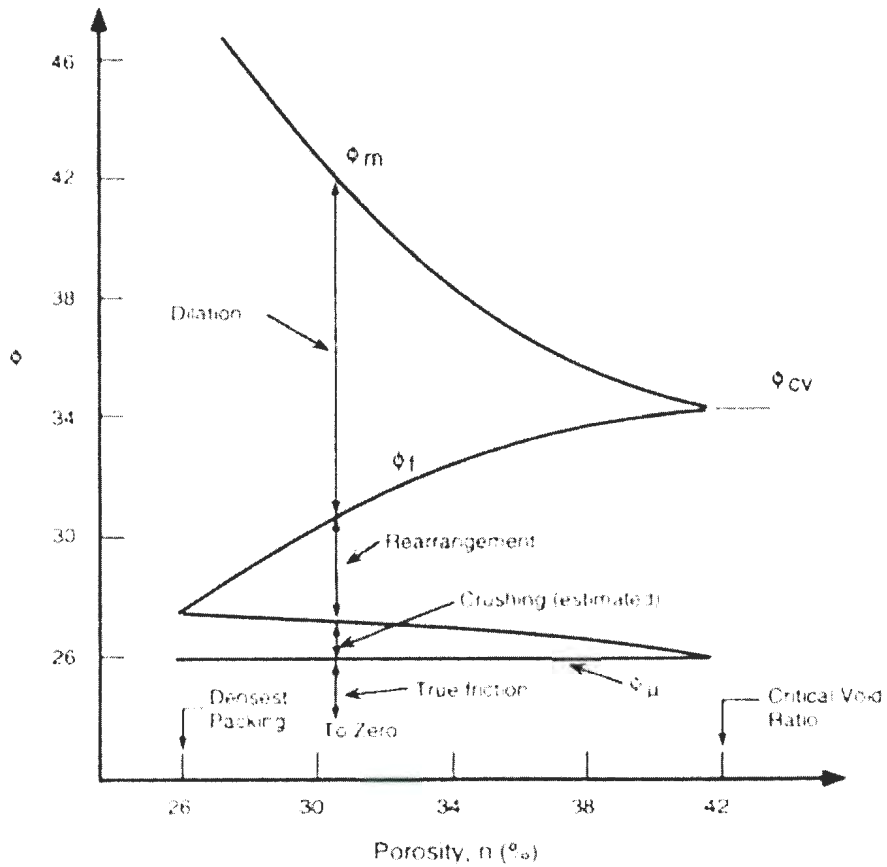


Figure 3-1: Contributions to the shear strength of granular soils (Mitchell, 1993).

Instead of relative density, the “state parameter concept” has also been successfully used to develop constitutive models for sands (e.g. Jefferies, 1993). The main advantage of this parameter is that it combines the influences of density and confining pressure on sands in a unique way as shown in Figure 3-2. The state parameter is a measure of how far the soil state is from the critical state in terms of density or void ratio.

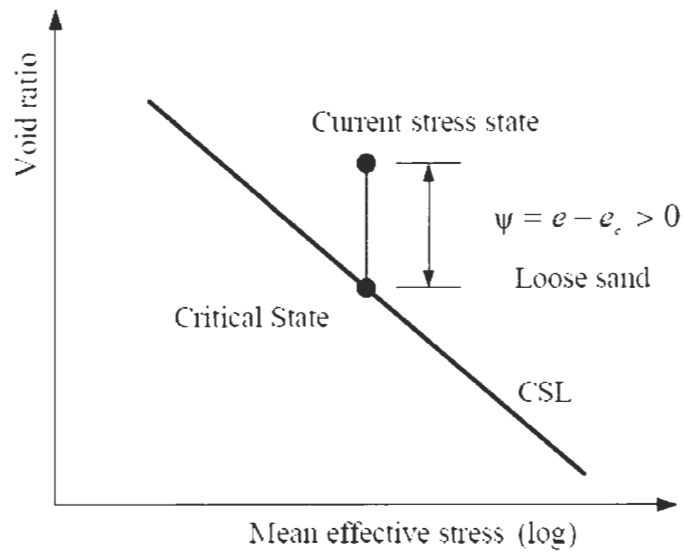


Figure 3-2: Definition of the state parameter

### 3.3 Typical Response of Sand in Triaxial Test

Typical stress-strain curves for dense and loose sand in drained triaxial tests are shown in Figure 3-3. In Figure 3-3(a) the deviator stress,  $q$ , is equal to  $\sigma_1 - \sigma_2$  for triaxial conditions. The axial strain is  $\epsilon_1$  and the deviator strain,  $\epsilon_q$  is equal to  $2(\epsilon_1 - \epsilon_3)/3$  for triaxial compression. Both  $\epsilon_1$  and  $\epsilon_q$  are commonly used to plot stress-strain curves in geotechnical engineering.

As shown in this Figure 3-3 dense sand shows a peak value of deviator stress before dropping to constant stress at larger strains. Conversely, loose sand does not show a peak but directly reaches to the same constant value of stress as the dense sand at large strains for identical mean effective stress conditions.

Figure 3-3(b) plots data in volumetric strain versus axial or deviator strain. Volumetric strain,  $\epsilon_v$ , is defined as  $\epsilon_1+2\epsilon_3$  for triaxial conditions with positive sign for compression. That means, positive volumetric strains represent contraction while negative volumetric strains denote dilation.

Dense sand contracts initially during shear and then dilates until a state is reached where volumetric strain remains constant. Loose sand contracts during shear until it reaches constant volume conditions at large strains.

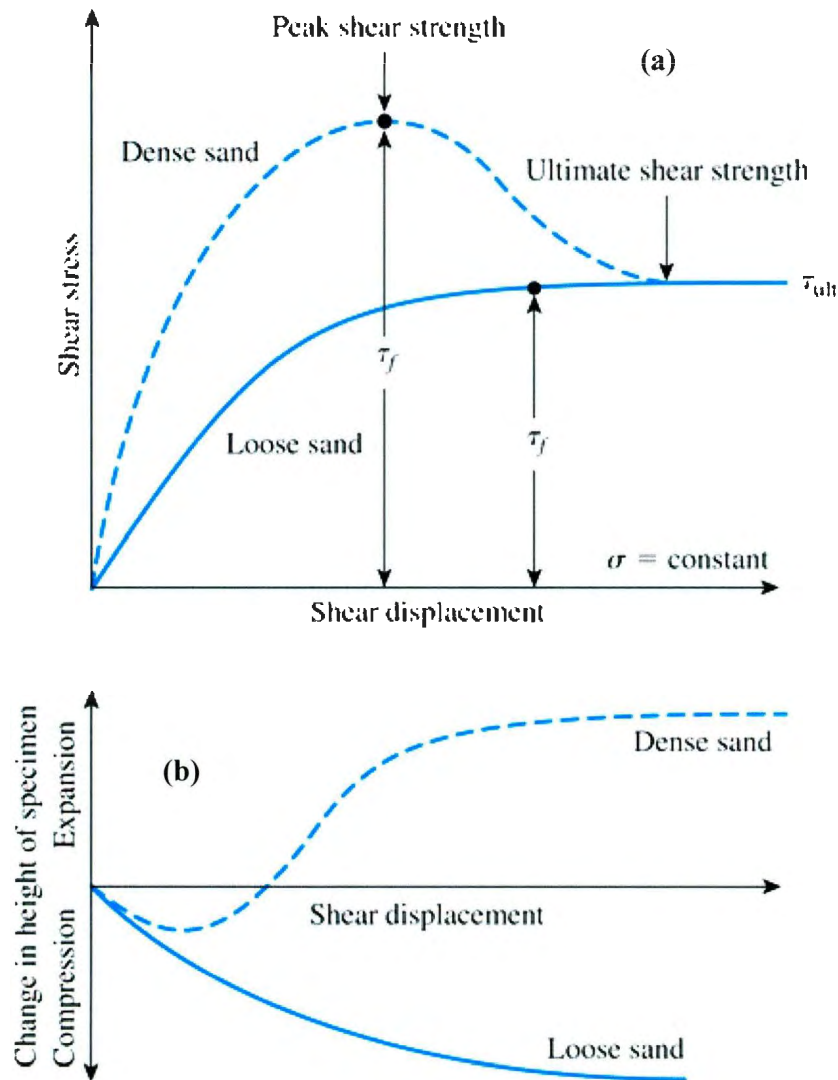


Figure 3-3: Schematic of typical results of a drained triaxial test on loose and dense sand (a) Deviator stress vs Axial strain (b) Volumetric strain vs Axial strain (Das, 2008)

The aim of constitutive modeling is to develop mathematical equations which represent the stress-strain behaviour not only in triaxial condition but also in other form of loading. To measure the stress-strain and strength properties of sand, a large number of sophisticated testing systems have been developed and a large number of plasticity

models have been proposed such as Mohr-Coulomb, NorSand, Bounding Surface and SANISAND (Taiebat and Dafalias, 2007). The stress-strain behaviour of sand depends not only on their density but also on the stress level. The true state of soils cannot be quantified simply by relative density. The location of its current stress and volume state relative to the critical state line could be the better option as used in NorSand model. In this research, constitutive models available for sand have been reviewed. Finally, the analyses have been performed using two constitutive models. The first one is the Mohr-Coulomb model, which has been widely used by previous researchers. The second one is the NorSand model which is an advanced soil constitutive models. The response of buried pipeline in sand using these models has also been compared.

### **3.4 Mohr-Coulomb Model**

Mohr-Coulomb soil model is a simple linear elastic-perfectly plastic model. It is widely used in geotechnical engineering to simulate material response under monotonic loading. Mohr-Coulomb model is one of the built-in soil constitutive models in ABAQUS finite element software for modeling geomaterials. The way it is implemented in ABAQUS is shown in Figure 3-4. The failure criteria in deviatoric plane are shown in Figure 3-5(a). The flow potentials in deviatoric and  $p$ - $q$  plane are shown in Figures. 3-5(b) and 3-5(c), respectively. As shown in this figures that the flow potentials are smooth surfaces to avoid numerical issues. The default deviatoric eccentricity ( $e=(3-\sin\phi')/(3+\sin\phi')$ ) is used.

The Mohr-Coulomb failure criterion assumes that the failure occurs when the shear stress on any point in a material reaches a value of  $\tau_f$  that depends linearly on the normal stress in the same plane (Figure 3-4) as defined in Equation 3.8.

$$\tau_f = c' + \sigma' \tan \phi' \quad (3.8)$$

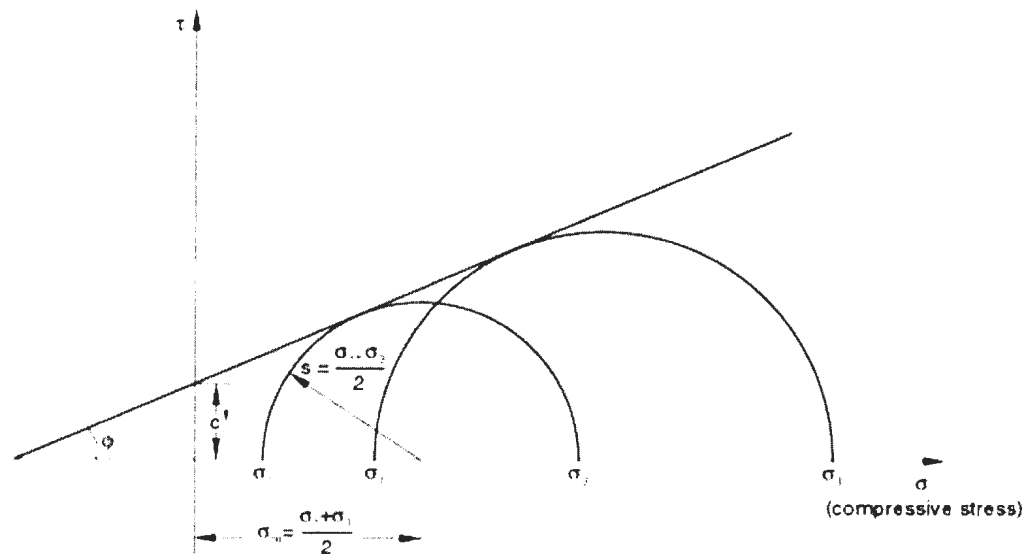
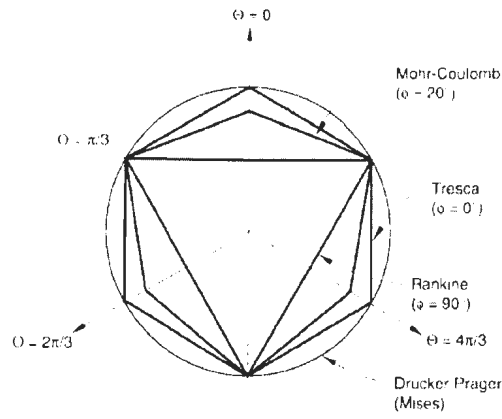


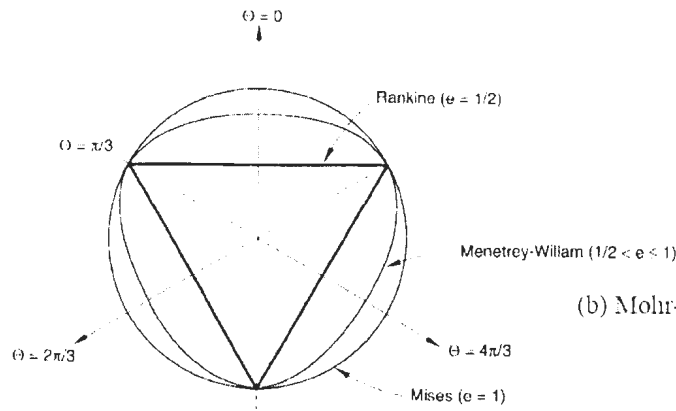
Figure 3-4: Mohr-Coulomb failure criteria

The material constant  $c'$  defines the cohesion and the friction angle  $\phi'$  controls the slope of the yield surface in the deviatoric plane as shown in Figure 3-4. The yield surface does not harden with plastic strain. In the case of  $\phi = 0^\circ$ , Mohr-Coulomb model reduces to the pressure-independent Tresca model with a perfectly hexagonal deviatoric section.

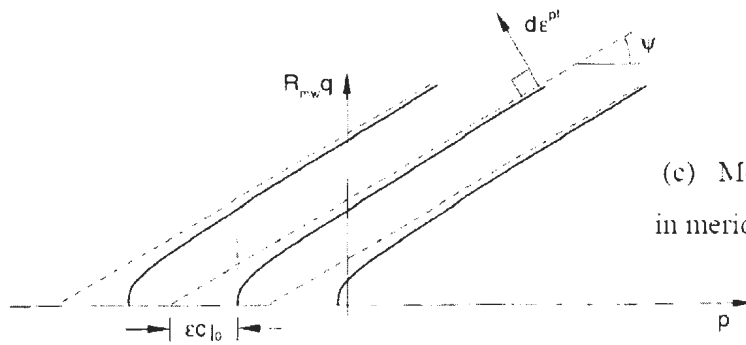
Within the Mohr-Coulomb framework, the soil is modelled as an isotropic dilatant elastic-perfectly plastic material. Elastic behaviour can be modelled using linear/non-linear elastic properties. Plastic flow in the meridional stress plane can be considered to be “associated” when the angle of internal friction  $\phi'$  and the angle of dilation  $\psi_m$  are equal and the meridional eccentricity,  $\varepsilon$  is very small (Figure 3c); however, plastic flow in this plane is in general “non-associated”. Plastic flow in the deviatoric stress plane is always “non-associated”. Therefore, the use of this Mohr-Coulomb model generally requires the non-symmetric matrix storage and solution scheme.



(a) Mohr-Coulomb failure criterion in deviatoric plane



(b) Mohr-Coulomb flow potential in deviatoric plane,



(c) Mohr-Coulomb flow potential in meridional plane

**Figure 3-5: (a) Mohr-Coulomb failure criterion in deviatoric plane, (b) Mohr-Coulomb flow potential in deviatoric plane and (c) Mohr-Coulomb flow potential in meridional plane (ABAQUS 6.7, 2007; Compressive stress is shown as negative)**

In short, Mohr-Coulomb soil constitutive model requires two strength parameters,  $c'$  and  $\phi'$ , where  $c'$  represents the part of strength that is independent of normal stress and  $\phi'$  is the angle of internal friction in terms of effective stress. It requires two additional elasticity parameters (Young's modulus,  $E$ , and Poisson's ratio,  $\nu$ ). A linear isotropic elastic modulus is used in this study. Moreover, the dilation angle ( $\psi$ ) is needed to be defined which is constant in built-in model. Applying normality to Mohr-Coulomb surface, i.e. using associated flow, implies that the dilation angle is equal to the friction angle. This results in unreasonably high volumetric strains and hence Mohr-Coulomb is typically used as a non-associated flow model. In general, the prediction using built-in Mohr-Coulomb is not satisfactory both for volume changes and pre-yield nonlinear behaviour.

### **3.5 NorSand Model**

NorSand is a generalized critical state model for soil based on the "state parameter" approach. It is an elasto-plastic critical state soil model first proposed by Jefferies (1993). It has associated plasticity but through the introduction of limited hardening, it simulates dilation similar to actual soil. Over the last 15 years, the NorSand model has been updated, primarily to incorporate varying critical image stress ratio,  $M_i$ , and to provide improved predictions under plane strain condition. The version of the NorSand presented here corresponds to the version given in Jefferies (1993).

It is claimed that, the NorSand was the first critical state soil model to realistically model sand. Unlike Cam-Clay, it predicts realistic dilatancy for dense sands (Jefferies and

Shuttle, 2005). Like Cam-Clay NorSand assumes normality, but NorSand also imposes a limit on the hardening of the yield surface which allows for more realistic prediction of dilatancy for dense soils.

A brief summary of NorSand model development is provided in the following sections. The NorSand has been developed based on two basic axioms: (i) a unique critical state exists, and (ii) soils move to the Critical State Line (CSL) with shear strain.

This is an idealized critical state model and with following four ideas (Shuttle and Jefferies, 2010):

1. There are infinite possible NCL in  $e$ - $\sigma_m$  space such that any yield surface does not necessarily intersect the CSL, with the position of the current yield surface in the  $e$ - $\sigma_m$  space being defined by  $\psi$ . Here,  $\sigma_m$  is the mean effective stress in three-dimensional stress space  $(\sigma_1 + \sigma_2 + \sigma_3)/3$ , which is equal to  $p'$  in triaxial condition. For convenience, all the effective stress components are presented without prime (') although author understands that in most of the geotechnical engineering textbook,  $\sigma$  is used for total stress and  $\sigma'$  for effective stress.
2. The state parameter  $\psi$  tends to zero as shear strain accumulates to a large value.
3. The minimum possible dilation rate (i.e. dilation at peak strength) is linearly related to  $\psi$ .
4. Principal stress rotation always softens (shrinks) the yield surface.

One of the main features of all versions of NorSand is that it has an infinity of normal consolidation lines (NCL) and not every yield surface is required to pass through the critical state which is a significant difference from Cam-Clay model. This behaviour was first reported by Tatsuoka and Ishihara (1974), from triaxial tests on Fuji River sand. They demonstrated that the normal consolidation line (NCL) for sands is not unique, instead being a function of density. Moreover, they showed that looser samples yield at higher deviator stress for a given mean effective stress. Jefferies and Been (2000) provided additional data to confirm this finding conducting tests on Erksak sand. The concept is illustrated in Figure 3-6. For every normal consolidation line there is a conjugate yield surface at each value of initial mean effective stress.

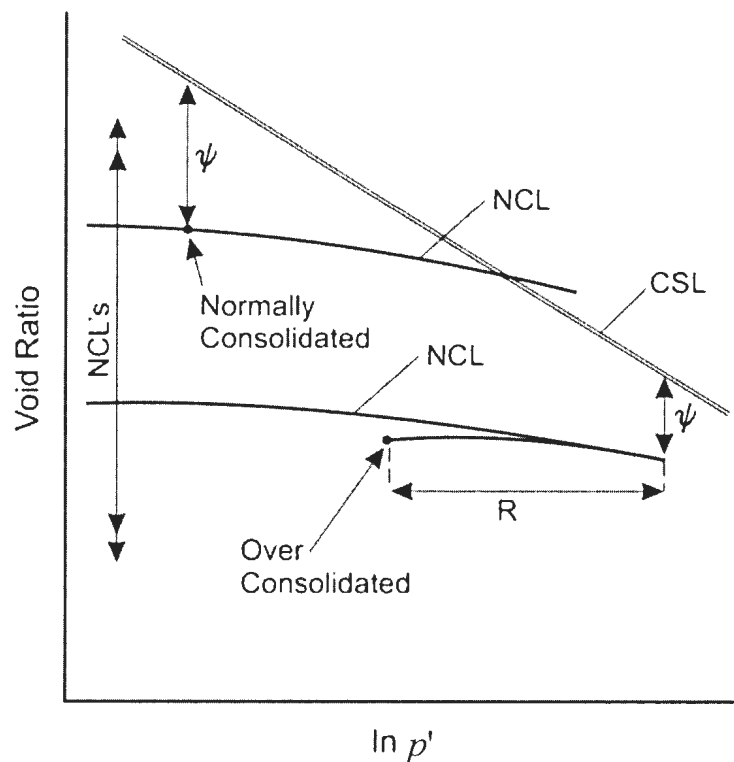


Figure 3-6: Typical CSL and NCL in  $e$ - $\ln p'$  plot

NorSand, in common with other plasticity models, comprises three items: (i) a yield surface; (ii) a flow rule, and (iii) a hardening law. These three items of the NorSand model are briefly discussed below. Further details are available in the articles by Jeffries and his co-workers (e.g. Jefferies, 1993 and 1997; Jefferies and Been, 2000; Jefferies and Shuttle, 2002; Shuttle and Jefferies, 2010).

Yield Surface and Flow Rule:

Although Cam-Clay model can successfully model soft clay in wet side, the dilatancy rule used in Cam-Clay does not match well with data obtained for sand especially dense sand. Based on experimental results, Nova (1982) proposed the following stress-dilatancy rule which has been used in NorSand model.

$$D^p = \frac{M - \eta}{1 - N} \quad (3.9)$$

The parameter  $N$  represents the volumetric coupling and its value varies between 0.2 and 0.4 (Nova 1982). The NorSand yield surface has the familiar bullet-like shape of the classical Cam Clay model but with one important addition. In triaxial condition the yield surface can be written as (Jefferies 1993):

$$\eta = \frac{M}{N} \left( 1 + (N - 1) \left( \frac{p}{p_i} \right)^{\frac{N}{N-1}} \right) \quad (3.10)$$

If  $N = 0$  the above equation becomes same as Cam-Clay model

$$\eta = M \left( 1 + \ln \left( \frac{p_t}{p} \right) \right) \quad (3.11)$$

The shape of the yield surface is a function of  $N$ . Yield surface hardening is constrained to match the computed maximum dilatancy to real sand behaviour. From experimental data, the maximum dilatancy has been found to be

$$D_{\max} = \chi \psi_i \quad (3.12)$$

Where  $\chi$  is a constant and the state parameter at image state is given by

$$\psi_i = \psi + \lambda \ln \left( \frac{p_t}{p} \right) \quad (3.13)$$

The maximum dilatancy is transformed to a 'limiting hardness' (a family of lines parallel to CSL in  $e$ - $\ln p$  space) and the yield surface is sized so that the dilatancy from normality matches reality.

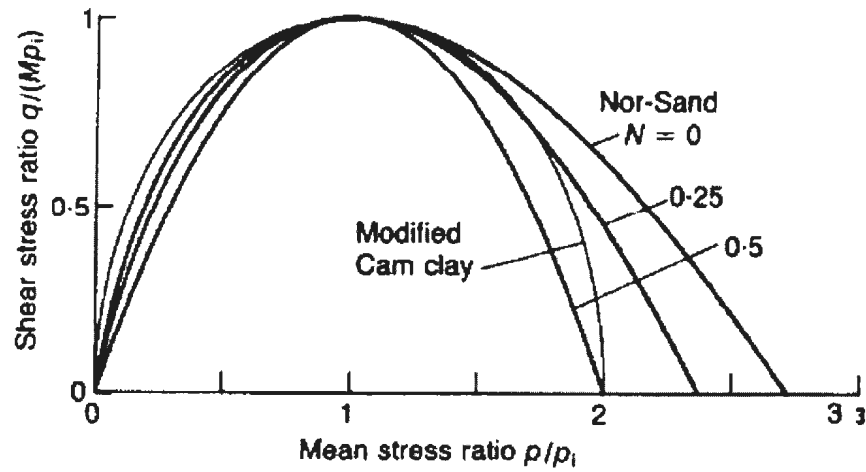


Figure 3-7: Yield surfaces in triaxial stress space (Jefferies, 1993)

Figure 3-7 shows the shape of the yield surface (Equation 3.10) as function  $N$ . As mentioned in previous sections that excessive dilation is one of the main limitations of the Mohr-Coulomb and dry side of Cam-Clay models. The plastic dilatancy  $D^p$  is determined from the idealized stress-dilatancy relation.

Hardening Law:

The third aspect of the model is the hardening law, which describes how the yield surface increases or decreases in size with plastic straining. Equations 3.14 and 3.15 describe a family of lines in  $e-\ln p$  space parallel to the CSL.

$$\left(\frac{p_i}{p}\right)_{max} = \left(1 + \frac{3.5\psi_i N}{M}\right)^{(N-1)/N}, \text{ if } N \neq 0 \quad (3.14)$$

$$\left(\frac{p_i}{p}\right)_{max} = \exp(-3.5\psi_i / M), \text{ if } N = 0 \quad (3.15)$$

A simple hardening rule that complies with the limited maximum hardness is a first order rate equation to bring the sand to its limiting hardness (Equation 3.16) or in an exponential rate equation (Equation 3.17):

$$\frac{\dot{p}_t}{\dot{\epsilon}_q} = H (p_{t,\max} - p_t) \quad (3.16)$$

$$\frac{\dot{p}_t}{\dot{\epsilon}_q} = H \exp^{(-\eta/M)} (p_{t,\max} - p_t) \quad (3.17)$$

where  $H$  is a proportionality constant and a new material property which can be compared to the role of  $1/\lambda$  in Cam-Clay. In the present NorSand UMAT, the exponential form (3.17) is used.

NorSand is an isotropic model hardening which expands or contracts the yield surface while retaining its shape. The current state parameter and the direction of loading controls whether the yield surface hardens or softens. The divergence of yield surface from critical state is used as the basis of the hardening law, and the hardening law acts to move the yield surface towards the critical state under the action of plastic shear strain – which directly captures the essence of critical state principles.

In summary, the NorSand model requires eight (8) input parameters that can be determined from laboratory test data. Two of them are critical state parameters, four

plasticity parameters, and two elasticity parameters. Table 3-1 shows the parameters required in NorSand model and their typical range.

**Table 3-1: Typical range of NorSand model parameters (Shuttle and Jefferies, 2010)**

<i>Property</i>	<i>Typical Range</i>	<i>Remark</i>
<i>CSL</i>		
$\Gamma$	0.9 – 1.4	'Altitude' of CSL, defined at 1 kPa
$\lambda$	0.01 – 0.07	Slope of CSL, defined on base e
<i>Plasticity</i>		
$M_{tc}$	1.2 – 1.5	Critical friction ratio, triaxial compression as reference condition
$N$	0.2 - 0.45	Volumetric coupling coefficient
$H$	50 – 500	Plastic hardening modulus for loading, often $f(\psi)$
$\chi_{tc}$	2.5 – 4.5	Relates minimum dilatancy to $\psi$ . Often taken as 3.5. Triaxial compression as reference condition
<i>Elasticity</i>		
$I_r$	100-800	Dimensionless shear rigidity
$\nu'$	0.1 – 0.3	Poisson's ratio, commonly 0.2 adopted

### 3.6 Advantages of NorSand in Modeling Soil/Pipeline Interaction

The concept of critical state (Roscoe et al., 1958) has been successfully applied to modeling the behaviour of cohesive soils. Because the behaviour of sand is somehow different from clay, some modification has been made later for modeling sand in critical state framework. Moreover, the Critical State Models like Cam-Clay or Modified Cam-Clay have some notable successes i.e. explaining the effect of void ratio on soil behaviour and effect of overconsolidation on clay strength. Unlike clay, for a particular  $\eta$ , sand does not possess a unique relationship between the void ratio  $e$  and  $p'$ . In fact, the density of a

typical sand in the pressure range before particle crushing cannot be altered considerably by a constant  $\eta$  compression, either isotropic ( $\eta = 0$ ) or anisotropic ( $\eta \neq 0$ ). Moreover, when the  $\eta$  of sand reaches its limiting value of  $M$  (the critical stress ratio) during plastic loading, it does not necessarily follow that the sand is at a critical state. The stress path can actually move along the  $\eta = M$  line, as for example in an undrained dilative shear path up to ultimate failure. These differences suggest that the well-established framework for clay modeling should not be directly used for sand modeling. NorSand has few parameters, most of which are familiar. The unfamiliar parameters are easily understood and measured. It really does not need much more effort than a Mohr Coulomb model (Shuttle and Jefferies, 2010).

For numerical modelling of sand, Mohr-Coulomb model is commonly used. However one might also want to use Cam-Clay model. Some key features of NorSand comparing with other constitutive models are given below, which should be considered in soil/pipeline interaction analyses:

- The basic problem is neither Cam-Clay nor the Modified Cam-Clay dilate anything like dense sand. NorSand can model dilation behavior of sand.
- Existing Cam-clay models fail to predict observed softening of dense sands properly.
- Like Cam-Clay, NorSand assumes normality but NorSand also imposes a limit on the hardening of the yield surface which allows more realistic prediction of dilatancy for dense soils.

- A significant difference from Cam-Clay is that NorSand has infinity of Normally Consolidation Lines (NCL) and not every yield surface is required to pass through the critical state. This behaviour was first reported by Tatsuoka and Ishihara (1974) from triaxial tests on fuji river sand, who demonstrated that NCL for sands are not unique, instead being a function of density.
- The hardening of the yield surface cannot be uniquely controlled by void ratio and the slopes of the NCL and the swelling line as for Original Cam-Clay (OCC) model or Modified Cam-Clay (MCC) model. In NorSand hardening is related to the plastic shear strain.
- To get the representative predictions for dense sand in the original and Modified Cam-Clay models, a high overconsolidation Ratio (OCR) must be used even if the sand is normally consolidated. In NorSand, the 'intrinsic state' of soil is separated from over consolidation and there is no need to assign an OCR to properly model dense normally consolidated sand (Jefferies, 1993).
- Mohr-Coulomb model cannot predict the softening behaviour whereas, NorSand realistically simulates softening behaviour.
- Constant dilation angle is generally used in Mohr-Coulomb model whereas in NorSand, the dilation angle changes with plastic deformation. Note that some researchers (e.g. Popescu et al., 2002) implemented the variation of dilation angle as a function of plastic shear strain.

## Chapter 4

### FINITE ELEMENT ANALYSES WITH MOHR-COULOMB SOIL CONSTITUTIVE MODEL

#### 4.1 General

The Finite Element software package ABAQUS/Standard 6.10 EF1 is used to simulate the pipeline/soil interaction both in two- and three-dimensional conditions. Comparison of numerical results with actual experiments is necessary to validate the numerical model. The model tests conducted at Cornell University (Trautmann and O'Rourke, 1983) are used for the numerical validation. Two soil constitutive models used in this study are Mohr-Coulomb model and NorSand soil constitutive model. In this chapter, the performance of Mohr-Coulomb model is presented. The performance of NorSand model is discussed in Chapter 5.

#### 4.2 Model Tests at Cornell University

A number of large-scale tests were performed at Cornell University to understand the soil/pipe interaction behaviour subjected to lateral and vertical loading (Trautmann and O'Rourke, 1983). The two-dimensional view of the experimental setup is shown in Fig. 4-1. The tests were performed in a tank of 1.2 m width, 2.3 m long and 1.2 m depth. Different types of fluvio-glacial sand having similar, but not identical, grain size characteristics (Olson, 2009), referred to as CU filter sand were used in the tests. To show the capability and limitations of the present FE analysis models, benchmark analyses have

been performed to simulate these tests using the same test conditions and same geotechnical properties of the soil used in the tests.

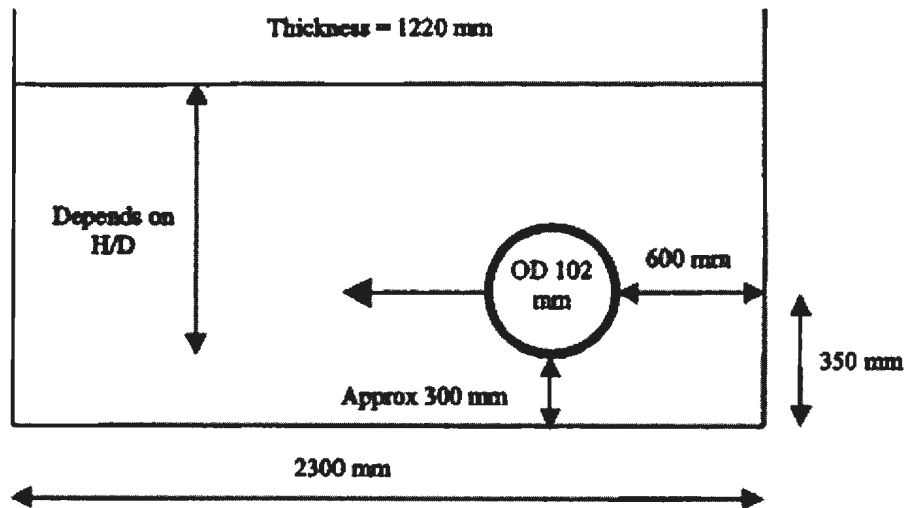


Figure 4-1: Two-dimensional view of experimental setup (Trautmann and O'Rourke, 1983)

The Cornell University (CU) filter sand has a coefficient of uniformity  $C_u$  of 2.6 and an effective grain size  $D_{10}$  of 0.2 mm. The tests were conducted in dry soil beds of three different relative densities having dry unit weight of  $14.8 \text{ kN/m}^3$  for loose,  $16.4 \text{ kN/m}^3$  for medium and  $17.7 \text{ kN/m}^3$  for dense sand, which corresponded to the relative density of 0, 45, and 80%, respectively. In practice, the sand around the pipeline is often compacted and could be in the state of medium to dense conditions. Hence, the tests in medium and dense cases are simulated in the present study. A 102 mm pipe with a wall thickness of 6.4 mm fabricated from ASTM Grade A-36 steel was used in model tests. The pipe was of welded seam, hot rolled construction and had rough, scaley surfaces with minor rust patches.

Geotechnical parameters for CU filter sand were obtained from the direct shear tests performed by Trautmann (1983). Tests were performed in 60 mm by 60 mm direct shear testing apparatus, using 50 mm thick specimens and a displacement rate of 0.56 mm/min. The relationship between the normal stress and shear stress at the peak is shown in Figure 4-2. As shown the angle of internal friction at the peak is  $42^\circ$  for dense sand while it is  $33^\circ$  for medium sand. Note that, these densities are slightly lower than the densities used in pipe loading tests, and therefore the peak of  $44^\circ$  for dense and  $35^\circ$  for medium sand are used in finite element analyses in the present study.

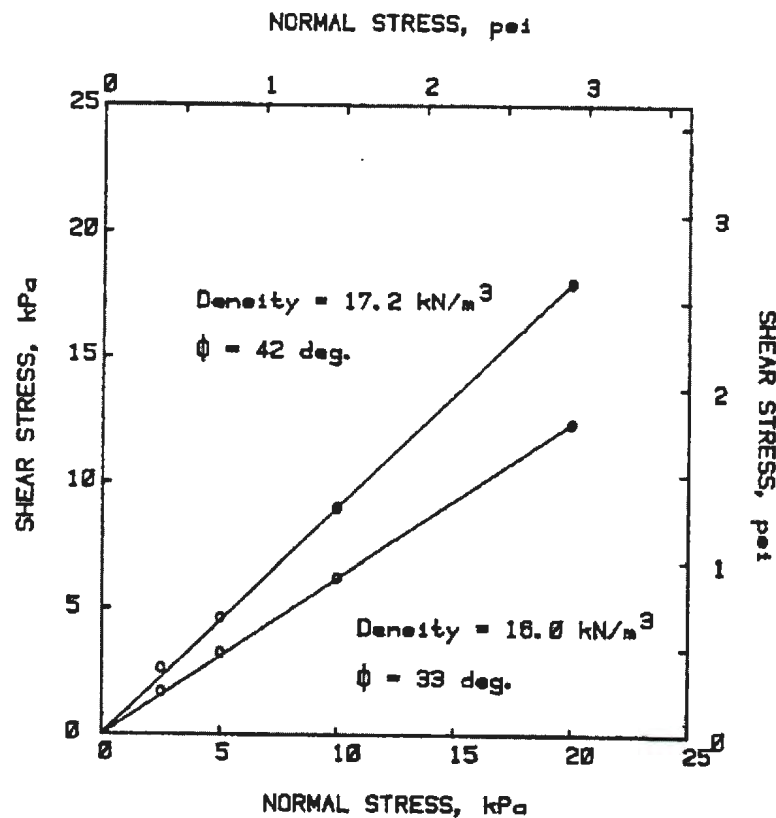


Figure 4-2: Relationship between normal stress and shear stress at the peak of Cornell University (CU) filter sand (Trautmann, 1983)

Pipe loading tests were conducted in several conditions varying the depth of embedment of the pipe and soil density. Experimental results were converted to dimensionless form to facilitate the comparison of experimental and analytical results. The dimensionless format also facilitates the application of the results to a wide variety of pipe diameter and depth of practical interest.

Figures 4-3 to 4-5 show the force-displacement curves for lateral loading obtained by Trautmann (1983) for loose, medium and dense sand, respectively. The vertical axis in this figure show the normalized lateral resistance  $F/(\gamma D H L)$ , where  $F$  is the measured lateral force,  $\gamma$  is the dry unit weight of the sand,  $H$  is the depth from the top of the soil to the base of the pipe for lateral movement which is denoted as  $H_b$  in the present study in order to avoid any confusion with depth of embedment used for vertical pipe loading,  $D$  is the external diameter of the pipe, and  $L$  is the length of the pipe involved in the test. The horizontal axis is the dimensionless pipe displacement expressed as  $Y/D$  which will be denoted as  $\delta_l/D$  for present analyses in which  $\delta_l$  is the measured lateral pipe movement. The arrows in these figures show the location of maximum load, which were used for further analyses of test data.

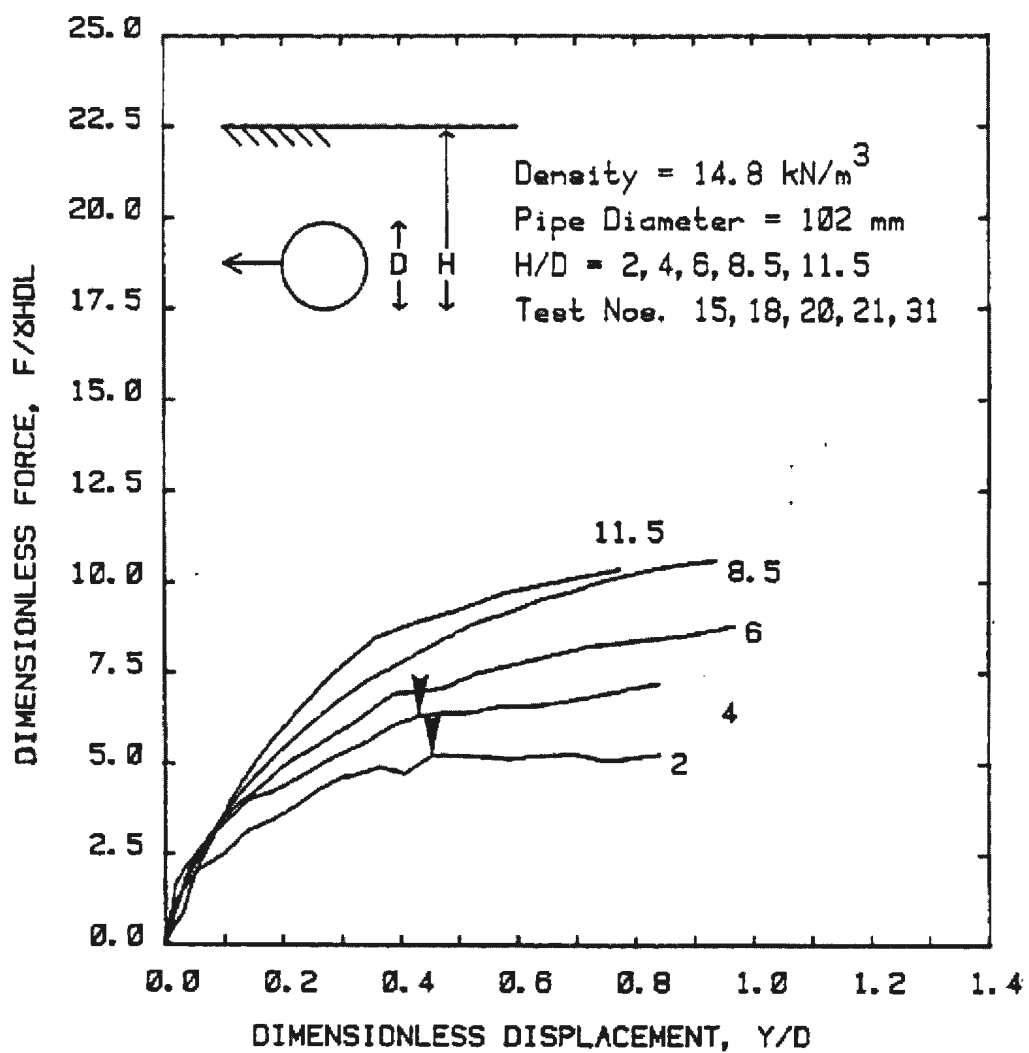


Figure 4-3: Force-displacement curve of lateral pipe tests in loose sand (Trautmann, 1983)

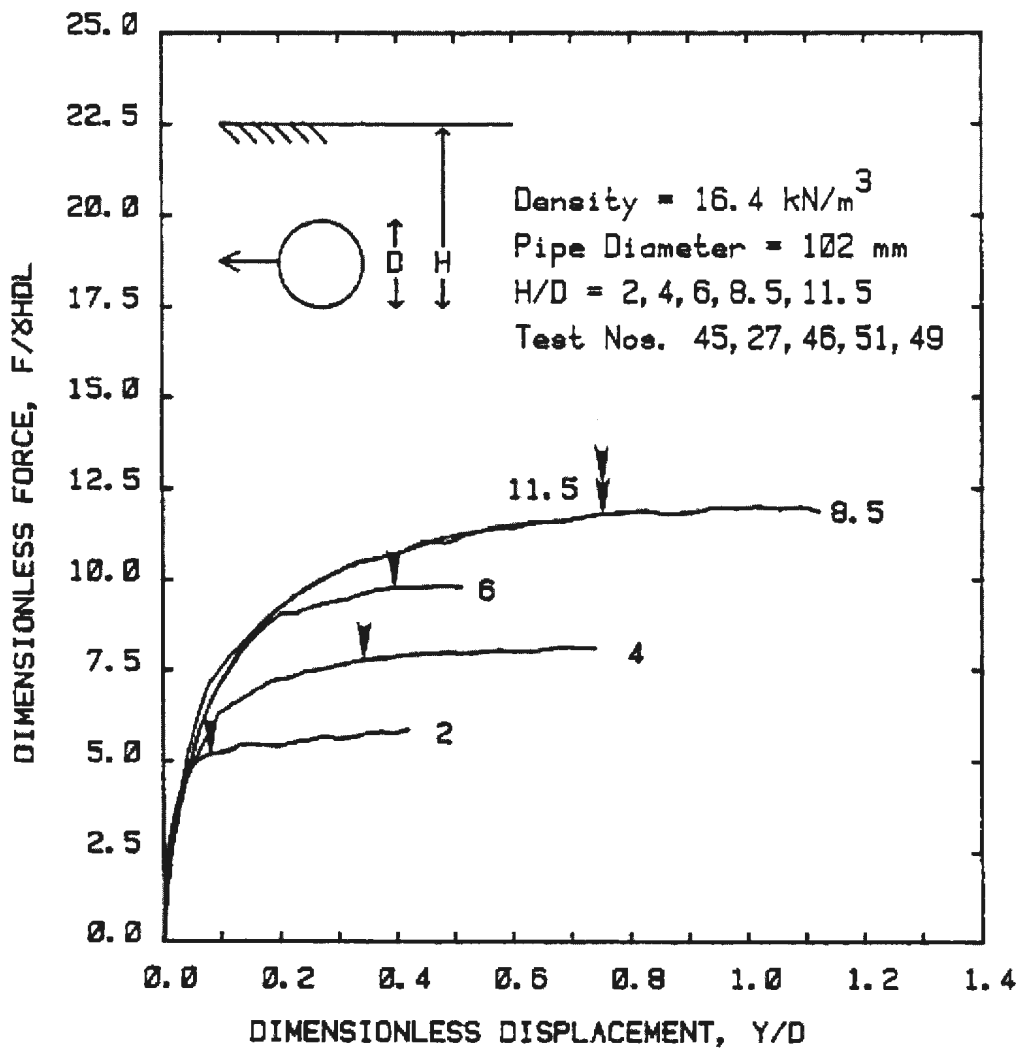


Figure 4-4: Force-displacement curve of lateral pipe tests in medium sand (Trautmann, 1983)

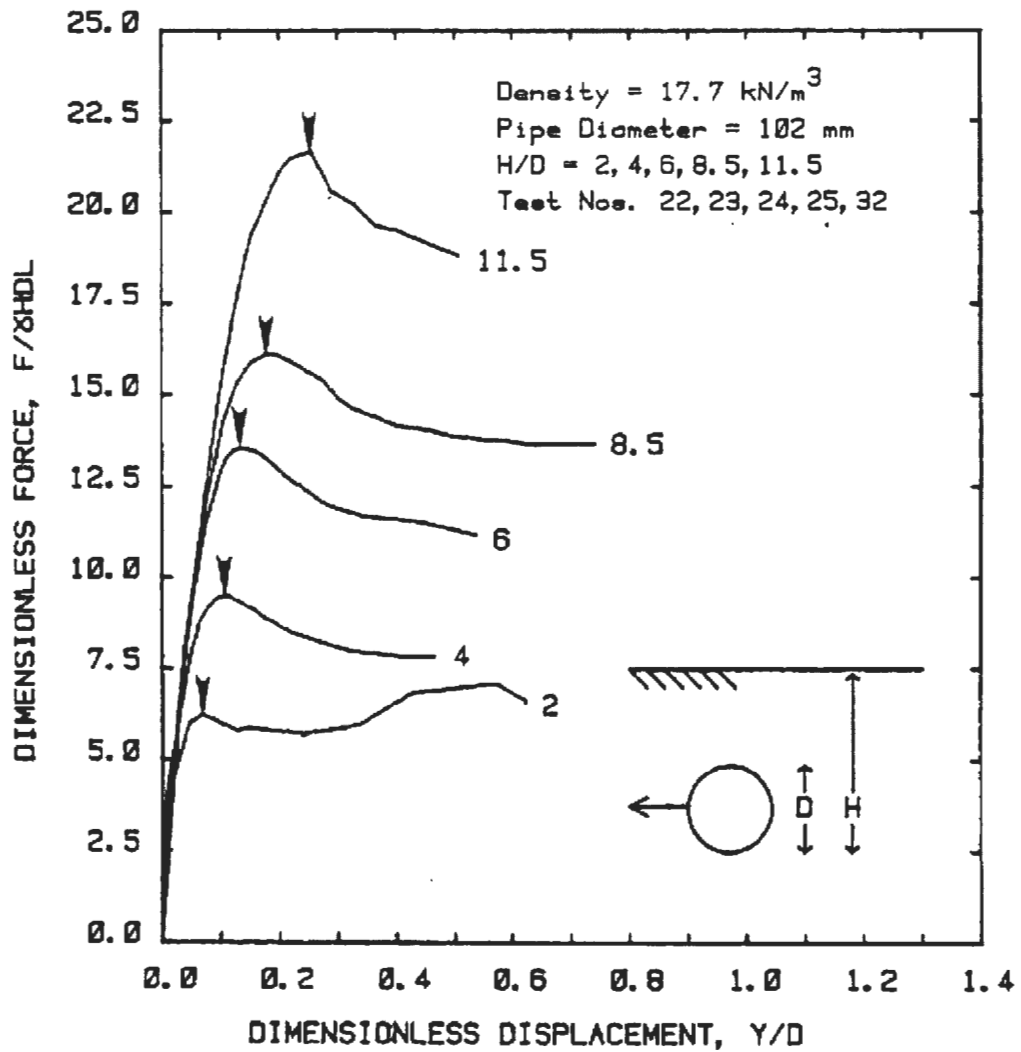


Figure 4-5: Force-displacement curve of lateral pipe tests in dense sand (Trautmann, 1983)

As shown in Figures. 4-3 and 4-4, for loose and medium sand, the dimensionless force gradually increases with displacement. However, for dense sand (Figure. 4-5), the dimensionless force reached to the peak after some displacement and then decreased. The peak force is the one of the most important factors that should be evaluated properly using appropriate soil constitutive model.

Figures 4-6 to 4-8 show the force-displacement curves for vertical loading obtained by Trautmann (1983) for loose, medium and dense sand, respectively. The parameter  $F$  in the vertical axis represents the measured vertical force and  $H_c$  is the depth from the top of the soil to the center of the pipe before the start of upward movement. In the horizontal axis,  $Z$  is the measured as upward pipe movement which will be denoted as  $\delta_u$  in the present study.

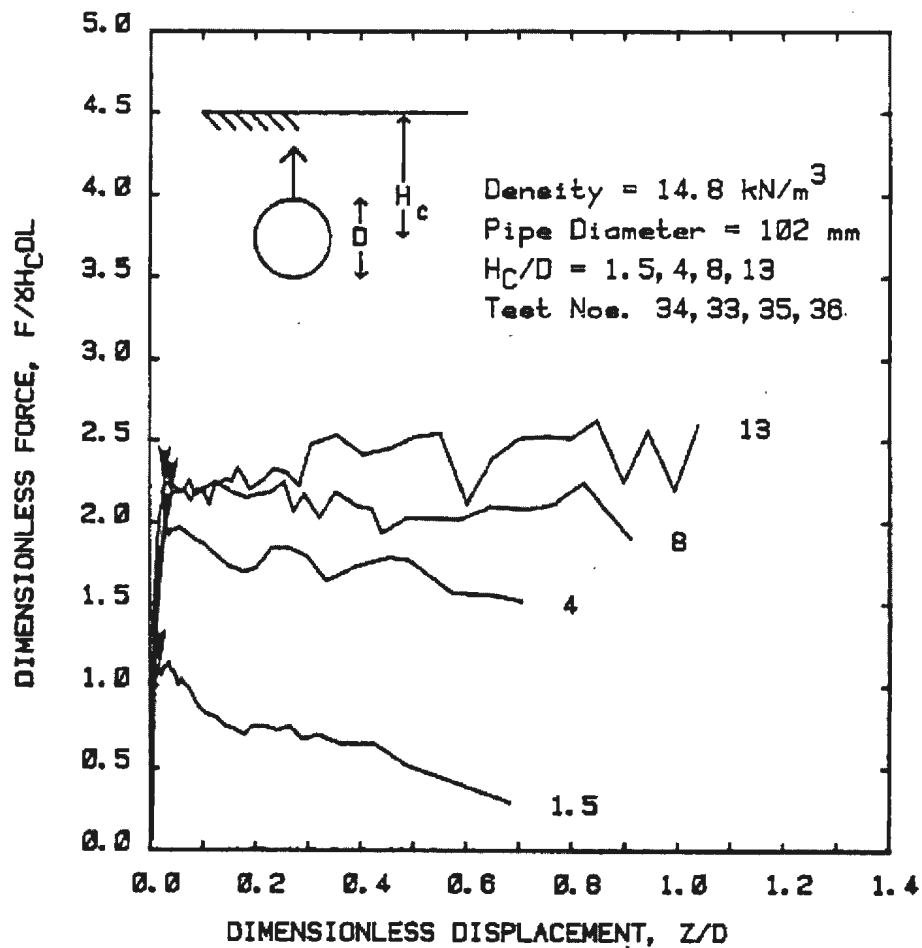


Figure 4-6: Force-displacement curves for uplift tests on buried pipe in loose sand (Trautmann, 1983)

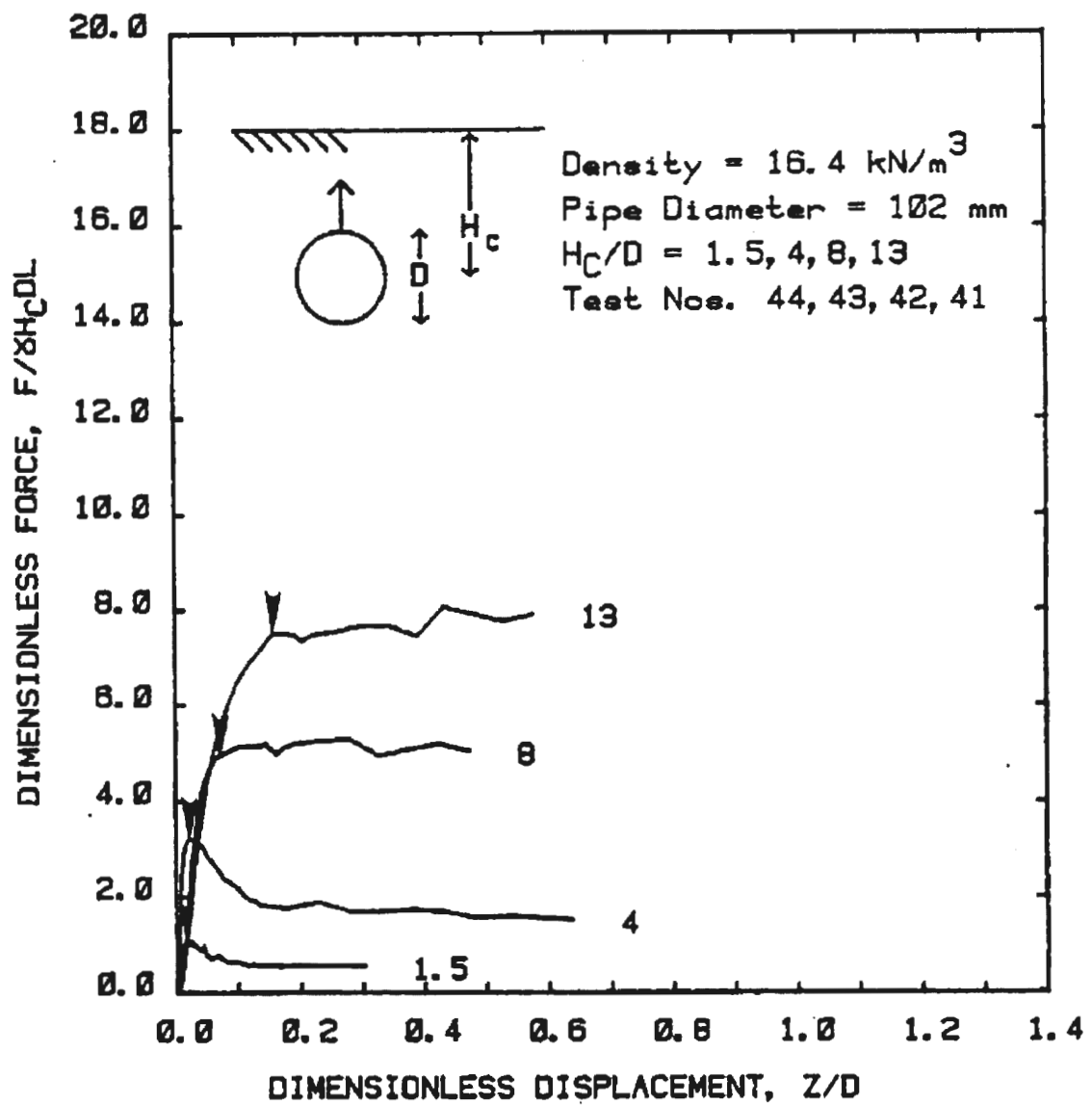


Figure 4-7: Force-displacement curves for uplift tests on buried pipe in medium sand (Trautmann, 1983)

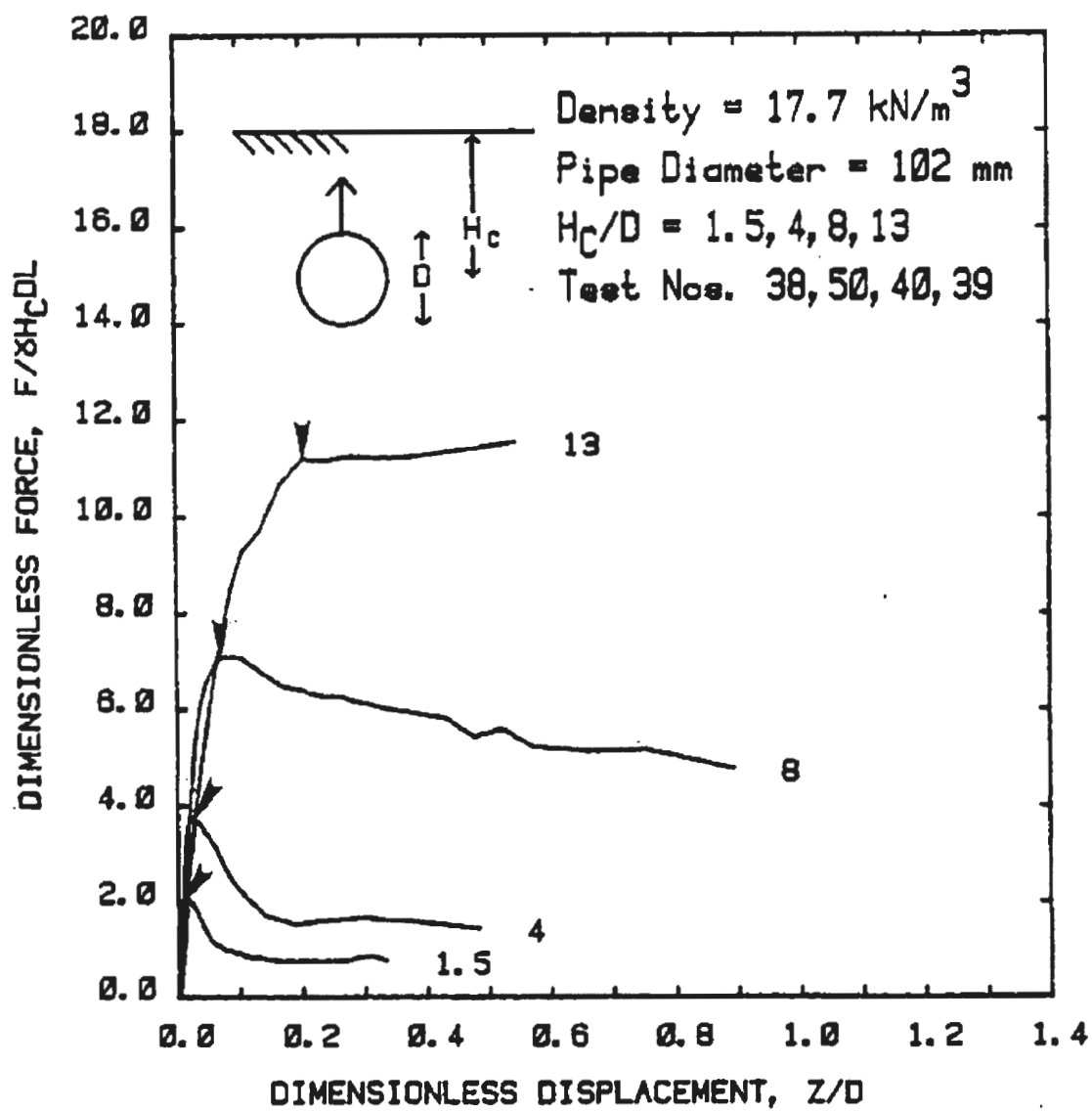


Figure 4-8: Force-displacement curves for uplift tests on buried pipe in dense sand (Trautmann, 1983)

As shown in Figures. 4-6 to 4-8, the shape of the force-displacement curve for upward loading is also highly dependent upon the depth of embedment. For example, a shallowly

embedded pipe in loose sand at  $H_c/D=1.5$  shows a significant reduction in normalized force after the peak. Moreover, for a given depth of embedment, for example  $H_c/D=4$ , the post-peak reduction of dimensionless force is more in dense sand as shown in Figure 4-8. Proper modeling of soil/pipe interaction behaviour should be able to capture this behaviour.

### 4.3 Finite Element Modeling

Numerical analyses in this study started with two-dimensional finite element simulation of lateral loading of above experiment (Trautmann and O'Rourke, 1983). Figure 4-9 shows the dimensions of the soil domain and typical finite element mesh used in the two-dimensional analyses.

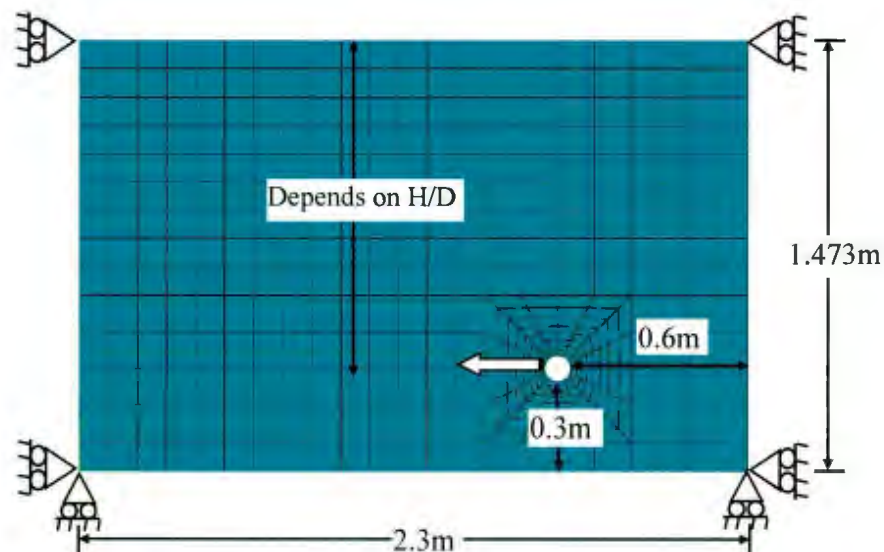


Figure 4-9: Structured meshing in ABAQUS

The dimensions are similar to the large-scale experiments (Figure 4-1) conducted by Trautmann and O'Rourke (1983). By simplifying the soil and pipeline as a two-dimensional plane strain system, the soil is discretized by 8-node biquadratic plane strain quadrilateral, reduced integration element, CPE8R. Reduced integration (i.e., four-point integration) for soil elements is used to improve the efficiency of computation. According to Bathe and Wilson (1976), four-point integration is generally the optimum integration order for eight-node rectangular elements. In order to prevent the spurious zero-strain modes, ABAQUS employs the reduced integration rule together with hourglass stiffness control to formulate the element stiffness matrix (HKS Inc. 2000). The bottom of the model (Figure 4-9) is restrained from any vertical movement, while all the vertical faces are restrained from any lateral movement using roller supports. No displacement boundary condition is applied on the top face, and the soil can move freely. A pipe is placed at the desired location. The depth of the pipe is measured in terms of  $H/D$  ratio, where  $H$  is the depth from the top of the soil to the center of the pipe for upward movement denoted as  $H_c$  or depth from the top of the soil to the base of the pipe for lateral movement denoted as  $H_b$  and  $D$  is the external diameter of the pipe. The values of  $H/D$  used in these analyses are 2.0 and 11.5 (for lateral movement) and 4.0 and 13.0 (for upward movement).

#### **4.3.1 Pipe/soil Interface**

The interface between pipe and soil is simulated using the contact surface approach available in ABAQUS/Standard. This approach allows the separation and sliding of finite amplitude and arbitrary rotation of the contact surfaces. The Coulomb friction model is

used for the frictional interface between the outer surface of the pipe and sand. In this method, the friction coefficient ( $\mu$ ) is defined as  $\mu = \tan(\phi_\mu)$ , where  $\phi_\mu$  is the pipe/soil interface friction angle. The pipe/soil interface friction angle,  $\phi_\mu$  depends on the interface characteristics and the degree of relative movement between the pipe and soil. The larger value of  $\phi_\mu$  indicates the characteristics of rough uncoated pipes with rusty or corroded surfaces and the lower values would correspond to pipes with smooth coating. The value of  $\phi_\mu$  varies between  $\phi'$  and  $\phi'/2$  (Yimsiri et al, 2004). A value of  $\mu=0.32$  is used in this study.

#### **4.3.2 Loading**

The numerical analysis is conducted in two main steps. The first step is a geostatic stress step that accounts for the effects of soil weight and defines the initial stress state in the soil. In the second step, the pipe is moved in the desired direction specifying a displacement boundary condition at the every node of the pipe.

#### **4.3.3 Soil Properties**

Clean, subangular, fluvio-glacial sand was used in model tests (Trautmann and O'Rourke, 1983). The sand has uniformity coefficient 2.6 and effective grain size 0.2 mm. The minimum and maximum dry unit weights are  $15.5 \text{ kN/m}^3$  and  $18.3 \text{ kN/m}^3$ , respectively. In this study, the tests in medium and dense soil conditions are simulated as the soil around the pipeline in the field is generally compacted. The tests simulated in this research were conducted in dry sand with unit weight of  $16.4 \text{ kN/m}^3$  and  $17.7 \text{ kN/m}^3$ , which gives relative density of 45% and 81% respectively.

As mentioned before, two soil constitutive models used in this study are Mohr-Coulomb model and NorSand soil constitutive model. In this chapter, the performance of Mohr-Coulomb model is shown first and Chapter 5 includes the performance of NorSand model.

The Mohr-Coulomb plasticity model is a built-in model in ABAQUS/Standard finite element software for modeling geomaterials. The input parameters required in Mohr-Coulomb model are: Young's Modulus ( $E$ ), Poisson's ratio ( $\nu$ ), angle of internal friction ( $\phi'$ ), dilation angle ( $\psi_m$ ) and unit weight of soil ( $\gamma$ ). The elastic modulus  $E$  can be determined from the unload-reload parts of drained triaxial tests data or from empirical relationships. In this study two finite element modeling is done for medium and dense soil. The values of  $E$  for medium and dense sands are estimated from test data presented by Turner and Kulhawy (1987). The Poisson's ratio of 0.2 is the best representative values of medium and dense sand (Jefferies and Been, 2006). The peak friction angle  $\phi'_{\text{peak}}$  and dilation angle  $\psi_m$  are derived from the direct shear test data presented by Trautmann, 1983. The dilation angle was estimated based on  $\phi'_{\text{peak}} = \phi'_{\text{critical}} + 0.8\psi_m$  given by Bolton (1986). The value of  $\phi'_{\text{critical}} = 31^\circ$  is used. Table 4-1 shows the values of the parameters used in finite element analyses.

Table 4-1: Geometry and Parameters used in finite element analyses

Parameter	Values	
<u>Pipe:</u>		
External Diameter, $D$	0.102 m	
Thickness, $t$	0.0064 m	
Elastic Modulus, $E_{\text{pipe}}$	$2.04 \times 10^8$ kN/m <sup>2</sup>	
Poisson's Ratio, $\nu_{\text{pipe}}$	0.3	
<u>Soil:</u>	Medium sand	Dense sand
Elastic Modulus, $E$	2950 kN/m <sup>2</sup>	3650 kN/m <sup>2</sup>
Poisson's Ratio, $\nu_{\text{soil}}$	0.2	
Critical State Friction Angle, $\phi'_{\text{critical}}$	31°	31°
Friction Angle, $\phi'$	35°	44°
Dilation Angle, $\psi_m$	5°	16°
Unit weight, $\gamma$	16.4 kN/m <sup>3</sup>	17.7 kN/m <sup>3</sup>
Interface Friction co-efficient, $\mu$	0.32	
Depth of pipe, $H/D$	2 and 11.5 (for pure lateral), 4 and 13 (for pure upward)	

#### 4.4 Mesh Sensitivity and Boundary Effects

The size and distribution of mesh have significant effects on numerical prediction. In addition, the locations of the boundaries are equally important for successful modeling. In this section these effects are shown.

#### **4.4.1 Mesh sensitivity**

In this study, ABAQUS CAE is used to generate finite element mesh. Once the soil domain is defined, auto generated default meshing option might be used to form the mesh. When it is used, the typical finite element mesh formed are shown in Figure 4-10. As shown in this figure that the mesh formed in this option is not in regular pattern. However, for better modeling, it is expected to have a structured mesh with denser elements near the pipe. Structured mesh has been generated in this study by zoning the soil domain using “bias” option available in ABAQUS. Typical structured mesh generated in this study is shown in Figure 4-9.

A mesh sensitivity study is performed first to select the appropriate mesh size and distribution for two-dimensional analyses. Starting with default meshing with ABAQUS and the parameters shown in Table 4-1, analyses have been performed with structured meshing shown in Figure 4-9 with different element numbers. Very little difference in peak pipe force is obtained if the mesh generation changed from the default to structured meshing system. However, the success with structured mesh without any numerical issue is higher than auto generated mesh. Moreover, the total number of element cannot be controlled in the auto generated default meshing in ABAQUS, which can be easily done in the structured meshing system. The structured meshing is very efficient with less numerical issues as the element shapes are regular than the auto generated default meshing. Therefore, the structured meshing is selected for further analyses to obtain good results and promote computational efficiency.

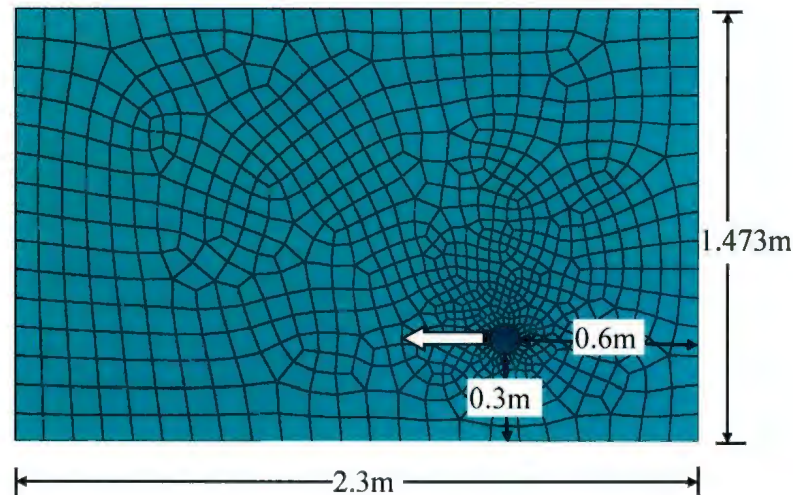


**Figure 4-10: Default meshing in ABAQUS**

#### **4.4.2 Boundary Effect**

Another critical issue that needs to be checked is the location of the bottom and right boundaries with respect to the location of the pipe. One might think that the bottom and right side of the tank is close to the pipe and might have some effect on load-displacement behaviour. In order to check the effects of bottom and right boundaries, which are relatively close to the pipe, analyses have also been performed with a larger soil domain where the bottom and right boundaries respectively are at 0.8 m and 1.1 m from the pipe (Figure 4-11). Very little difference in calculated lateral resistance using these two different soil domains (Figure 4-12) indicates that the dimensions of the soil domains shown in Figure 4-10 are sufficiently large and therefore boundary effects are not expected on predicted lateral resistance, displacement and failure mechanisms. Therefore, in the following section analyses are done using finite element mesh shown in Figure 4-9.

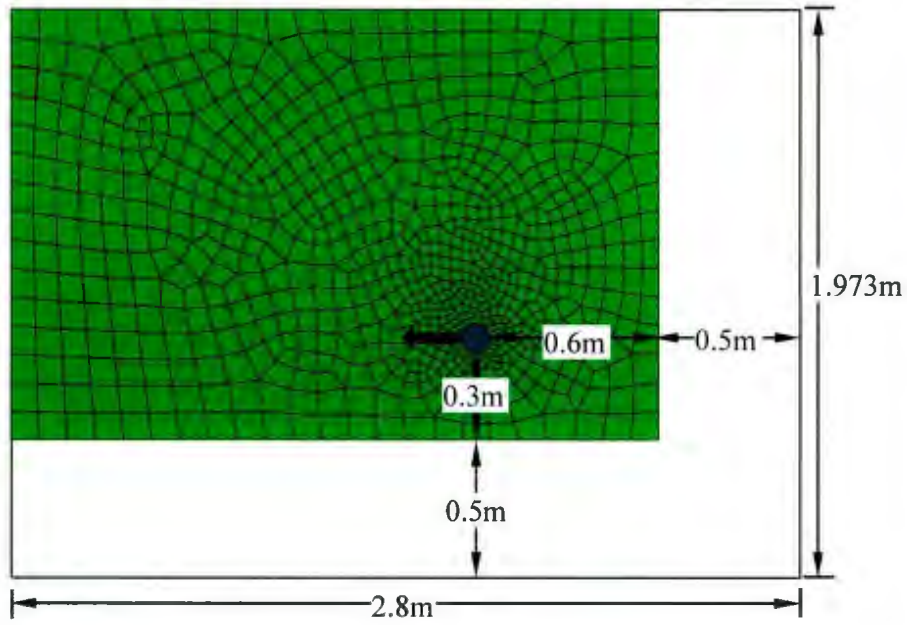


Figure 4-11: Location of right and bottom boundaries

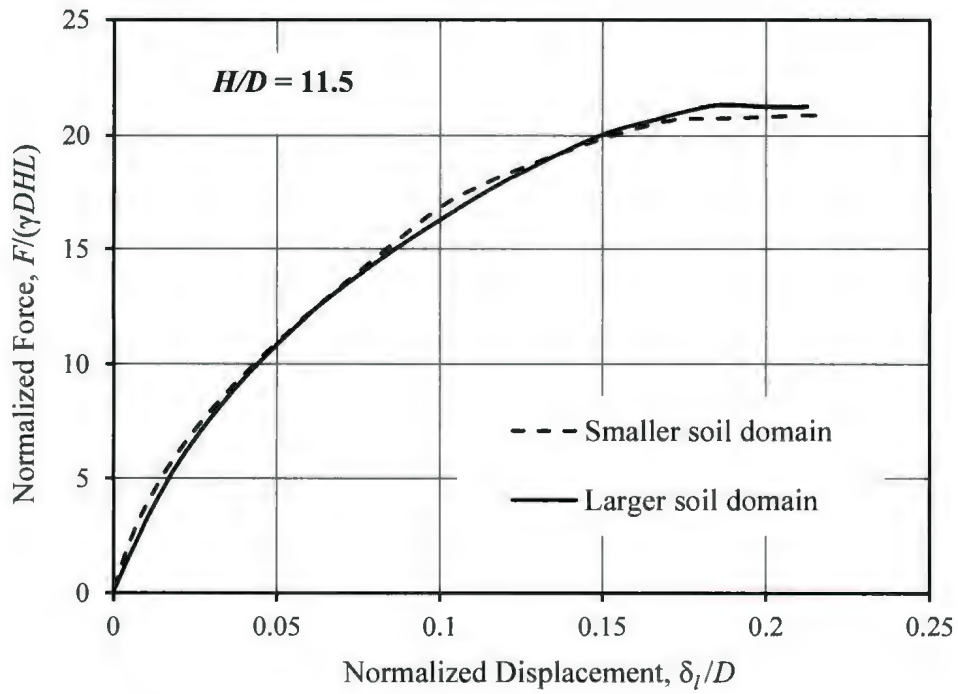


Figure 4-12: Bottom and right boundary effects in 2D analysis

#### 4.5 Geostatic Loading Step

Finite element analyses are performed for varying  $H_b/D$  and density of the soil (medium and dense sand). The parameters used in these analyses are shown in Table 4-1. For lateral pipe movement, two  $H_b/D$  ratio of 2 and 11.5 were taken. The initial stress or the geostatic stress step definition is very important for numerical analyses. The stress values and the stress contours at the geostatic step were checked carefully before going for further analysis. It is to be noted here that even if the initial stresses is not specified properly the analysis might get through the geostatic step, but might have error or give inaccurate results in the subsequent loading step. Also there would be higher soil displacements at this stage as ABAQUS attempts to bring it in an equilibrium condition. In this study, the initial condition of stress is given which is closed to the *in situ* stress condition. Then the geostatic step is applied. The following checks after the geostatic step are done.

- The vertical stress (S22 in 2-D and S33 in 3-D) after geostatic step is closer (or equal) to what is defined the 'initial conditions' and also the contours of this stress are parallel.
- The soil displacements (U2 in 2-D and U3 in 3-D) after geostatic step are very small.

Figure 4-13 shows the typical vertical stress contours after geostatic step. Figure 4-13 (a) is for shallow embedment ( $H_b/D=2$ ) of pipe in medium sand, and Fig. 4-13(b) is for deep burial condition ( $H_b/D=11.5$ ) of pipe in dense sand. As shown in these figures, the vertical stress contours after geostatic stress step are parallel and the value of stress is

same as *in situ* stress. Although it is not shown here, the vertical displacements after the geostatic step is very negligible ( $<10^{-6}$  m). That means the analyses in the geostatic step have been completed successfully.

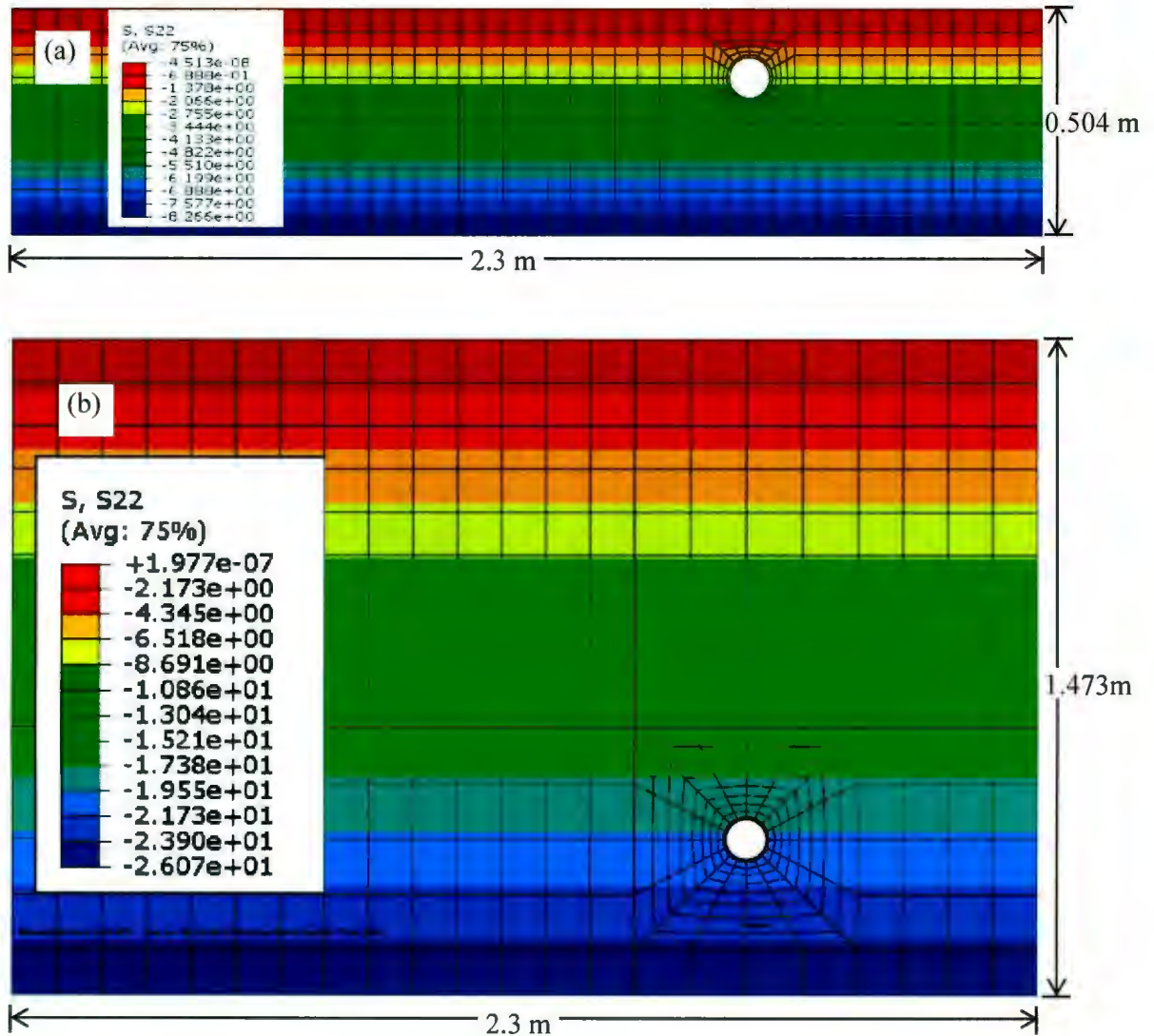


Figure 4-13: Geostatic loading (a) for analysis with medium dense sand for  $H_v/D = 2$  (b) for analysis with dense sand for  $H_v/D = 11.5$ .

#### 4.6 Pure Lateral Loading

A two-dimensional finite element model is developed for lateral loading of pipe with geometry exactly similar to the experimental setup used by Trautmann (1983) as shown in Figure 4-1. Although the test setup is three-dimensional, the analysis presented in this section is in two-dimensional plane strain condition. The ratio of the pipe diameter to the pipe wall thickness is selected as  $D/t = 16$ . The analyses are performed for one shallow ( $H_b/D=2$ ) and one deep ( $H_b/D=11.5$ ) burial condition. In both cases the bottom of the pipe is at 300 mm above the floor of the tank (Figure 4-1). Similar to the experimental setup the pipe is placed at 600 mm left from the right wall of the tank and is moved laterally to the left until sufficient post-peak load-displacement response is observed. The Mohr-Coulomb model implemented in ABAQUS requires a non-zero cohesion to avoid numerical issue. The cohesion value of  $1.0 \text{ kN/m}^2$  is used in this study.

Figure 4-14(a) and Figure 4-14(b) show the comparison between the experimental and numerical results for shallow burial conditions ( $H_b/D=2$ ) with medium ( $\gamma = 16.4 \text{ kN/m}^3$ ) and dense sand ( $\gamma = 17.7 \text{ kN/m}^3$ ). Figure 4-15(a) and 4-15(b) show the similar comparison for deep burial conditions ( $H_b/D=11.5$ ). As shown, the peak resistance obtained from numerical analyses is reasonably matched with experimental results. However, the post-peak behaviour such as the post-peak softening could not be modeled properly using the Mohr-Coulomb soil model. Also the force displacement curve obtained from the numerical analysis does not match well with experimental results for  $H_b/D=11.5$ .

Although the modulus of elasticity for sand has been selected from experimental observation, the force-displacement curve in Figure 4-15(b) shows that a higher modulus of elasticity of sand than the value selected here might give better comparison with test results. Finite element results with a higher value of  $E$  ( $=11,000 \text{ kN/m}^2$ ) is also shown in Figure 4-15(b), which gives a closer result with test data.

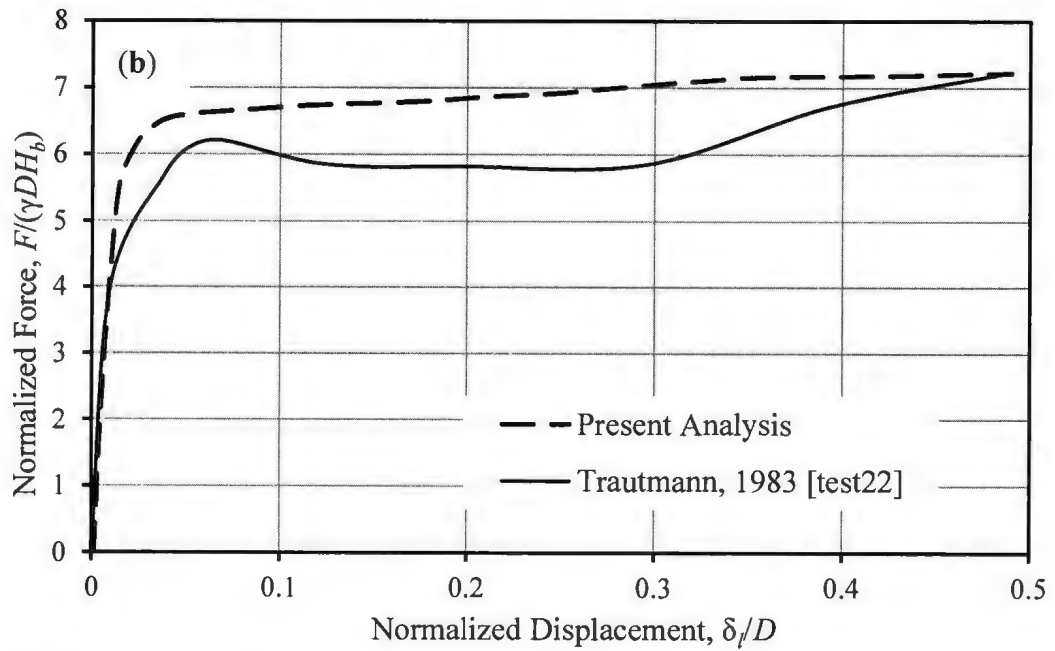
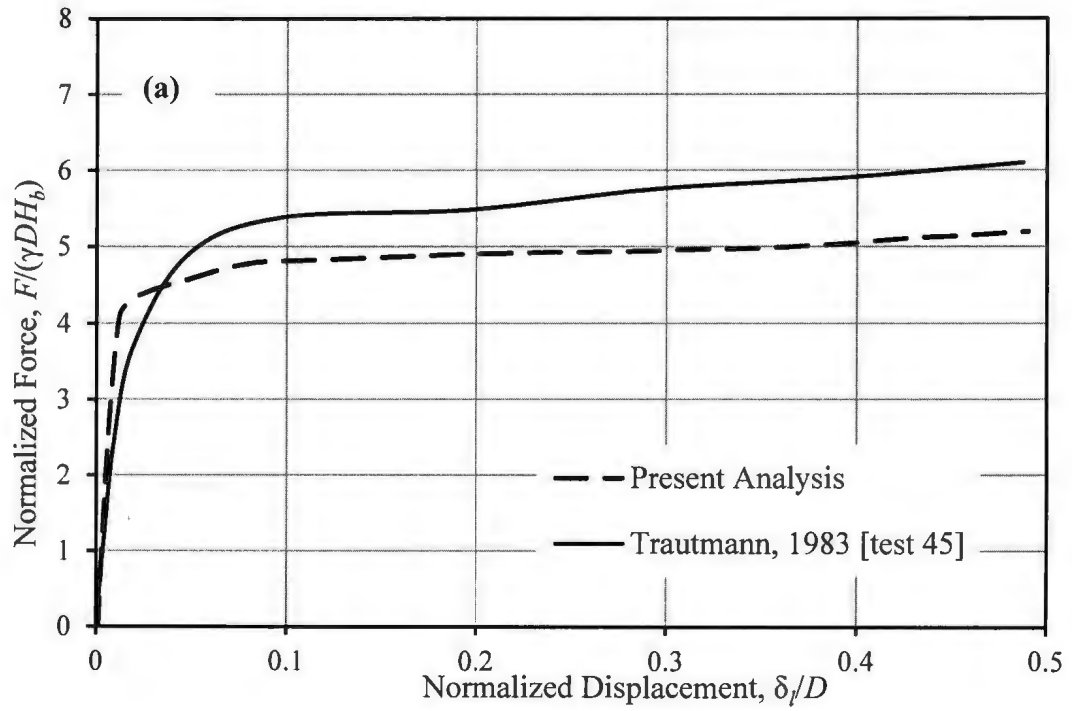


Figure 4-14: Normalized force-displacement curve for lateral loading in (a) Medium dense sand with  $H_v/D = 2$  and (b) Dense sand with  $H_v/D = 2$

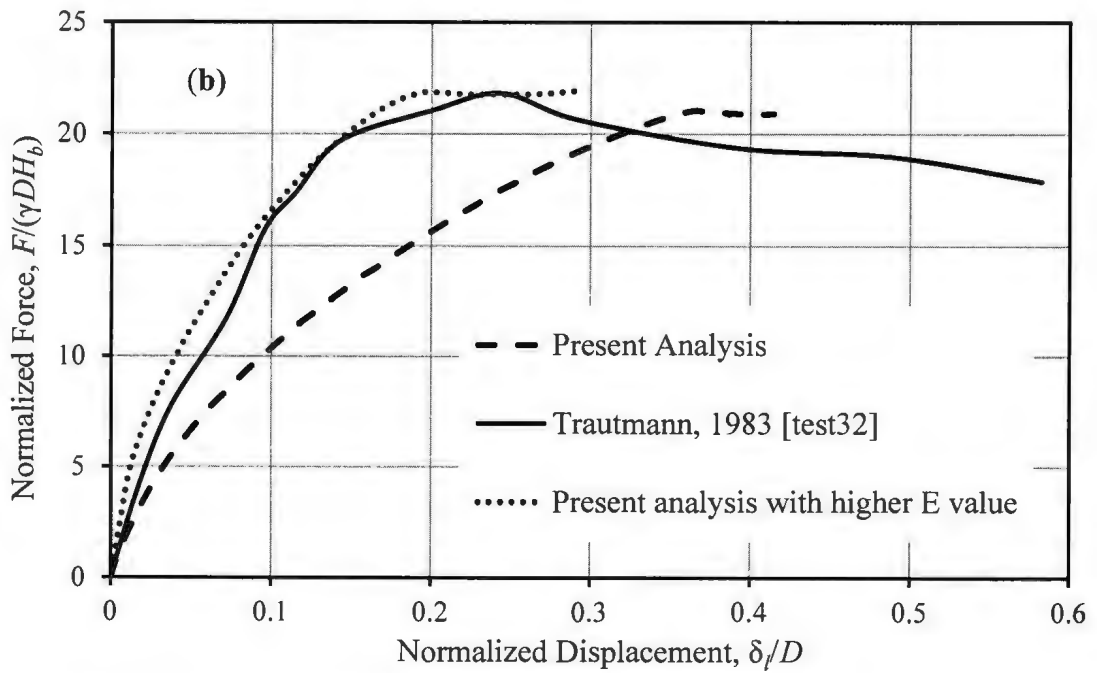
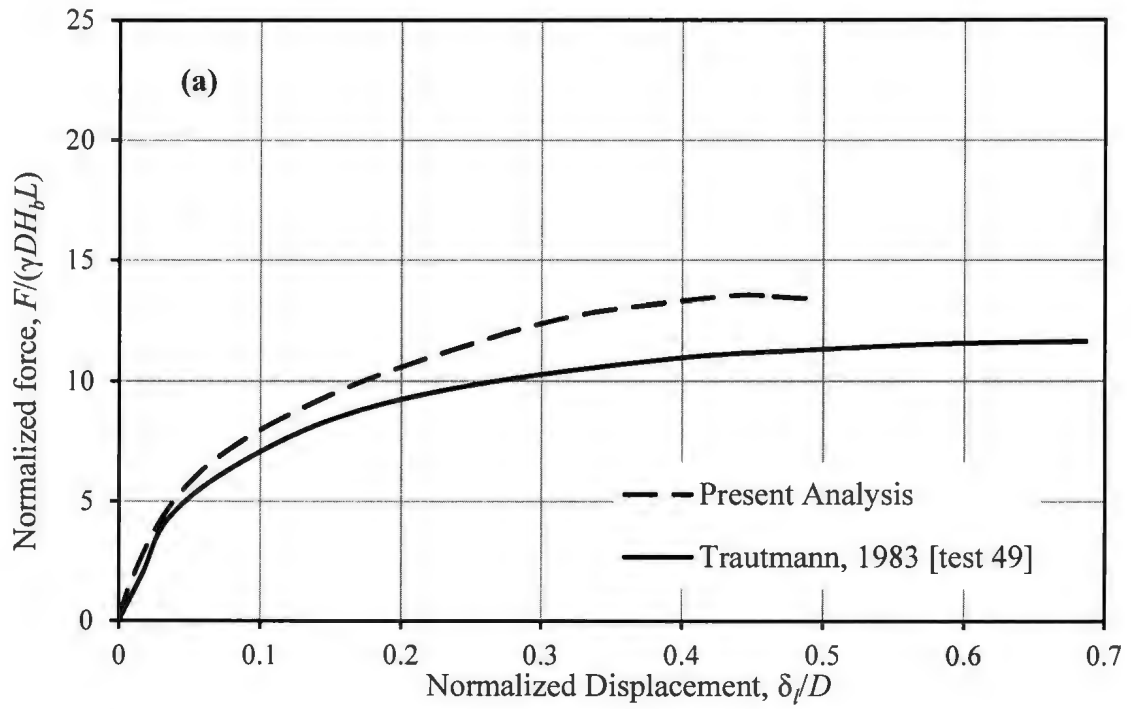


Figure 4-15: Normalized force-displacement curve for lateral loading in (a) Medium dense sand) with  $H/D = 11.5$  and (b) Dense sand with  $H/D = 11.5$

#### 4.7 Pure Vertical (Upward) Loading

A two-dimensional finite element model is developed for upward loading of pipe with geometry exactly similar to the experimental setup used by Trautmann (1983). The experimental set up used by Trautmann (1983) for upward loading is little different from the setup for lateral loading as shown in the figures 4-16 and 4-17. The ratio of the pipe diameter to the pipe wall thickness is same as lateral loading of  $D/t = 16$ . The analyses are performed for one shallow ( $H_c/D=4$ ) and one deep ( $H_c/D=13$ ) burial condition. In both cases the bottom of the pipe is at 300 mm above the floor of the tank.

Figure 4-16(a) and 4-16(b) show the comparison between the experimental and numerical results for shallow burial conditions ( $H_c/D=4$ ) for both medium and dense sand. Figure 4-17(a) and 4-17(b) show the comparison between the experimental and numerical results for deep burial conditions ( $H_c/D=13$ ) with medium and dense sand. As shown, the peak resistance obtained from numerical analyses reasonably matched with experimental results. However, the post-peak reduction of vertical force could not be simulated using the Mohr-Coulomb model.

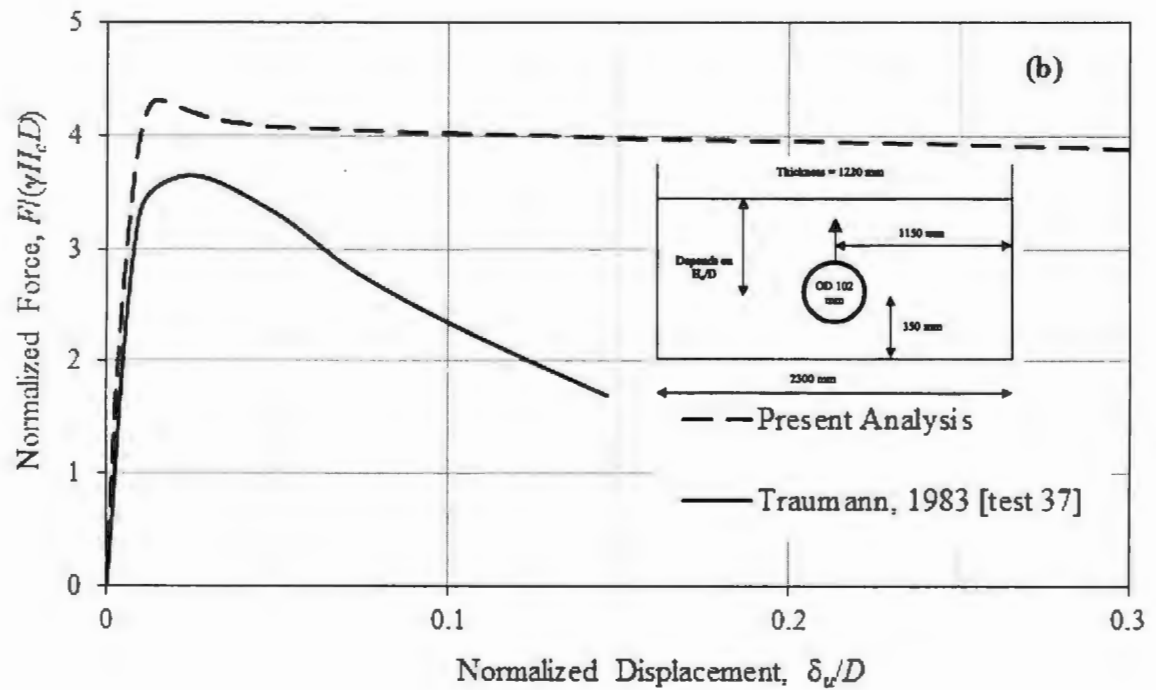
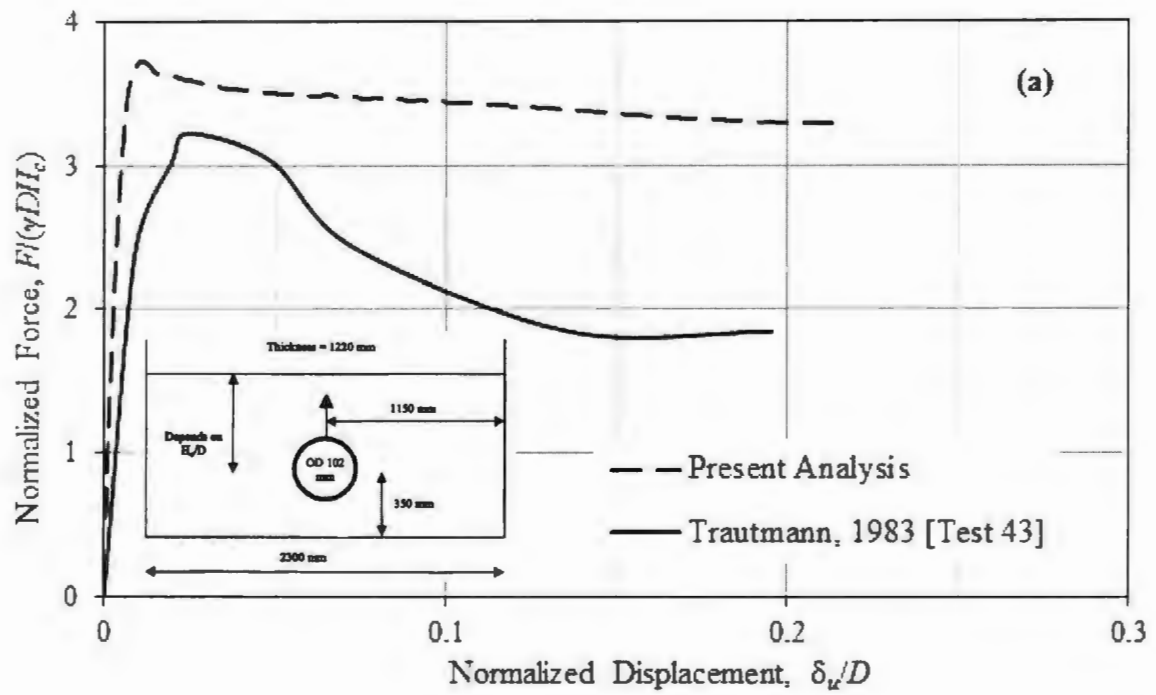


Figure 4-16: Normalized force-displacement curve for upward loading in (a) Medium dense sand with  $H_c/D = 4$  and (b) Dense sand with  $H_c/D = 4$

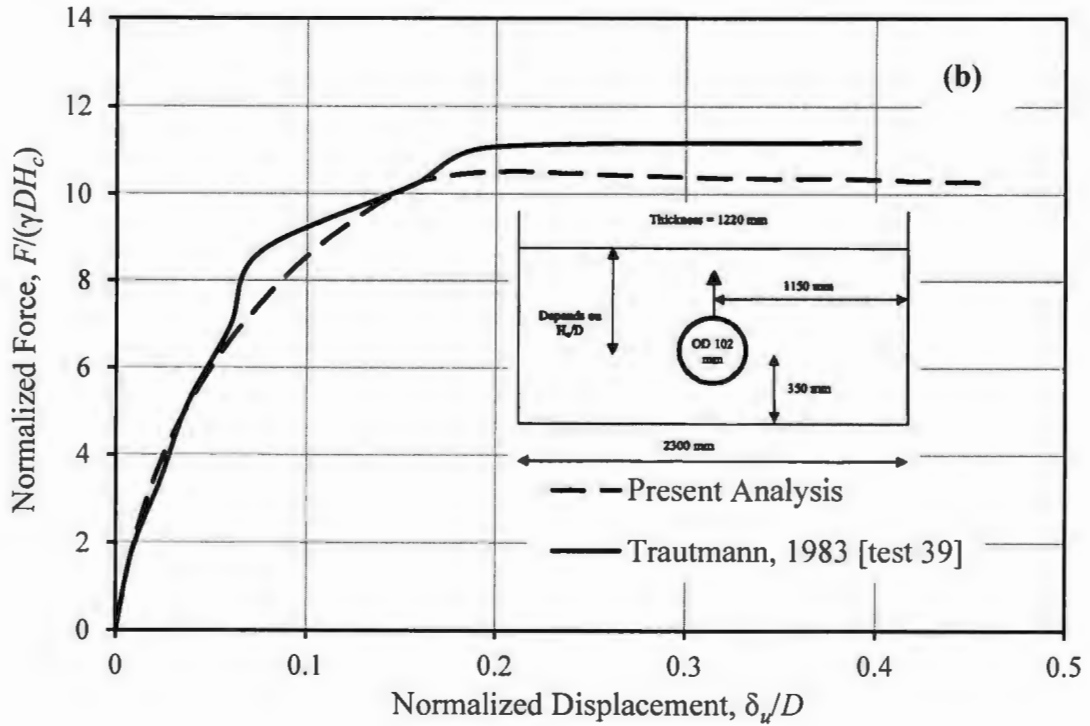
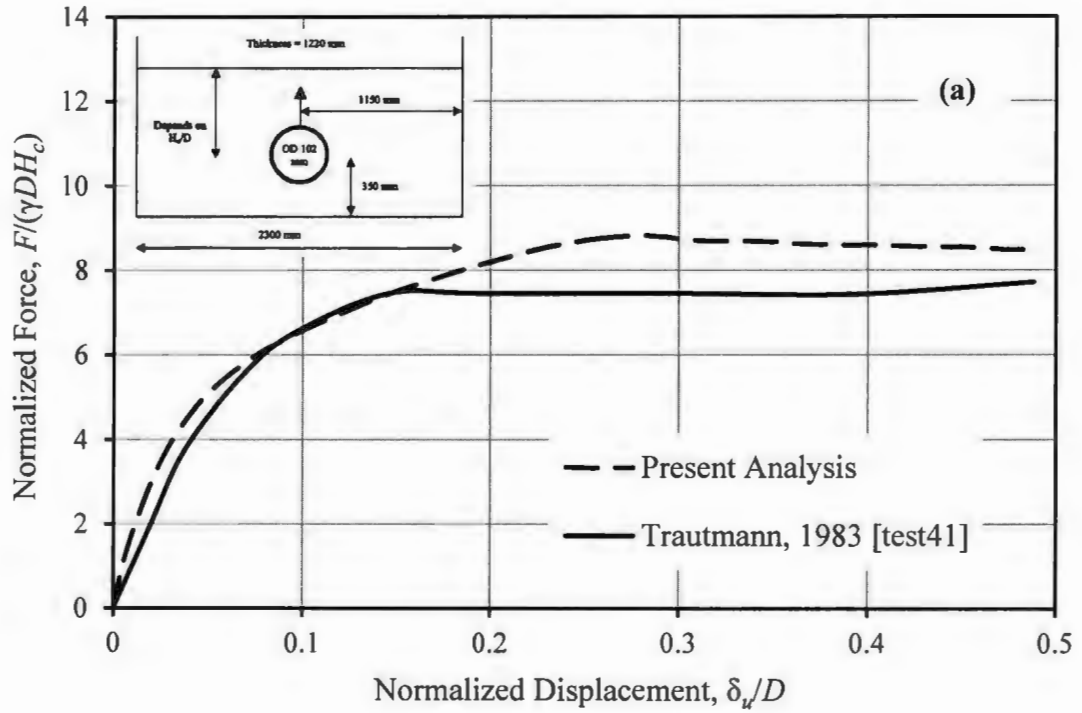
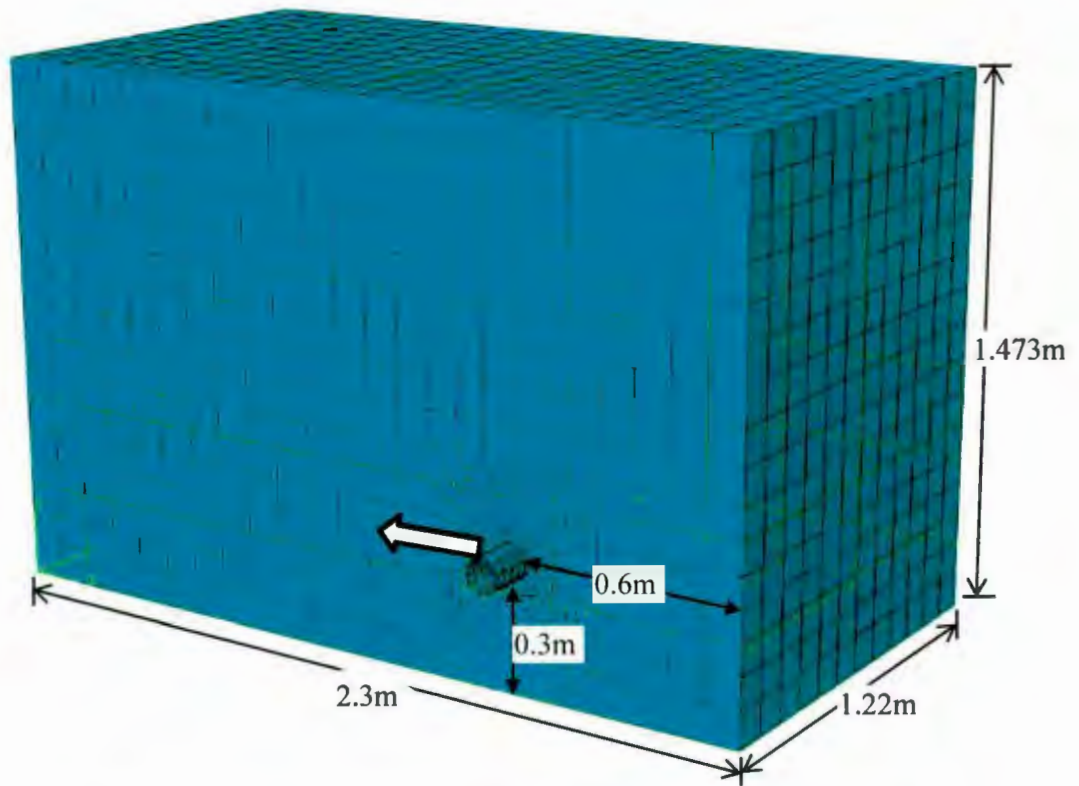


Figure 4-17: Normalized Force-Displacement curve for upward loading in (a) Medium dense sand with  $H_c/D = 13$  and (b) Dense sand with  $H_c/D = 13$

#### 4.8 Three-Dimensional Analyses

The tests conducted by Trautmann (1983) are in fact in three-dimensional condition, although in previous sections, it is modeled in a two-dimensional plane strain condition. In their experiment, a model pipe of 0.61 m length was moved laterally in a 2.3m×1.22m×1.473 m (length×width×thickness) tank filled with dry sand. In this section, the same problem in three-dimensional condition is analyzed. The main purpose of this simulation is to check whether the difference between 2D simulation and test results is due to three dimensional effects or not. The three-dimensional finite element model shown in Figure 4-18 is formed with the geometry exactly similar to the experimental setup by Trautmann (1983). For soil, 8-node linear brick, reduced integration, hourglass control elements (C3D8R) and for pipe, 4-node three-dimensional bilinear rigid quadrilateral (R3D4) elements are used. All the vertical faces are modeled using roller supports and therefore the interface between tank and soil is not modeled properly in this case. This time, a rigid pipe is used in the analysis to improve the computational time and the reference point is defined at the center of the pipe. The pipe is moved laterally by applying a displacement boundary condition at the reference point without any imposed vertical restraint. Typical vertical stress contours after geostatic loading are shown in Figure 4-19.



**Figure 4-18: Typical meshing for lateral 3-D soil/pipe interaction analysis**

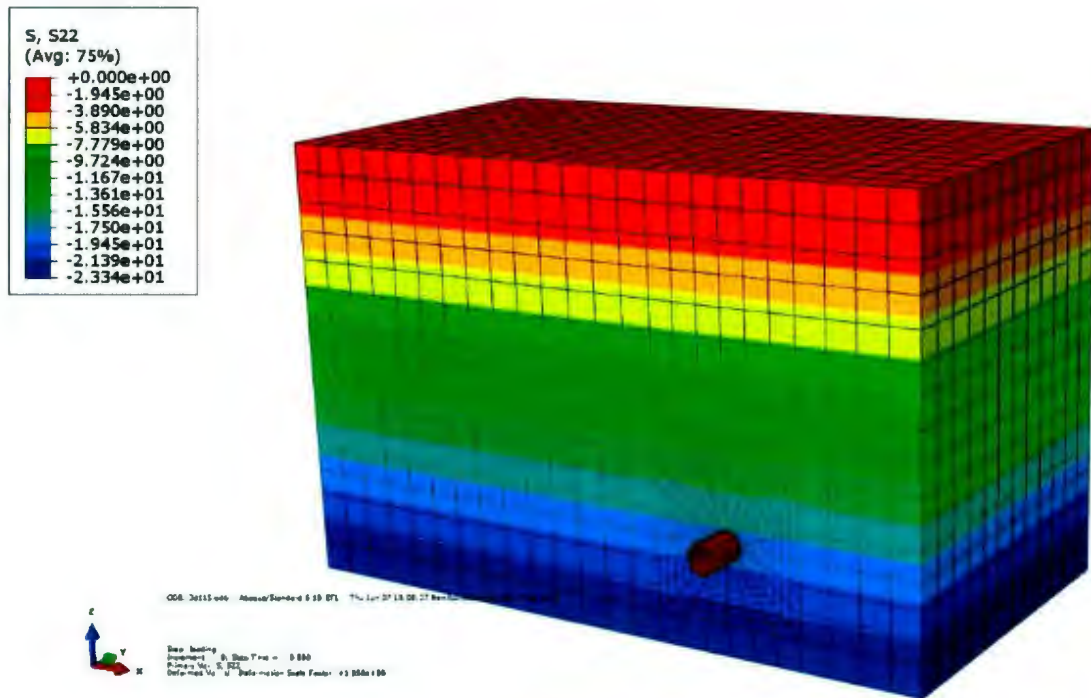


Figure 4-19: Typical geostatic loading for lateral 3-D pipe-soil interaction analysis

#### 4.8.1 Pure Lateral Loading

The same soil parameters listed in Table 4-1 are used except Young's modulus of elasticity,  $E$  as  $11000 \text{ kN/m}^2$  as the force-displacement curve matched better with this value as shown in Figure. 4-15(b) for two-dimensional cases. Three-dimensional lateral pipe displacement analyses are done for the dense sand i.e. for  $\gamma = 17.7 \text{ kN/m}^3$ . The FE results obtained from the three-dimensional model are compared with the two-dimensional results presented in the previous sections and also with the test results as shown in Figure 4-20(a) and Figure 4-20(b).

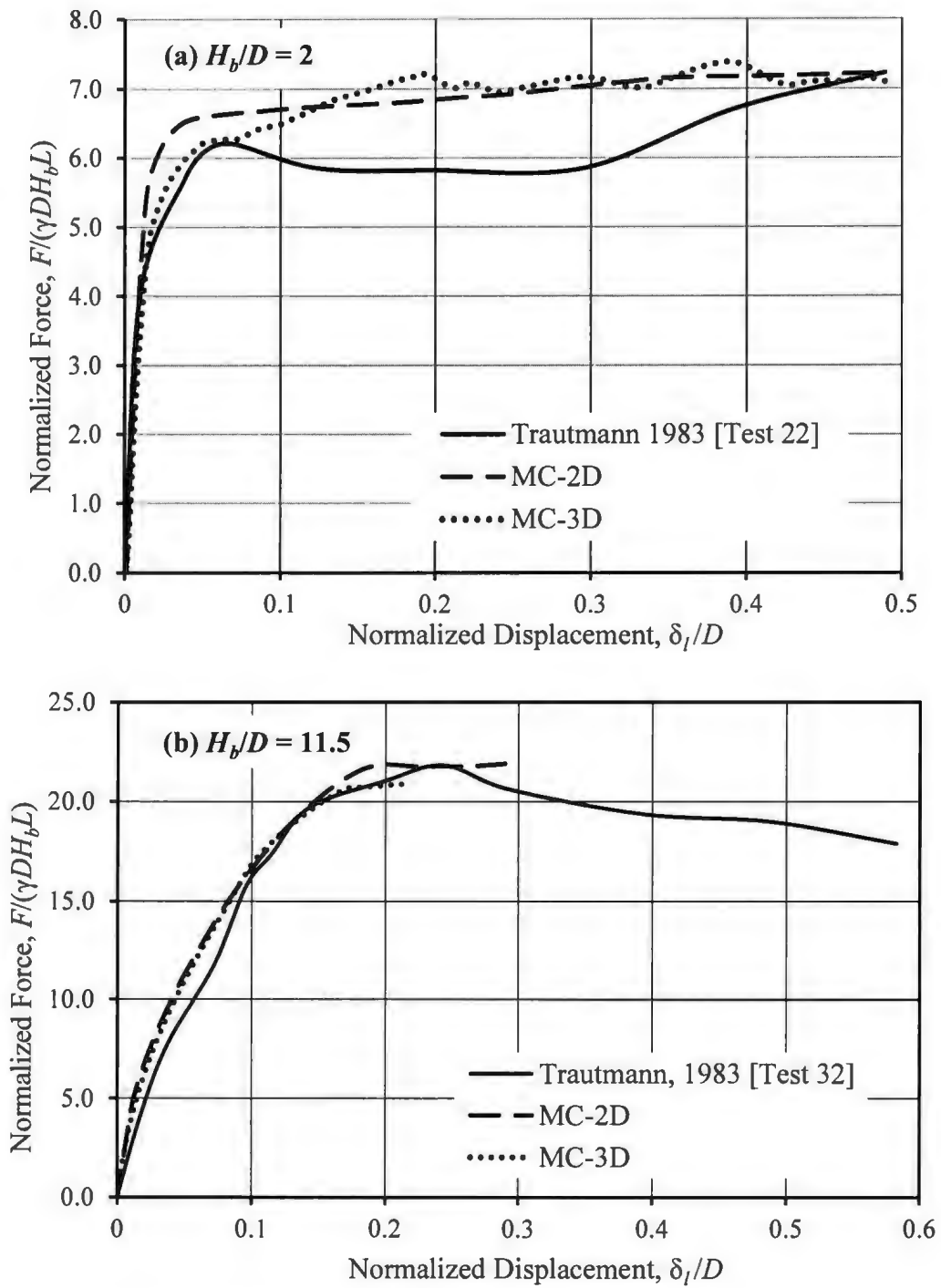


Figure 4-20: Normalized Force-displacements curves from Lateral-3D analysis for dense sand (a)

$H_v/D = 2$  (b)  $H_v/D = 11.5$

As shown, the force-displacement curves obtained from the two-dimensional modeling is very similar to that of the three-dimensional analysis. That means any discrepancies between the model test and finite element results are not for the three-dimensional effects. One of the possible reasons of discrepancies is the use of appropriate soil model. The Mohr-Coulomb plasticity model may not simulate the soil behaviour properly in this case. An advanced soil constitutive model might be used for better modeling this behaviour.

Figure 4-21 shows the shear strain in the soil around the pipe at a post-peak displacement. Two different soil failure mechanisms are observed: local (punching) failure for deep burial condition (Figure. 4-21b) and general shear failure for shallow pipe burial condition (Figure. 4-21a). PEMAG gives the plastic strain magnitude which is used to show the strain localization and failure type (local or general). PEMAG is defined as

$$\sqrt{\frac{2}{3}} \varepsilon^{pl} : \varepsilon^{pl} .$$

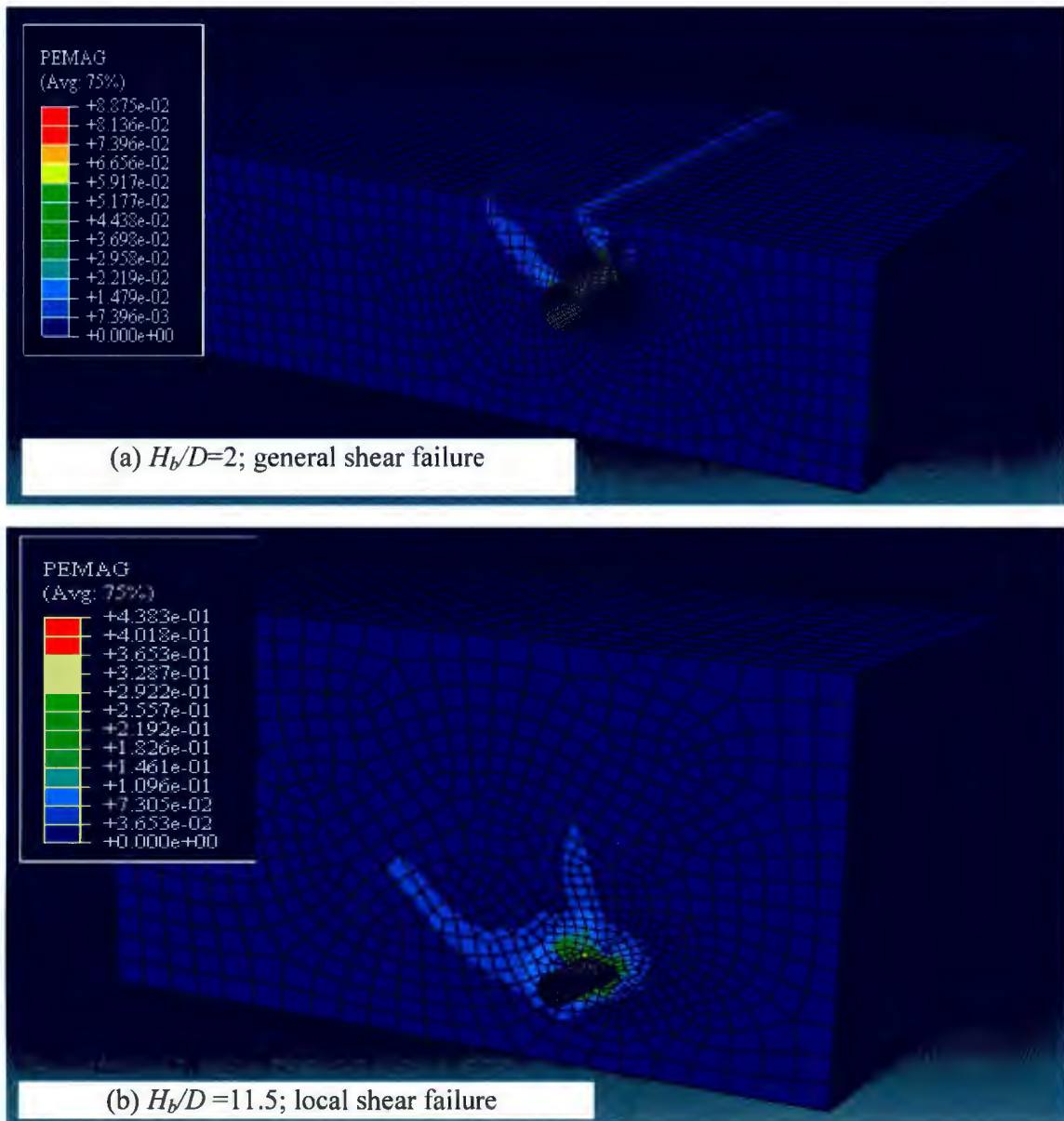


Figure 4-21: Shear failure pattern under lateral loading (a)  $H_b/D = 2$  (b)  $H_b/D = 11.5$ .

#### 4.9 Summary

The main focus of this chapter is to present some finite element analyses using built-in Mohr-Coulomb soil constitutive model and the comparison of the results with available model test results. Previous model tests show that the force-displacement response of pipelines buried in sand subjected to pure lateral or vertical (upward) load depends on depth of embedment and density of soil. For the pipelines in dense sand there is a post-peak reduction in force for both lateral and vertical (upward) loading. It is found that the finite element simulation with structured mesh has less numerical difficulties. The elastic modulus controls the shape of the initial part of the load-displacement curve. The use of a constant elastic modulus may not be the right procedure to simulate soil/pipeline interaction behaviour and therefore in the following chapter the shear modulus as a function of mean stress is used. The finite element simulation with built-in Mohr-Coulomb soil constitutive model with constant dilation angle cannot simulate the post-peak reduction in force as observed in model tests, however, the initial part of the force-displacement curve could be simulated with refined value of soil parameters.

## Chapter 5

### FINITE ELEMENT ANALYSES WITH NORSAND SOIL CONSTITUTIVE MODEL

#### 5.1 General

The finite element analyses presented in Chapter 4 is based on built-in Mohr-Coulomb model in ABAQUS. Not only in this study but also some previous studies recognized that that there are some limitations in Mohr-Coulomb soil constitutive model for modeling soil/pipeline interaction behaviour. Therefore, in this chapter modeling has been performed using an advanced soil constitutive model, NorSand.

This chapter has been organized in the following way. Firstly, the implementation of NorSand model in ABAQUS FE software using the user defined subroutine is briefly discussed. The parameters require to be defined in the ABAQUS input file for proper communication with UMAT are also discussed in this section. In the second part of this chapter, triaxial tests for a wide range of initial condition are simulated. These simulations are done to show that the NorSand UMAT can successfully model a wide range of soil condition that might occur in soil/pipeline interaction events. In the third part of this chapter, some soil/pipeline interactions for pure lateral and pure vertical (upward) loading are simulated and the results are compared with similar analyses using Mohr-Coulomb model. Finally, the finite element simulations have been performed for oblique lateral-vertical (upward) loading.

## 5.2 Implementation of NorSand Model into ABAQUS

ABAQUS/Standard has interfaces that allow the user to implement any general constitutive equations and the user-defined material model can be implemented in ABAQUS/Standard by using user subroutine, UMAT. When none of the built-in constitutive models available in the ABAQUS material library accurately represents the behaviour of the material to be modeled, the UMAT can be called. It updates the stresses and solution-dependent state variables to their values at the end of the increment for which it is called and provides the material Jacobian matrix,  $\partial\Delta\sigma/\partial\Delta\varepsilon$ , for the mechanical constitutive model implement in ABAQUS.

The first version of NorSand UMAT has been developed by Dasari and Soga (2000) for a joint industry program on soil/pipeline interaction. The original NorSand model proposed by Jefferies (1993) was implemented into ABAQUS/STANDARD Version 5.8. This version of UMAT has been received with the permission to modify it for the present study. A rapid change in ABAQUS software development has been occurred over the last decade and a number of versions have been released after the Version 5.8. The analyses presented in this study have been conducted using ABAQUS/STANDARD Version 6.10 EF1. The development of input files with UMAT in version 6.10 EF1 is different from Version 5.8. In addition, the compilers required for Version 6.10-EF1 and 5.8 are quite different. The present study using Version 6.10 EF1 requires Intel Visual Fortran 10.1/11.1 and Microsoft Visual C++ 2008 SP1 (Visual C++ 9.0). The following are some

of the important command lines included in the input file to activate NorSand UMAT during analyses.

\*MATERIAL, NAME=SOIL

\*DEPVAR (Allocated space at each material point for solution dependent state variables)

18 (There are 18 solution-dependent-state variables in the code)

\* USER MATERIAL, TYPE=MECHANICAL, CONSTANTS = 11, UNSYMM

$M, \lambda, \Gamma, N, H, A, n, v, \chi$ , ISWIT, TOL

(The above 11 constants are passed to the UMAT. Among them the first 9 are geotechnical properties required in NorSand model. The details of these constants are shown in Table 5-1).

\*INITIAL CONDITIONS, TYPE=SOLUTION, USER

(This is to specify initial condition (e.g. initial effective stresses, initial void ratio) via user subroutine SDVINI)

**Table 5-1: Input parameters required for UMAT**

$M_{tc}$	Critical stress ratio in triaxial compression
$\lambda$	Slope of the Critical state line in $e-\ln p$ graph
$\Gamma$	Critical void ratio at $p'=1$ kPa
$N$	$N$ in Nova's flow rule
$H$	Hardening modulus

A	Shear modulus multiplier (Equation 5.1)
n	Pressure exponent
$\nu$	Poisson's ratio
$\chi$	Maximum dilation coefficient
ISWIT	Switch to use constant or exponent $H$
TOL	Tolerance for stress integration

It is to be noted here that the NorSand model is also implemented in ABAQUS ALE for modeling ice gouging effect (Eskandari et al., 2011)

### 5.3 NorSand Model Parameters

Most of the model parameters listed in Table 5-1 are common in geotechnical modeling. Detailed information about these parameters are available in Jefferies and Been (2006). The parameters which are used differently in this study are discussed below.

#### 5.3.1 Modulus of Elasticity

In Chapter 4, constant modulus of elasticity ( $E$ ) is used in the simulations with Mohr-Coulomb model. It is also shown that the value of  $E$  has a significant effect on force-displacement behaviour as shown in Figure. 4-15(b). The elasticity is an important parameter that must be selected properly to simulate correct shape of load-displacement curve. Experimental studies (e.g. Janbu, 1963; Hardin and Black, 1966) show that the elastic moduli of granular materials increase with the increase in mean stress ( $p'$ ). It has

been also shown that the elastic modulus depends on void ratio. Various expressions have been proposed in the past in order to account the effects of void ratio and mean stress on elastic moduli. Yimsiri (2001) compiled all the available expression in the literature. All expressions of shear modulus ( $G$ ) can be written in the following general form.

$$G = Ap^n \quad (5.1)$$

The value of  $A$  depends on void ratio or density. Yimsiri (2001) showed that the value of  $n$  recommended by previous researchers varies between 0.4-0.61, with most cases  $n = 0.5$ . It is to be noted here that some authors (e.g. Jefferies 2006) used shear rigidity  $I_r$ , which can be also expressed in above form. In the NorSand UMAT  $G = Ap^n$  is used.

### 5.3.2 Critical Stress Ratio in three-dimensional stress space

The use of a constant value of  $M$  for all loading conditions is not realistic. Experimental observation shows that the value of  $M$  changes with Lode angle ( $\theta$ ). For example, the values of  $M$  in triaxial compression, triaxial extension and plane strain conditions are different. Several mathematical function of  $M(\theta)$  has been proposed in the past (e.g. Matsuoka and Nakai, 1974; Lade and Duncan, 1975, Banerjee et al., 1985) to capture this variation. The simplest form of variation is the Mohr-Coulomb hexagonal model in the  $\pi$ -plane. However, the hexagonal variation has sharp corners which cause numerical difficulties. Therefore, in this study the value of  $M$  varies with  $\theta$  according to the following function proposed by Banerjee et al. (1985).

$$M(\theta) = \frac{2k M_{tc}}{(1+k) - (1-k) \sin 3\theta} \quad (5.2)$$

where  $\theta$  is Lode angle,  $M_{tc}$  is critical state stress ratio in triaxial compression and

$k = \frac{3 - \sin \phi'}{3 + \sin \phi'}$ . Note that, the Lode angle  $\theta = 30^\circ$  represents triaxial compression while  $\theta$

$= -30^\circ$  represents triaxial extension and the plane strain condition is in between  $+30^\circ$  and

$-30^\circ$ . The variation of  $M$  with  $\theta$  in  $\pi$ -plane is shown in Figure 5-1.

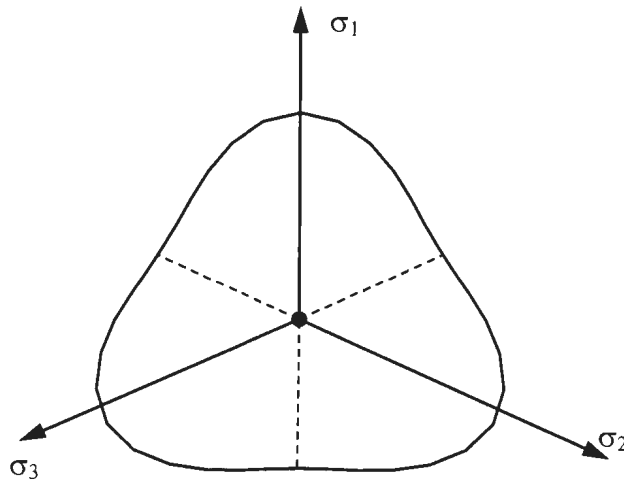


Figure 5-1: Variation of  $M$  in  $\pi$ -plane used in UMAT

In this study, the value of  $M$  in triaxial compression ( $M_{tc}$ ) is given as a geotechnical parameter in the input file. In the subroutine NorSand UMAT, the value of  $M$  is updated as shown in Figure 5-1.

#### 5.4 Simulation of Triaxial Tests using NorSand UMAT

To show the effectiveness of the implemented NorSand soil constitutive model in ABAQUS using the user defined subroutine UMAT, some triaxial tests under various conditions are simulated. In the first set of analyses four triaxial compression tests are simulated. The test condition and material properties used in the analyses are shown in Table 5-2. The main purpose of the selection of these four tests is to cover a wide range of soil conditions that might be encountered in pipe/soil interaction analyses. The test D667, D662, D682 and D685 corresponds to tests on very dense, dense, loose and very loose sands, respectively.

**Table 5-2: Triaxial test data on Erksak sand (Regenerated from Been et al., 1991)**

Test Name	Initial condition			End of test			
	Void Ratio	p' (kPa)	$\psi_i$	$\sigma'_3$ (kPa)	p' (kPa)	q (kPa)	e
D667	0.590	130	-0.161	130	253	355	0.702
D662	0.677	60	-0.084	60	104	131	0.752
D682	0.776	500	0.044	500	812	938	0.725
D685	0.812	200	0.067	200	283	273	0.749

Jefferies and Been (2006) compiled a large number of laboratory data and reanalyzed them in the framework of NorSand soil constitutive model. The parameter used in the present numerical analyses are obtained from their work and listed in Table 5-3.

**Table 5-3: Model parameters of NorSand for simulating triaxial tests**

<u>Parameters</u>	<u>D667</u>	<u>D662</u>	<u>D682</u>	<u>D685</u>
Void ratio, $e$	0.590	0.677	0.776	0.812
$p_{max}$ (= $p'$ at the tip of the yield surface, $\eta=0$ )	130	60	500	200
Critical stress ratio in triaxial compression, $M_{tc}$	1.3	1.26	1.18	1.18
Slope of the Critical state line in $e-\ln p'$ graph, $\lambda$	0.014			
Critical void ratio at $p' = 1\text{kPa}$ , $\Gamma$	0.8			
$N$ in Nova's flow rule, $N$	0.25			
Hardening modulus, $H$	500	450	250	200
Shear modulus multiplier, $A$	9000	8000	1500	1500
Pressure exponent, $n$	0.5			
Poisson's ratio, $\nu$	0.25			
Maximum dilation coefficient, $\chi$	3.8	4	4	4.5
Tolerance for stress integration, $TOL$	0.001			

An axisymmetric 4-noded single element (CAX4) is chosen to simulate a soil element in triaxial condition as shown in Figure 5-2. The soil specimen was consolidated isotropically to initial consolidation pressure as shown in third column of Table 5-2. The initial consolidation pressure is applied on the soil specimen in numerical simulation by surface pressure on the top and right vertical faces. It is to be noted here that the application of surface pressure on the bottom and left faces is meaningless as they are restraint from any displacement in the vertical and lateral directions, respectively. After the application of confining pressure, the vertical load is applied on the soil specimen by setting vertical downward displacement of top two nodes in incremental form. Note that these four tests are on normally consolidated sand. The effects of overconsolidation are discussed later.

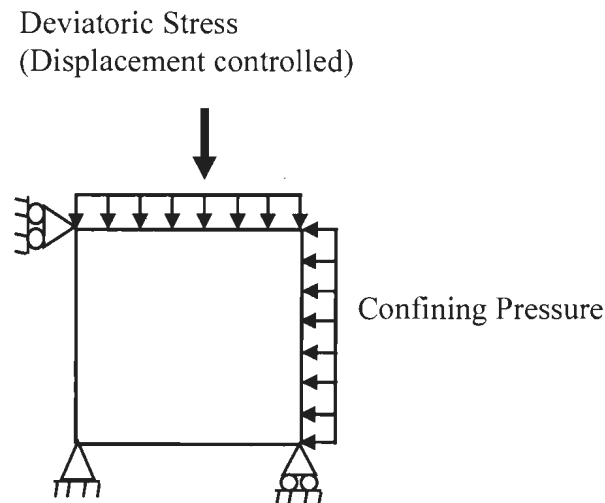


Figure 5-2: Axisymmetric 4-noded element CAX4 for FE simulation of triaxial tests.

In Figures 5-3 to 5-6, the numerical results are presented in the form of deviatoric stress versus axial strain and volumetric strain versus axial strain plots. The laboratory test data

are also shown in this figure for comparison. The results from numerical simulation using the NorSand UMAT show a very good fit with the test results.

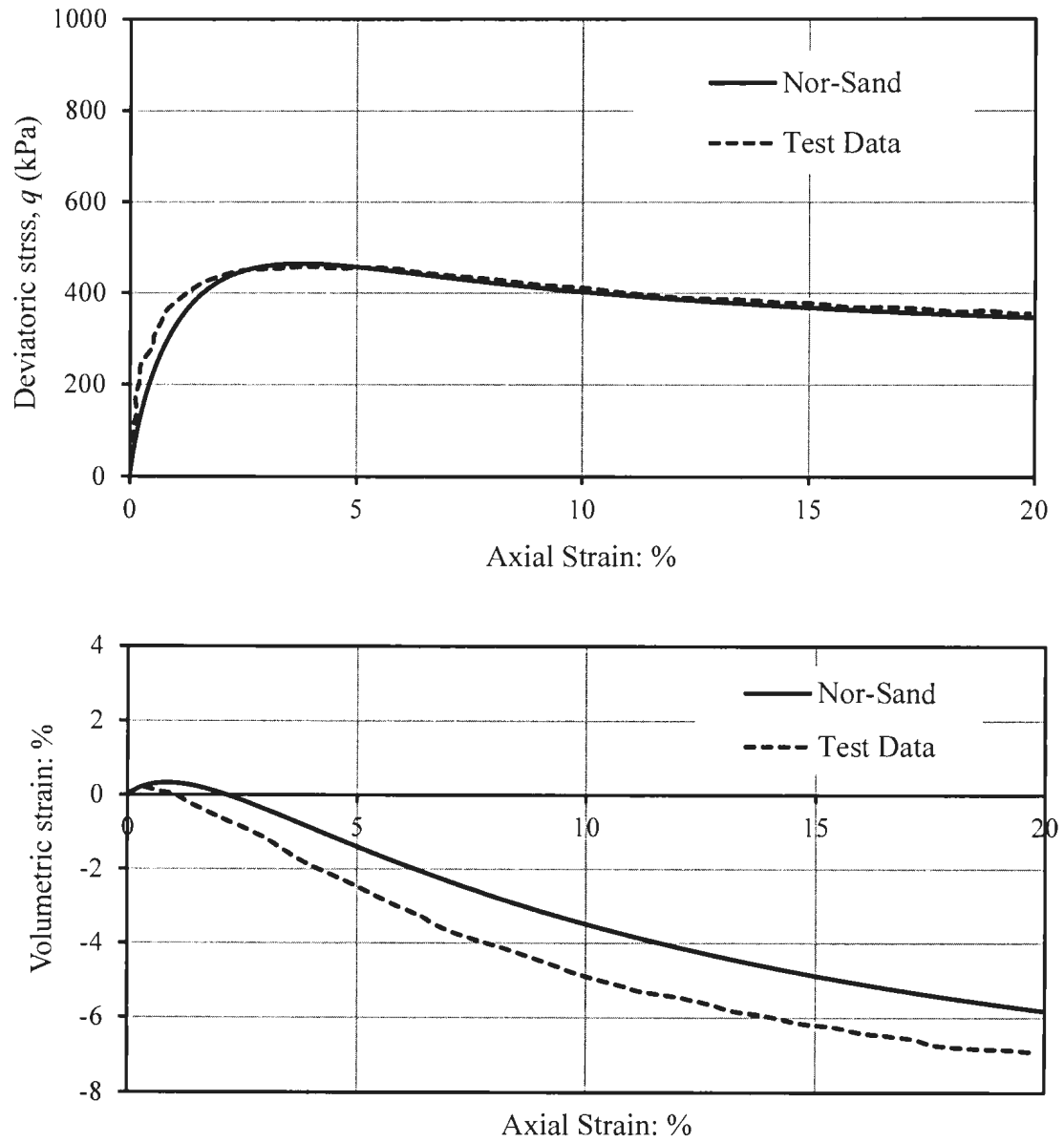


Figure 5-3: Finite element simulation (Very Dense Sand)

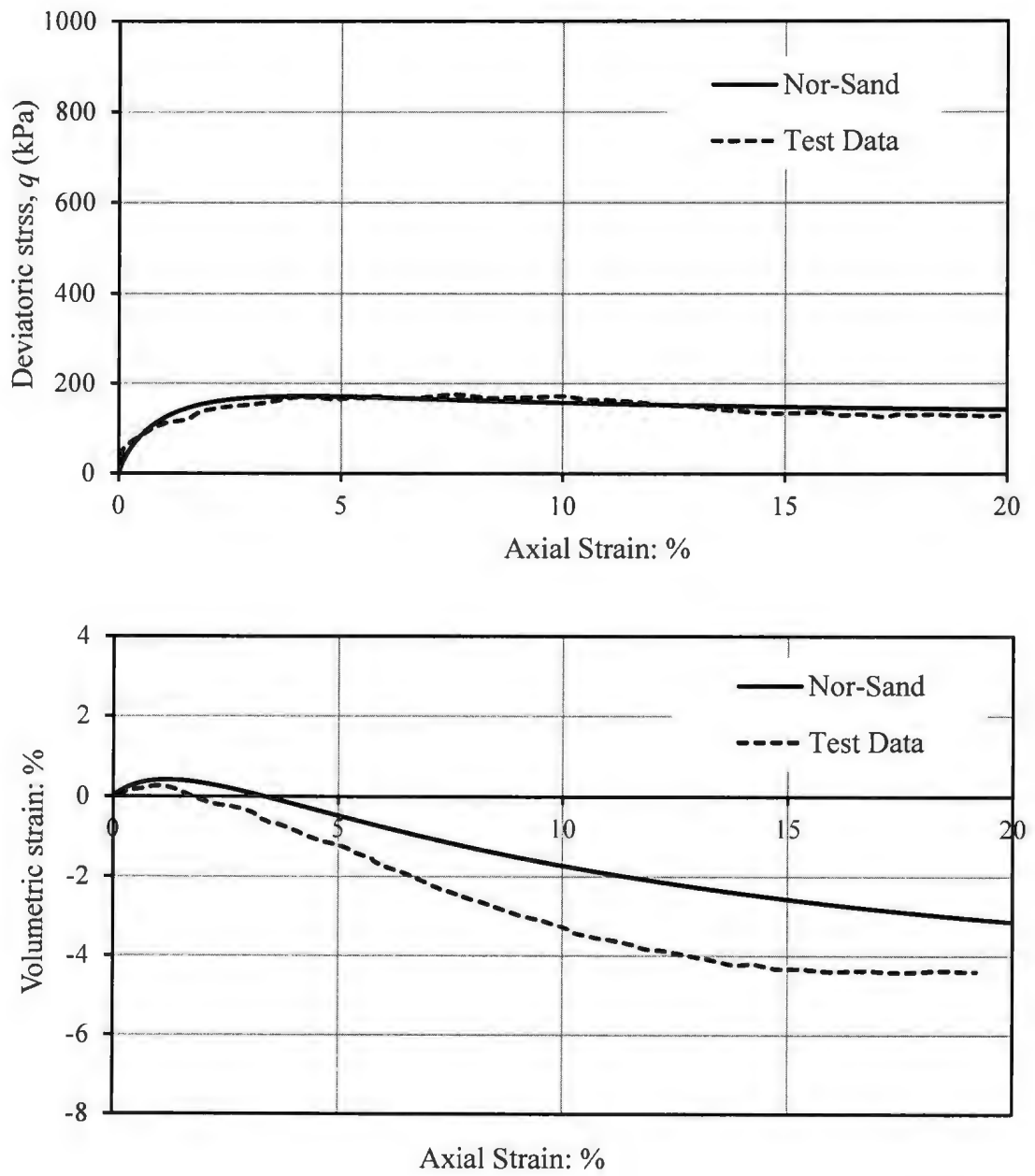


Figure 5-4: Finite element simulation (Dense Sand)

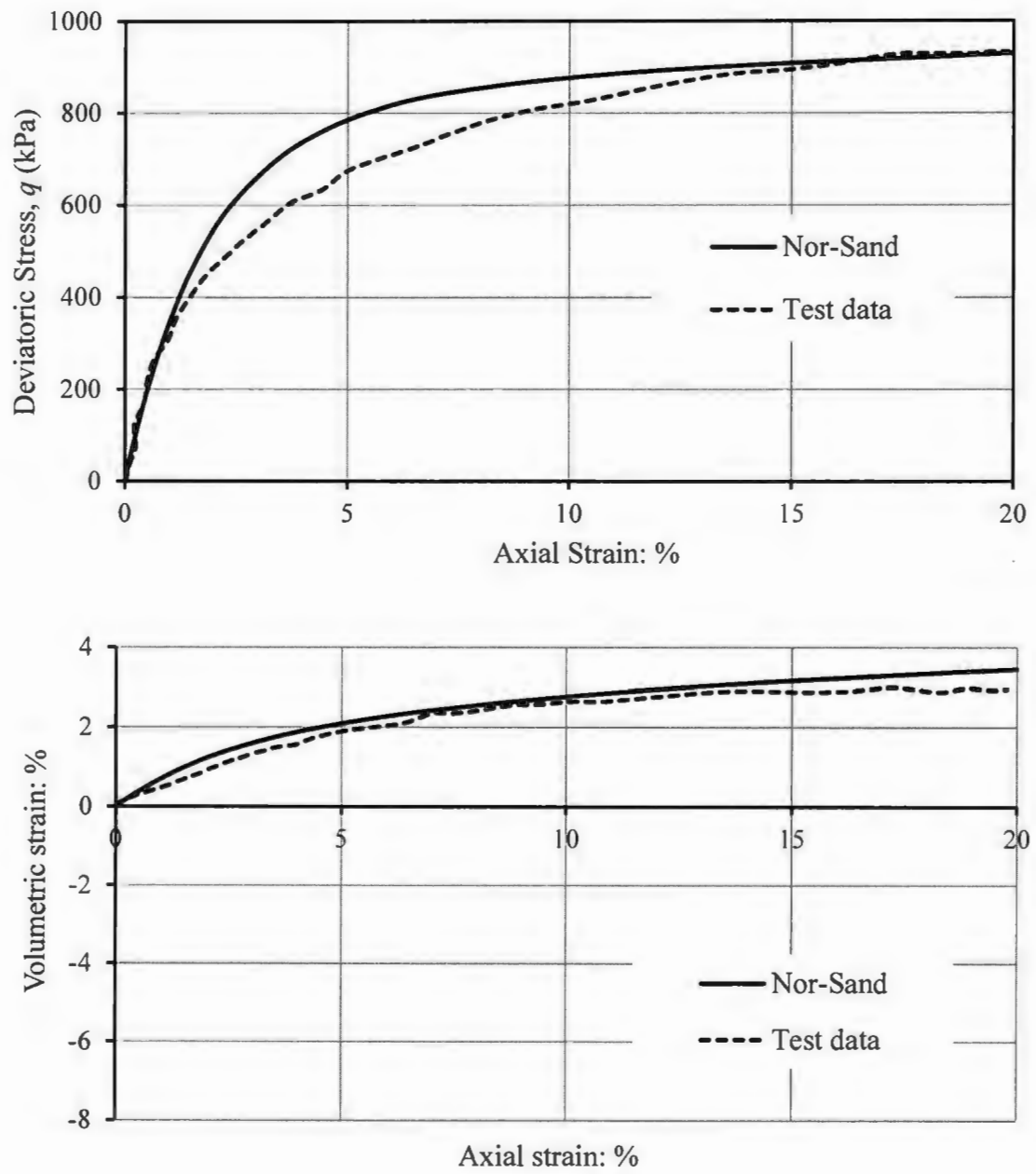


Figure 5-5: Finite element simulation (Loose Sand)

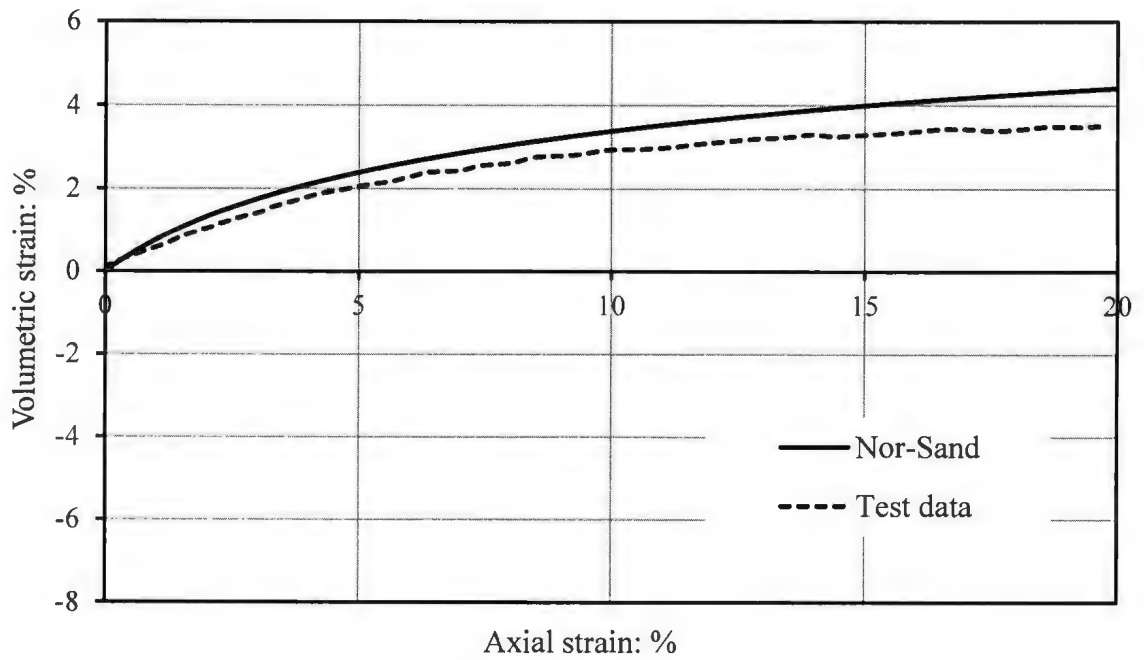
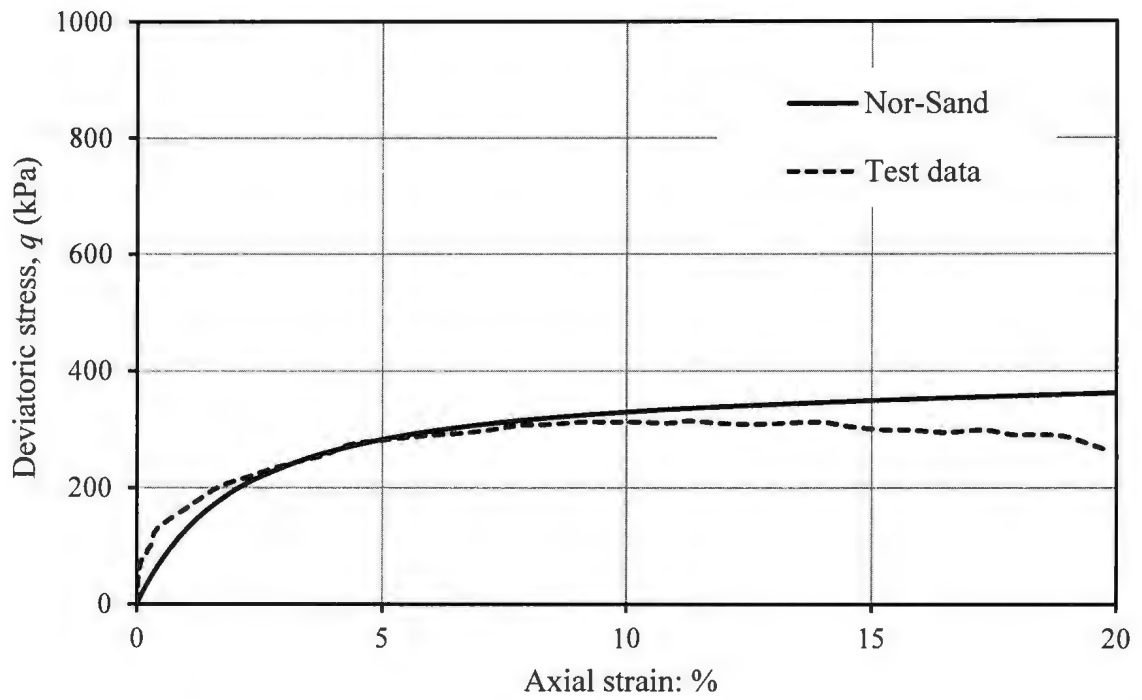


Figure 5-6: Finite element simulation (Very Loose Sand)

After simulation of four triaxial tests listed in Table 5-2, tests similar to D682 are simulated for three different void ratios. As discussed in Chapter 3 NorSand model can capture the possible infinite number of normally consolidated lines. Figure 5-7 shows three normally consolidated lines (NCL) at three different densities. Three soil specimens are consolidated isotropically along these NCL to  $p' = 500$  kPa and then unloaded to  $p' = 300$  kPa and then sheared in triaxial compression. This created some overconsolidation ratio. The purpose of this simulation is to show the effects of density and overconsolidation of sand using NorSand UMAT. Figure 5-8 shows the variation of deviatoric stress with axial strain. The initial void ratios of the soil specimens A and B are very close to the critical state void ratio at their initial stress level. Therefore, the deviatoric stress reaches to the peak and remains almost constant as typically observed in loose sand. Note that the initial value of  $p'$  for specimen A is higher than that of specimen B and therefore the deviatoric stress at the ultimate condition is higher for specimen A. The specimen B is overconsolidated and yielding occurs at a deviatoric stress of 195 kPa which is the intersection of the initial yield surface and stress path shown in Figure 5-10. Therefore, the stress strain behaviour before 195 kPa of deviatoric stress is nonlinear elastic as shown in Figure 5-8. Figure 5-9 also shows for lower initial void ratios (0.6 and 0.7) the stress strain plot is similar to the behaviour typically observed in dense sand with strain softening.

Figure 5-9 shows the volumetric strain versus axial strain plots for four different initial conditions, which is similar to typical triaxial results on dense to loose sands.

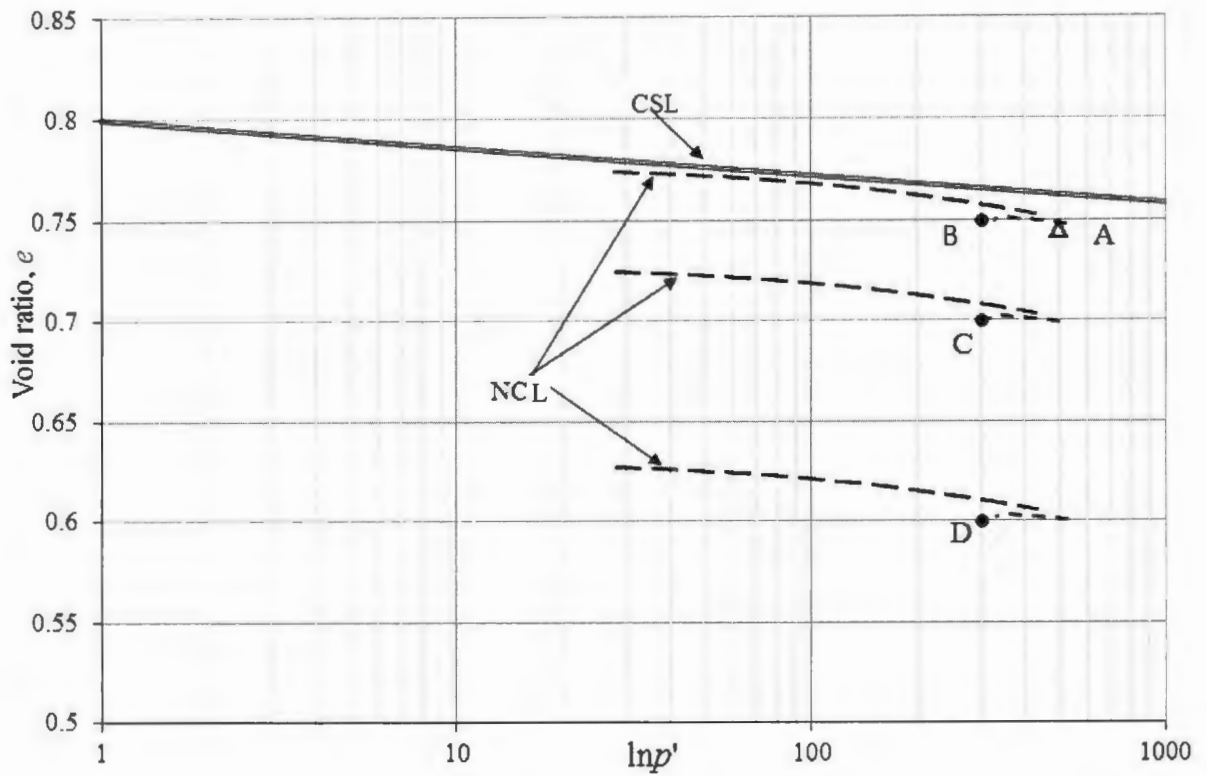


Figure 5-7: Void ratio in  $e-\ln p'$  plot for different densities

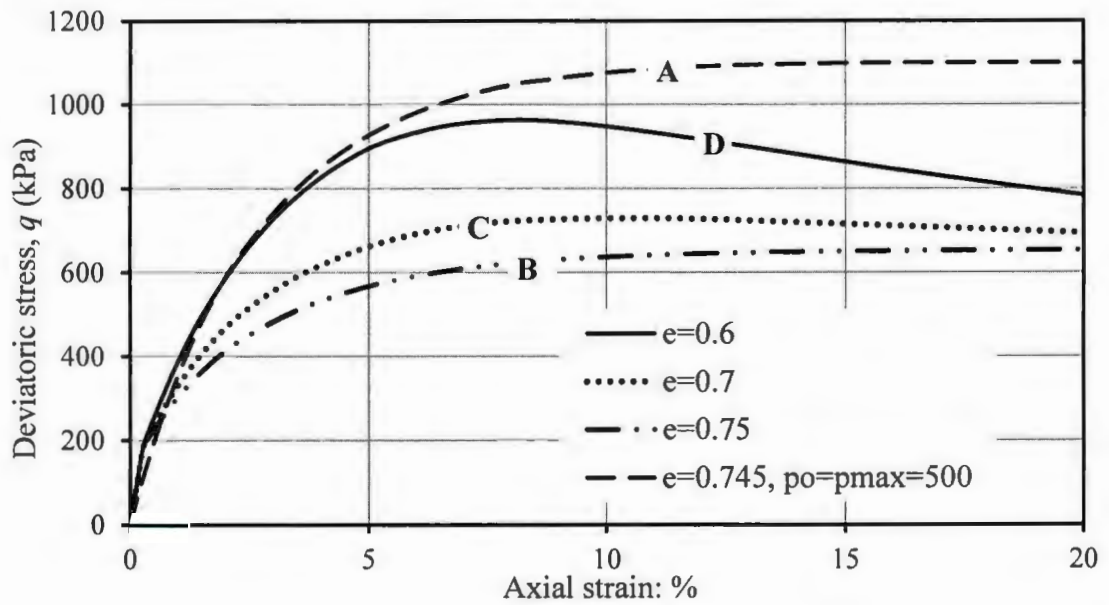


Figure 5-8: Deviatoric stress vs. axial strain plot for different void ratios

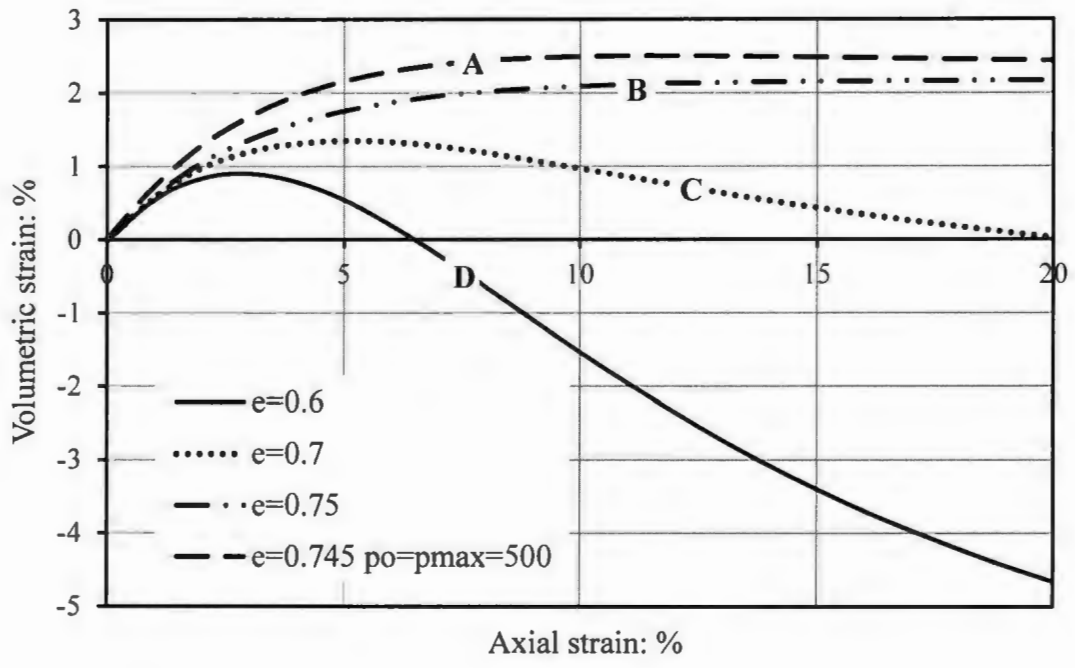


Figure 5-9: Volumetric strain vs. Axial strain plot for different void ratios

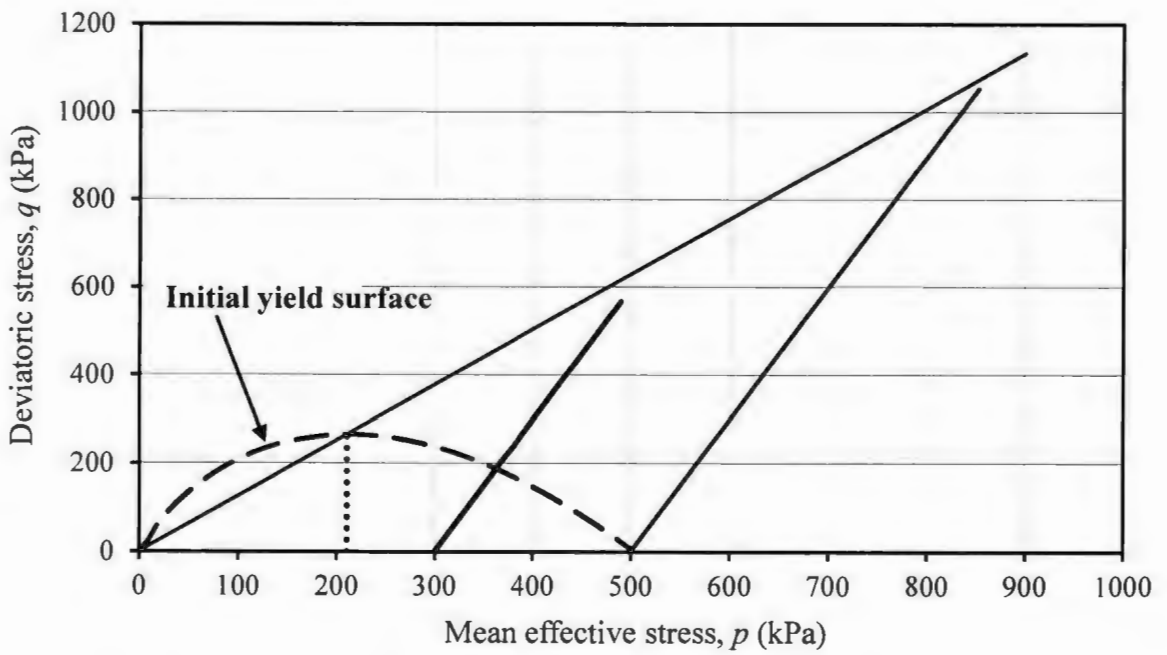


Figure 5-10: Deviatoric stress vs. mean effective stress plot for over-consolidated sand

From the above analyses it can be concluded that the NorSand model has been properly implemented in ABAQUS FE software using the UMAT.

## **5.5 Modeling of soil/pipeline interaction using NorSand UMAT**

The two- and three-dimensional finite element modelling using Mohr-Coulomb soil constitutive model is presented in Chapter 4. In this section, finite element analyses using the NorSand UMAT are presented. The main purpose of these analyses is to show the effects of advanced soil constitutive model on soil/pipeline interaction analyses.

### **5.5.1 Input Parameter for NorSand Model**

Table 5-4 shows the values of input parameters used in all the analyses presented in the following sections using the NorSand UMAT unless otherwise mentioned. These are the typical values of Erksak 330/0.7 sand (Jefferies and Been, 2006). This sand is chosen in this study as Jefferies and his coworkers validated the NorSand model by comparing a large number of laboratory tests on this sand. In general the data shown in Table 5-4 represents the dense state of Erksak 330/0.7 sand. The critical stress ratio in triaxial compression is 1.26 which corresponds to an critical angle of internal friction of 31°. It is to be noted here that while the peak angle of internal friction is higher in dense sand, the angle of internal friction at the critical state is almost constant irrespective of density. The value of  $\lambda$  and  $\Gamma$  are chosen from typical test data on this sand compiled by Jefferies and Been (2006). The  $N$  value of Nova's flow rule typically varies between 0.2 and 0.45 (Jefferies and Been, 2006) and in this study 0.25 is used. Jefferies and Been (2006)

suggested that the plastic hardening modulus ( $H$ ) of sand typically varies between 50 and 500 and in this study 200 is used. Several researchers showed that a value of pressure exponent ( $n$ ) of 0.5 best represents the elastic behaviour of sand. The maximum dilation coefficient varies between 2.5 and 4.5 and a value of 4 is used in this study.

**Table 5-4: Parameters used for soil/pipeline interaction analyses with NorSand UMAT**

<u>Parameters</u>	<u>Input Value</u>
Initial void ratio ( $e_m$ )	0.677
Critical stress ratio in triaxial compression ( $M_{tc}$ )	1.26
Slope of the Critical state line in $e$ - $\ln p$ graph ( $\lambda$ )	0.014
Critical void ratio at $p'=1$ kPa ( $\Gamma$ )	0.8
$N$ in Nova's flow rule ( $N$ )	0.25
Hardening modulus ( $H$ )	200
Shear modulus multiplier ( $A$ )	1000
Pressure exponent ( $n$ )	0.5
Poisson's ratio ( $\nu$ )	0.2
Maximum dilation coefficient ( $\chi$ )	4
Tolerance for stress integration	0.001

### 5.5.2 Input parameters for Mohr-Coulomb model

The finite element results using NorSand UMAT are also compared with FE analyses using the built-in Mohr-Coulomb model. In Mohr-Coulomb model, the dilation angle and the peak friction angle are required as input parameters which are obtained from the parameters listed in Table 5-4 in order to maintain consistency in input parameters between these two models.

The angle of dilation ( $\bar{\psi}$ ) in plane strain condition can be simply defined by the ratio of volumetric strain rate and shear strain rate as:

$$\sin \bar{\psi} = \frac{-(\dot{\epsilon}_1 + \dot{\epsilon}_3)}{(\dot{\epsilon}_1 - \dot{\epsilon}_3)} \quad (5.3)$$

where  $\dot{\epsilon}_1$  and  $\dot{\epsilon}_3$  are the strain rate in the major and minor principal strain directions, respectively. The minus sign arises simply from the convention that compressive strains are taken as positive and is introduced so that the angle of dilation is positive when the soil expands.

Houlsby (1991) indicated that care should be taken in the extension of the definition of the angle of dilation to other than plain strain conditions. He showed that for triaxial condition the following expression should be used.

$$\sin \bar{\psi} = \frac{-(\dot{\epsilon}_1 + 2\dot{\epsilon}_3)}{(\dot{\epsilon}_3 - \dot{\epsilon}_3)} \quad (5.4)$$

Note that the Equation 5.4 reduces to Equation 5.3 for plane strain condition.

In NorSand model the stress-dilatancy relationship is developed from triaxial test results.

The peak dilatancy rate is defined as (Jefferies 1993):

$$D_{\min} = \frac{-\dot{\epsilon}_v}{\dot{\epsilon}_q} = \frac{-(\dot{\epsilon}_1 + 2\dot{\epsilon}_3)}{\frac{2}{3}(\dot{\epsilon}_1 - \dot{\epsilon}_3)} = \chi \psi_i \quad (5.5)$$

Where  $\psi_i$  is the initial state parameter. Combining Equations 5.4 and 5.5 we find

$$\sin \bar{\psi} = \frac{2}{3} \chi \psi_i \quad (5.6)$$

Using the parameters listed in Table 5-4, the value of  $e_c$  is calculated. The initial value of state parameter  $\psi_i$  ( $=e_c - e_{in}$ ) is then calculated, which is used to calculate the value of  $\bar{\psi}$  ( $=9^\circ$ ). Once the value  $\bar{\psi}$  is known, the peak friction angle is calculated from  $\phi'_p = \phi'_c + 0.8\bar{\psi}$  (Bolton, 1986), which is equal to  $39^\circ$  in this case. The other parameters used in the analyses with Mohr-Coulomb model are shown in Table 5-5.

**Table 5-5: Parameters used for soil/pipeline interaction analyses with Mohr-Coulomb model**

<u>Parameters</u>	<u>Values</u>
Pipe:	
External Diameter, $D$	0.102 m
Thickness, $t$	0.0064 m
Elastic Modulus, $E_{\text{pipe}}$	$2.04 \times 10^8$ kN/m <sup>2</sup>
Poisson's Ratio, $\nu_{\text{pipe}}$	0.3
Soil:	Dense sand
Elastic Modulus, $E$	11000 kN/m <sup>2</sup>
Poisson's Ratio, $\nu_{\text{soil}}$	0.2
Critical State Friction Angle, $\phi'_{\text{critical}}$	31.5°
Friction Angle, $\phi'$	39°
Dilation Angle, ( $\bar{\psi}$ )	9°
Unit weight, $\gamma$	17.7 kN/m <sup>3</sup>
Interface Friction coefficient, $\mu$	0.32
Depth of pipe, $H/D$	2 and 11.5 (pure lateral loading), 4 and 13 (pure upward loading)

## 5.6 Pure Lateral Loading

Figure 5-11(a) shows the comparison between the numerical results with Mohr-Coulomb and NorSand soil constitutive models for shallow burial conditions ( $H_b/D=2$ ). As shown in this figure the normalized force reaches to the peak after a very small displacement. With Mohr-Coulomb model, a slight increase in force might be the effect of constant dilation angle used in the analysis. On the other hand, with NorSand model the vertical force reached to the peak and then reduced. Note that similar type of post peak reduction of lateral force was observed in model tests as shown in Figure 4-5. The constant dilation angle in Mohr-Coulomb model cannot simulate such behaviour. Some of the previous studies therefore used very simplified model of reduction of dilation angle with plastic shear strain (e.g. Daiyan et al. 2010a and b, Nobahar et al., 2007). Figure 5-11(a) also shows that the peak force developed at lower lateral displacement with Mohr-Coulomb model. One of the reasons is that a constant elastic modulus is used in Mohr-Coulomb model. If a lower value of elastic modulus is used the peak will be developed at larger displacement as shown in Chapter 4 (Figure 4-15b).

Figure 5-11(b) shows the similar comparison for deep burial conditions ( $H_b/D=11.5$ ) with dense sand ( $\gamma = 17.7 \text{ kN/m}^3$ ). As shown in this figure there is no significant reduction in lateral force after the peak even with NorSand model. This is the effect of depth of embedment on lateral force. It is to be noted here that if the soil is very dense the reduction of lateral force after the peak can be simulated using NorSand model. Such

behaviour cannot be simulated if the built-in Mohr-Coulomb model with constant dilation angle is used.

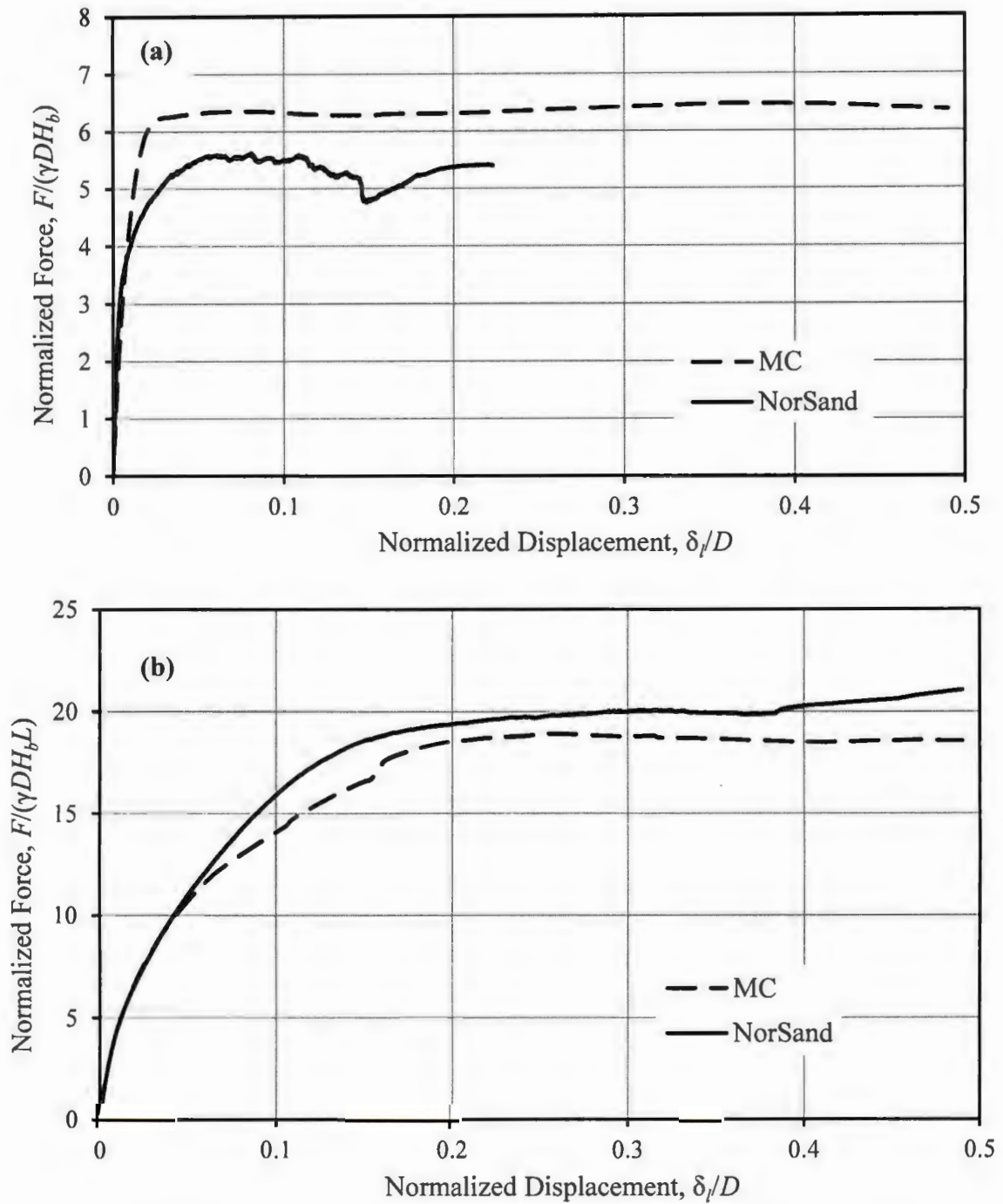


Figure 5-11: Normalized force-displacement curve with (a)  $H_v/D = 2$  (b)  $H_v/D = 11.5$

### 5.7 Pure Vertical (Upward) Loading

The effects of advanced soil constitutive model on soil/pipeline interaction analyses for pure upward loading are also checked in this study. The same finite element models presented above are used. In this case, instead of lateral displacement, vertical (upward) displacement is applied in the loading stage. Again two soil constitutive models, Mohr-Coulomb and NorSand, are used and analyses are performed for dense sand.

Figure 5-12 shows the comparison between the numerical results with Mohr-Coulomb and NorSand soil constitutive models for shallow burial conditions ( $H_c/D=4$ ). As shown in this figure that both models shows a post-peak reduction in vertical force. However, the reduction is higher with NorSand model. Note that in Mohr-Coulomb model a constant dilation angle is used. One of the reasons of post-peak reduction of vertical force is that after some vertical movement of the pipe the failure plane reaches to the ground surface as shown in Figure 5-13.

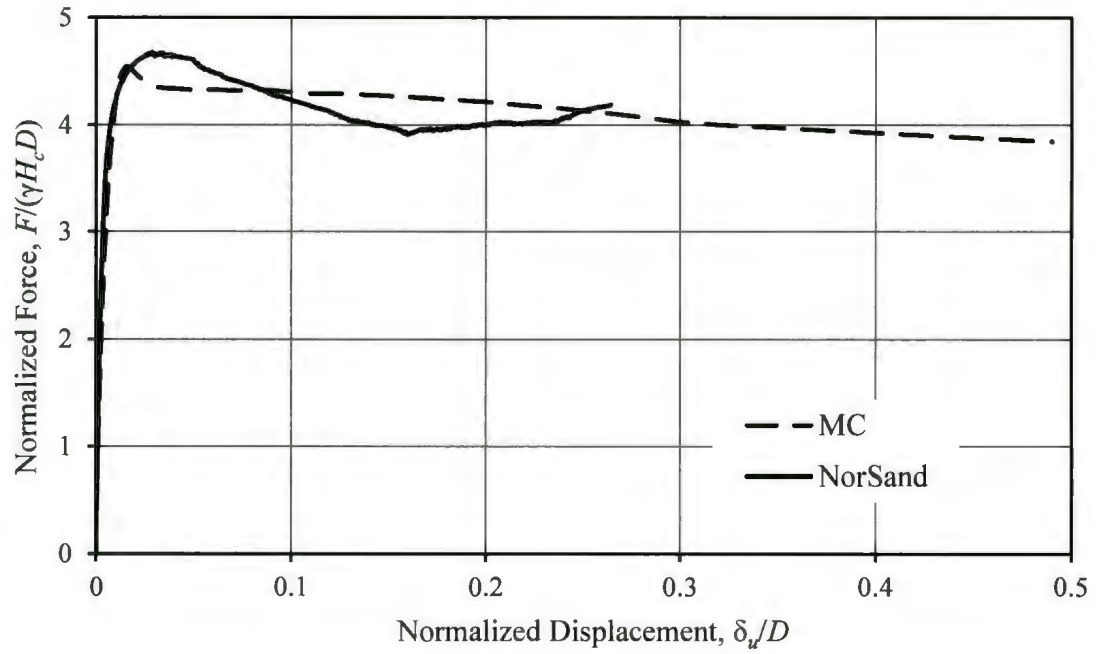


Figure 5-12: Vertical Force vs. vertical Displacement curve for  $H_c/D=4$

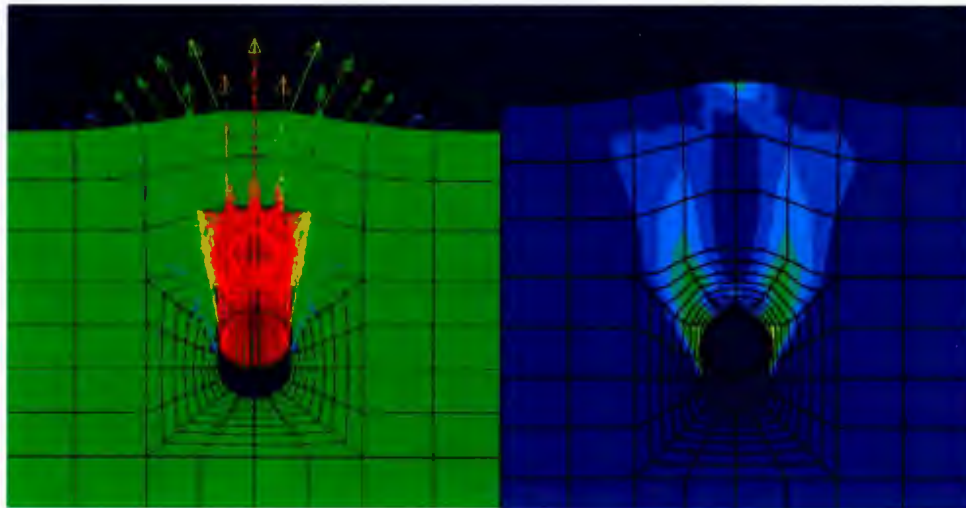


Figure 5-13: Displacement and plastic strain plot for pure upward loading in dense sand

As the pipe moves up, the length of the failure plane is reduced and therefore vertical force is reduced. On the other hand, in NorSand model, in addition to reduction in the

length of the failure plane as in Mohr-Coulomb model, the dilation angle is also reduced with shear strain. Therefore, the post-peak reduction is higher in NorSand model.

The vertical force versus vertical displacement plots for deep burial conditions ( $H_c/D=13$ ) are shown Figure 5-14 with two soil constitutive models. As shown in this figure some reduction in vertical force is predicted using NorSand model while it is almost constant after the peak when Mohr-Coulomb model is used. This is again because in NorSand model, the dilation angle of dense sand is reduced with the increases in shear strain.

In both shallow and deep burial conditions, NorSand predicts slightly higher peak vertical force. It is also to be noted here that the predicted vertical force with the vertical displacement is very similar to the measured values in model test as shown in Chapter 4 (Figures 4-7 and 4-8)

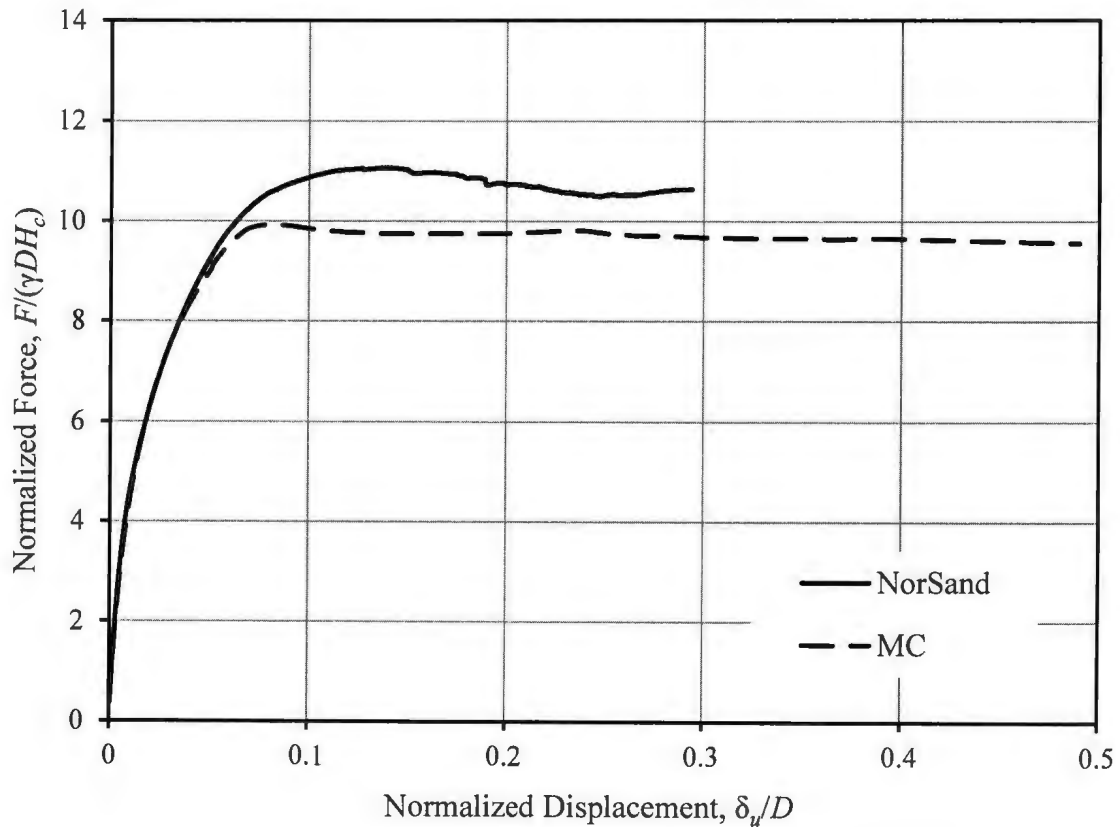


Figure 5-14: Vertical force vs. vertical displacement curve for  $H_v/D=13$

### 5.8 Oblique Loading

In the simplified methods currently used in engineering practice, the modeling of soil/pipeline interaction is performed using three independent springs in three orthogonal directions. However, in reality, it is very rare to have pure lateral or pure vertical movement of soil relative to the pipe. In most cases, the soil movement perpendicular to a pipeline has both horizontal and vertical components, i.e., the loading on the pipe from the movement of soil is in oblique direction. In the following sections finite element modeling of soil/pipeline interaction events in dense sand for lateral-vertical (upward)

oblique loading with an advanced soil constitutive model, NorSand is presented. It is to be noted here that there are some studies on lateral-vertical oblique soil/pipeline interactions for clay available in the literature (e.g. Daiyan et al., 2009; Guo 2005). Cathie et al., 2005 also provided an overview of the oblique loading and soil-pipeline interaction. However, the research on oblique loading in sand is very limited (e.g. Nyman, 1984; Daiyan *et al.*, 2011). There is no study on lateral-vertical oblique soil/pipeline interactions in sand with an advanced soil constitutive model as presented in the following sections.

In previous sections, the finite element results for pure lateral and pure vertical (upward) loading with two constitutive models have been compared. In this section, the response under oblique loading is investigated with NorSand soil constitutive model.

Two-dimensional finite element analyses have been performed for a pipeline embedded at  $H_b/D=11.5$  in dense sand ( $\gamma = 17.7 \text{ kN/m}^3$ ). The parameters and the geometry of the model kept exactly same as previous analyses. Similar to previous analyses, after the geostatic step, the pipe has been moved at an oblique angle using displacement boundary condition. The definition of oblique angle for 2-D analyses is shown in Figure 5-15 where  $\alpha$  is equal to  $90^\circ$  for pure horizontal and  $0^\circ$  for pure upward movement.

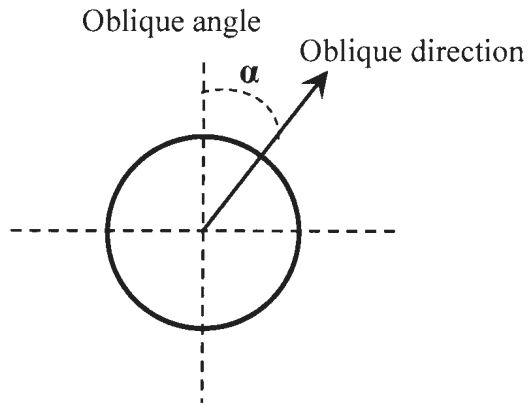


**Figure 5-15: Definition of oblique angle in 2-D oblique loading**

In finite element analyses, the components of nodal force on the pipe acting in the horizontal and vertical directions are printed in ABAQUS data file for all the nodes on the pipe for each increment. Summing them up, the horizontal ( $F_{oh}$ ) and vertical forces ( $F_{ov}$ ) are obtained. The components of displacement in the horizontal ( $\delta_{oh}=\delta_o\cos\alpha$ ) and vertical ( $\delta_{ov}=\delta_o\sin\alpha$ ) are also obtained, where  $\delta_o$  is the oblique displacement. The numerical simulations are done for five oblique angles  $15^\circ$ ,  $30^\circ$ ,  $45^\circ$ ,  $60^\circ$  and  $75^\circ$ , in addition to lateral ( $90^\circ$ ) and vertical loading ( $0^\circ$ ).

### **5.8.1 Force-Displacement Curves**

In Figures 5-16 and 5-17, the normalized force-displacement curves are shown for horizontal and vertical components of oblique loading, respectively. The vertical axis of Figure 5-16 represents the lateral force imposed on the pipe by the lateral component of oblique displacement, which is normalized as  $F_{oh}/(\gamma DH_b)$  in which  $F_{oh}$  is the horizontal

component of force,  $\gamma$  is the dry unit weight of the sand,  $H_b$  is the depth from the top of the soil to the base of the pipe, and  $D$  is the external diameter of the pipe. The horizontal axis is the dimensionless pipe displacement expressed as  $\delta_{oh}/D$ , in which  $\delta_{oh}$  is the horizontal pipe displacement in oblique loading. Similarly, the vertical axis of Figure 5-17 shows the vertical component of force. In this figure,  $H_c$  is the depth from the ground surface to the center of the pipe. The other parameters are same as horizontal components. The horizontal axis of this figure shows the dimensionless pipe displacement expressed  $\delta_{ov}/D$  in the vertical direction.

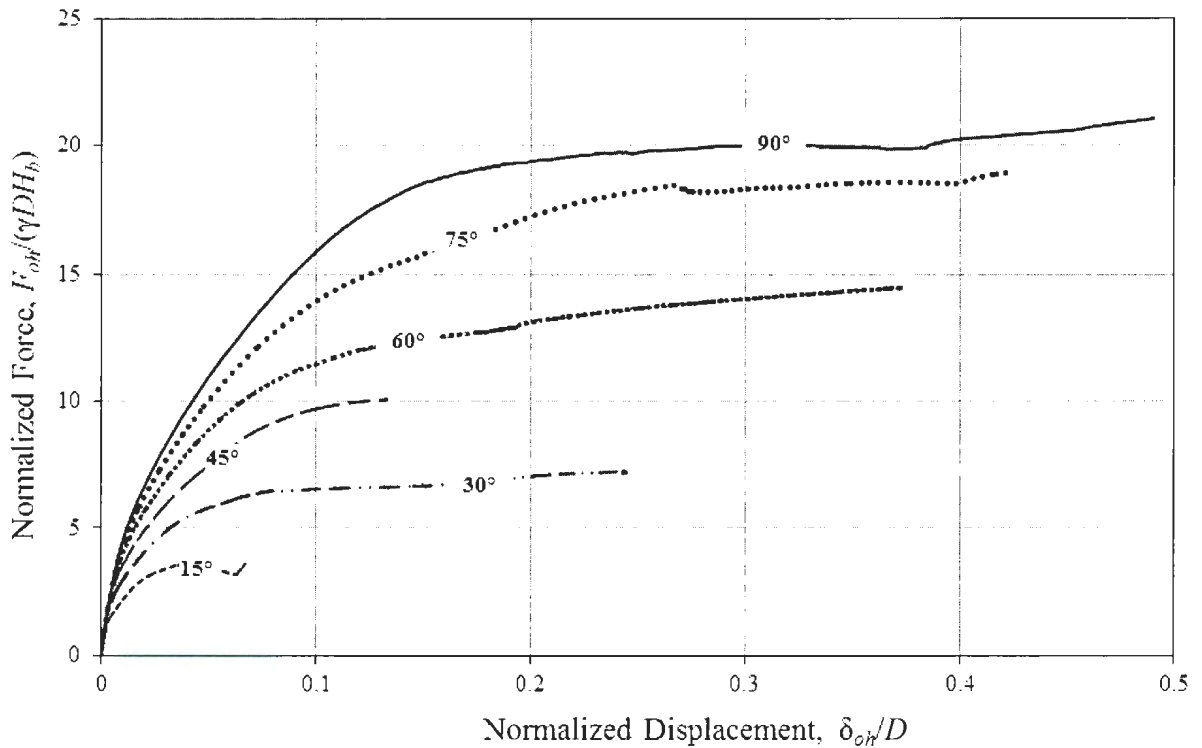


Figure 5-16: Force-displacement curves for horizontal component in oblique loading

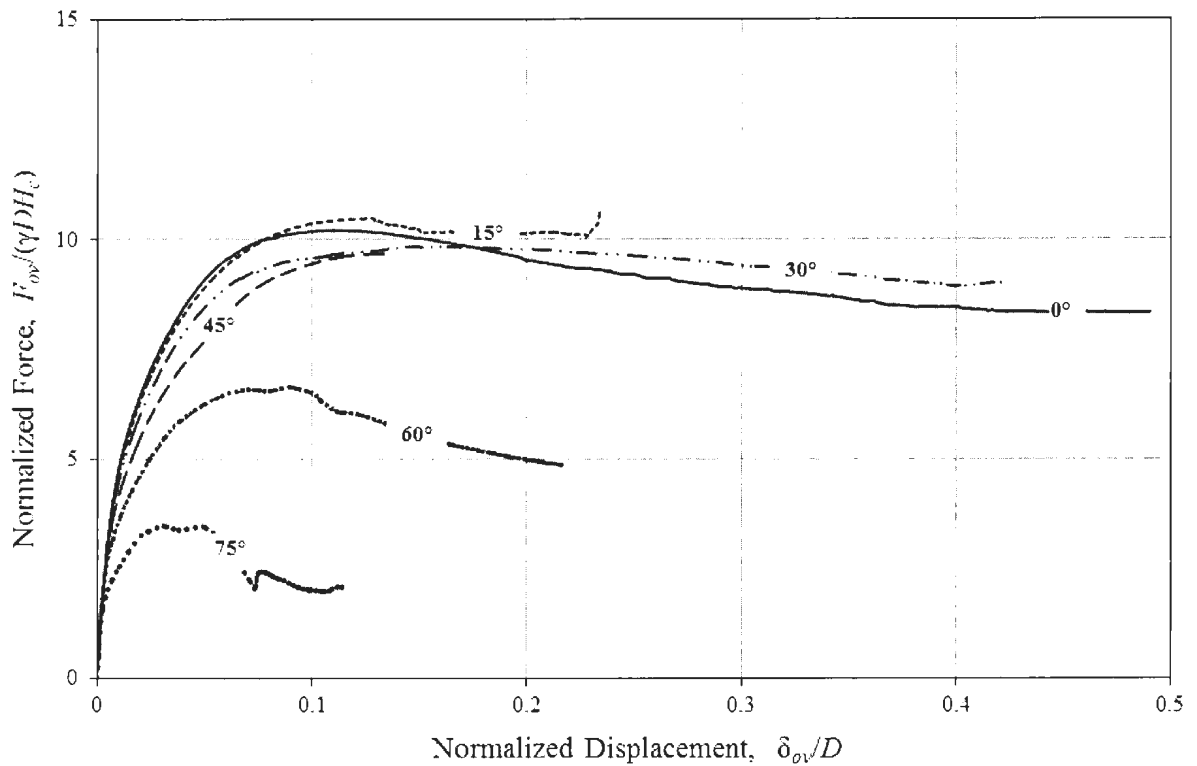


Figure 5-17: Force-displacement curves for vertical component in oblique loading

Figure 5-16 shows that for oblique loading angle greater than  $30^\circ$  the horizontal component of force ( $F_{oh}$ ) gradually increases with horizontal displacement ( $\delta_{oh}$ ). The rate of increase of force is very small at large displacement. For a very small oblique angle (e.g.  $\alpha=15^\circ$ ) the horizontal component of force reached to the peak and then decreased with further displacement.

The pattern of the vertical component of force displacement curve shown Figure 5-17 is different from the horizontal component shown in Figure 5-16. The vertical component of force reached to the peak and then decreased with increase in vertical displacement. The vertical displacement required to reach to the peak is relatively small for higher oblique

angles. For example, the peak vertical force is obtained at  $\delta_{ov}/D \approx 0.05$  for oblique angle of  $75^\circ$ , while the peak is at  $\delta_{ov}/D \approx 0.1$  for pure vertical loading ( $\alpha=0^\circ$ ).

Guo (2005) conducted finite element analyses of buried pipelines in clay subjected to combined horizontal and vertical (upward) movements in the oblique direction in undrained condition. The calculated force is normalized by undrained shear strength of clay ( $c_u$ ) and the diameter of the pipe ( $D$ ). Figure 5-18(a) shows that the force on the pipe gradually increases with displacement and reaches to the peak and remains almost constant at large displacement. Figures 5-18(b) and (c) show the variation of normalized horizontal  $N_h (=F_{oh}/c_u D)$  and vertical  $N_v (=F_{ov}/c_u D)$  force components with horizontal ( $u$ ) and vertical ( $v$ ) displacement components, respectively. A comparison between Fig. 5-17 and Fig. 5-18(c) show that while there is a significant softening response in the vertical force component in drained analysis in sand (Figure 5-17) it is less in undrained response for the pipelines buried in clay, at least for the cases analyzed.

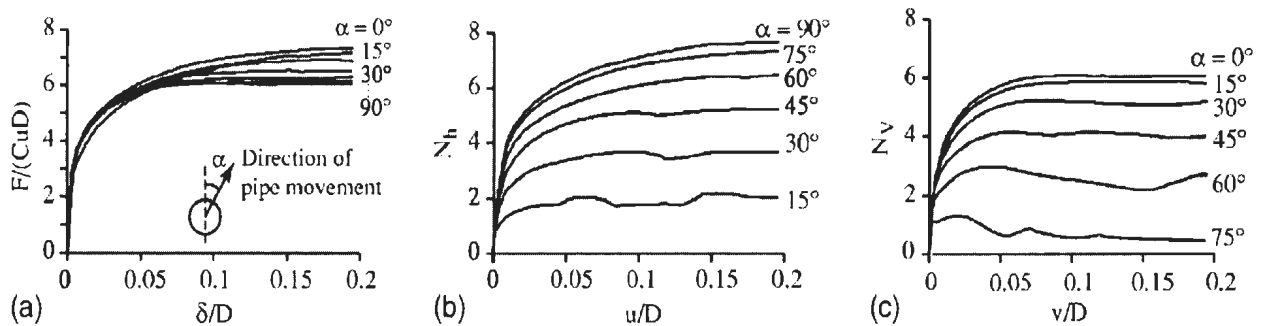


Figure 5-18: Force–displacement responses for oblique loading for  $H/D=3.03$ : (a) total, (b) horizontal, and (c) vertical forces (Guo, 2005)

Daiyan et al. (2011) conducted a series of finite element analyses to understand soil/pipeline interaction behaviour for combined horizontal and vertical (upward) movements of the pipeline buried in dense sand. The built-in Mohr-Coulomb soil constitutive model available in ABAQUS FE software is used with varying dilation angle as a function of plastic strain. Comparing the Figures 5-16, 5-17 and 5-19, it can be shown that there are some similarities between the force displacement curves. However, more analysis is required for direct comparison between these results and to show the effects of soil constitutive model on the response of pipeline subjected to oblique loading.

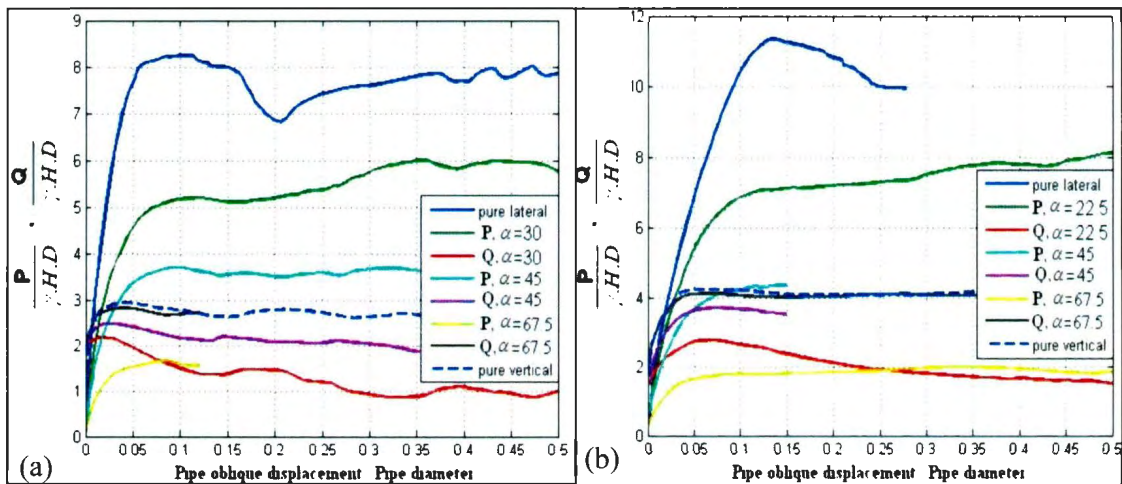


Fig. 5-19: Force–displacement responses for oblique loading: (a)  $H/D = 2$  and (b)  $H/D = 4$  (P: lateral component, Q: vertical component of load) (Daiyan, 2011)

### 5.8.2 Peak Forces Caused by Oblique Soil Movement

The peak force and the displacement at the peak are the two important parameters required in the design of buried pipelines. In this section the peak force exerted on the pipe for different oblique angles is investigated.

The peaks of the horizontal and vertical components of the force are obtained from the load displacement curves shown in Figures 5-16 and 5-17 respectively. Five commonly used procedures for estimating the peak force from a force-displacement curve are: (i) the point of intersection of the two straight line portions of the force-displacement curve (Wantland et al., 1982), (ii) the point at which the force displacement curve becomes flat, which is very similar to Terzaghi's bearing capacity failure, (3) the point of intersection of the tangent on the later part of the curve with vertical axis (Neely et al. 1973), (iv) the point at which the stiffness is one fourth of the initial elastic stiffness (Rowe and Davis 1982), and (v) the maximum force. Pike and Kenny (2011) showed that there are some differences in estimated peak force based on these methods. In this study, the peak force is obtained from the maximum value. When the maximum force is not evident in a force-displacement curve as shown in Figure 5-16 for large oblique angles, where the lateral component of force is continuously increasing, the force at  $\delta_{oh}=0.025(H+D/2)$  (ALA, 2002) is considered as the peak force.

The normalized peak force components in the horizontal and vertical directions are plotted against oblique angle in Figure 5-20. As shown in this figure that the peak of the horizontal component gradually increases with increase in oblique angle. On the other hand the peak vertical component remains almost constant with oblique angle until  $45^\circ$  and then decreases gradually.

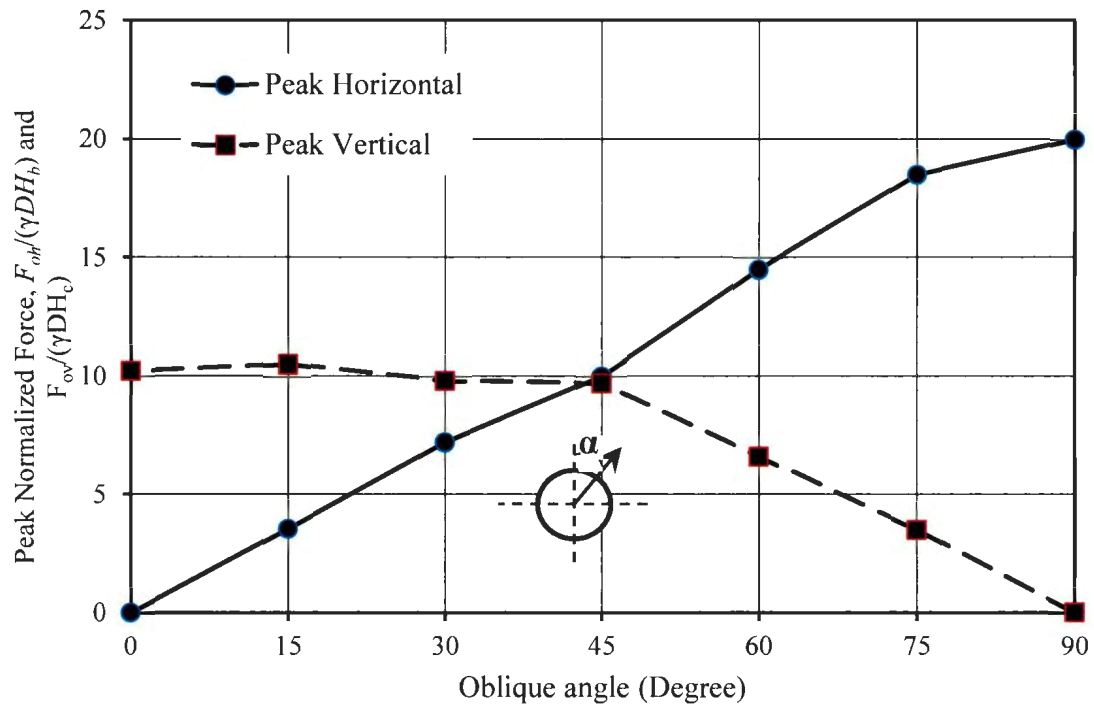


Figure 5-20: Variation of horizontal and vertical interaction factors with oblique angles

Daiyan et al. (2009) performed series of finite element analyses for pipelines buried in clay. The soil has been modeled using undrained shear strength of clay. Based on their finite element analyses and Response Surface Methodology (RSM), they proposed two equations for lateral and vertical interaction which is shown in Figure 5-21 as a function of oblique angle.

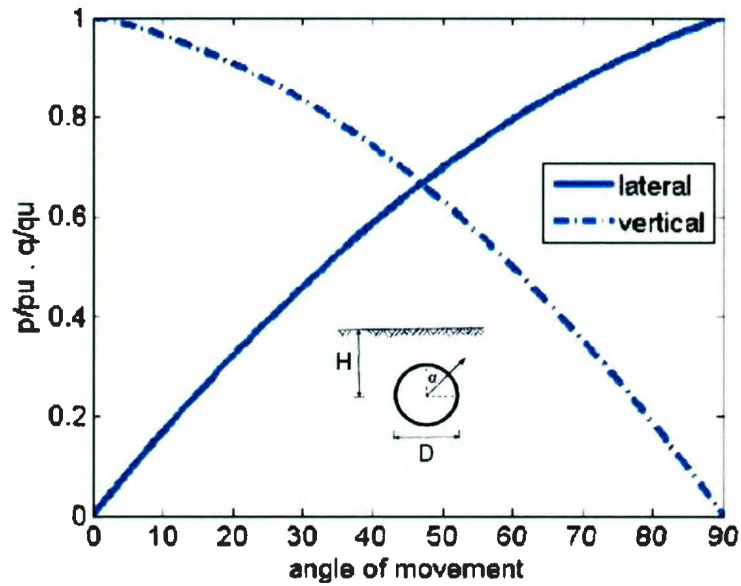


Figure 5-21: Normalized lateral and vertical components of peak oblique load on the pipeline in clay (Daiyan et. al, 2009)

A comparison between Figures 5-20 and 5-21 shows that the effect of oblique angle on vertical component of peak force in dense sand considered in the present study is different from the clay.

### 5.8.3 Failure envelopes under oblique loading

The failure envelopes under oblique loading can be developed by plotting the horizontal and vertical components of force at ultimate (peak) states, which is shown in Figure 5-22 for the present study. Another way to present these results is to plot the lateral and vertical components of force normalized by the ultimate forces corresponding to purely horizontal and vertical (upward) pipe movements, respectively. Figure 5-23 shows this plot.

The numerical results obtained from the present finite element analyses are also compared with previous studies. Using a limit equilibrium approach, Nyman (1984) proposed an equation for calculating oblique load capacity of a buried pipeline. He developed the equation based on Meyerhof's method for analysis of inclined anchor plates (Figure 5-24 a). The analogy between buried pipe and inclined anchor is shown in Fig. 5-24(b). He assumed that the resultant soil forces are collinear with the direction of pipe movement.

The mathematical relationship proposed by Nyman (1984) is:

$$p_{u\bar{\alpha}} = (1 - \beta)q_{u0} + \beta p_{u0} \quad (5.7)$$

Where  $p_{u0}$  is the ultimate lateral load for an oblique interaction angle,  $\alpha$  measured from a vertical axis,  $q_{u0}$  and  $p_{u0}$  are respective the ultimate vertical and lateral loads per unit length of pipe which are denoted as  $F_{oh}$  and  $F_{ov}$ , respectively, in this study and  $\beta$  is an inclination factor defined as:

$$\beta = \frac{0.25\alpha}{90-0.75\alpha} \quad (5.8)$$

Here  $\alpha$  is in degree.

Based on Nyman (1984), Guo (2005) proposed the following two modified form of equations for estimating oblique load capacity.

$$\left(\frac{p}{p_{u0}}\right)^2 + \frac{q}{q_{u0}} = 1 \quad (5.9)$$

$$\left(\frac{p}{p_{u0}}\right)^2 + \left(\frac{q}{q_{u0}}\right)^2 = 1 \quad (5.10)$$

The first one is very similar to Nyman (1984). Both of these equations are plotted in Figure 5-23. Guo also claimed that all the experimental and numerical data on clay he compiled fall within these two curves. For comparison the numerical results obtained by Daiyan et al. (2011) are also plotted in this figure.

While the numerical results with NorSand UMAT show the similar trend, some of the data are outside the range proposed by Guo (2005). However, more analyses are required for different densities and burial depths to confirm this trend.

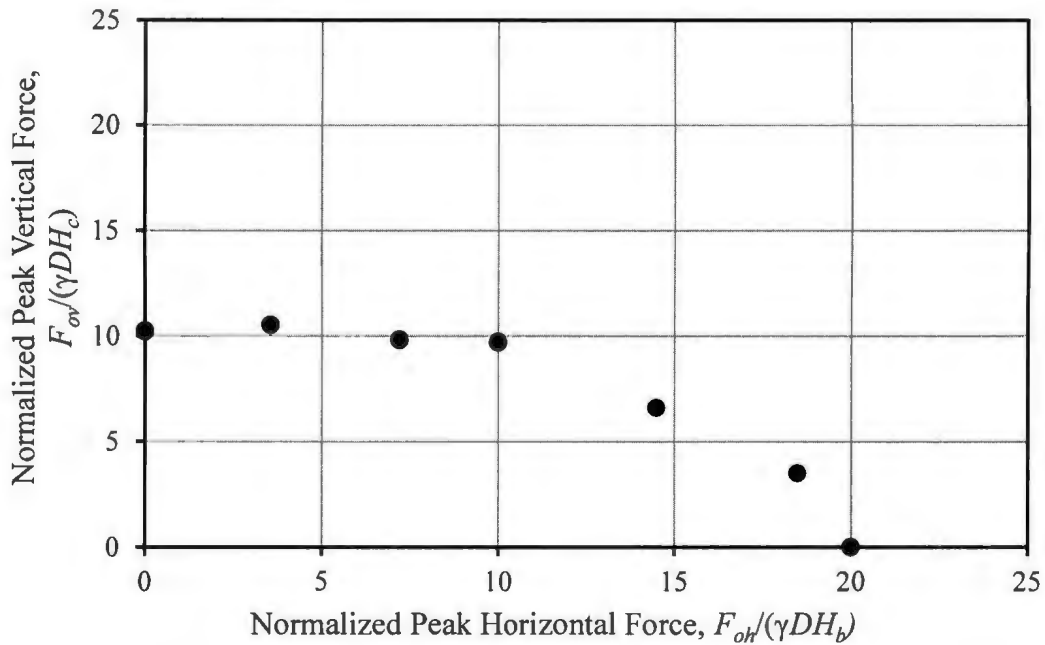


Figure 5-22: Lateral-vertical bearing factor interaction diagram as a function of the oblique angle

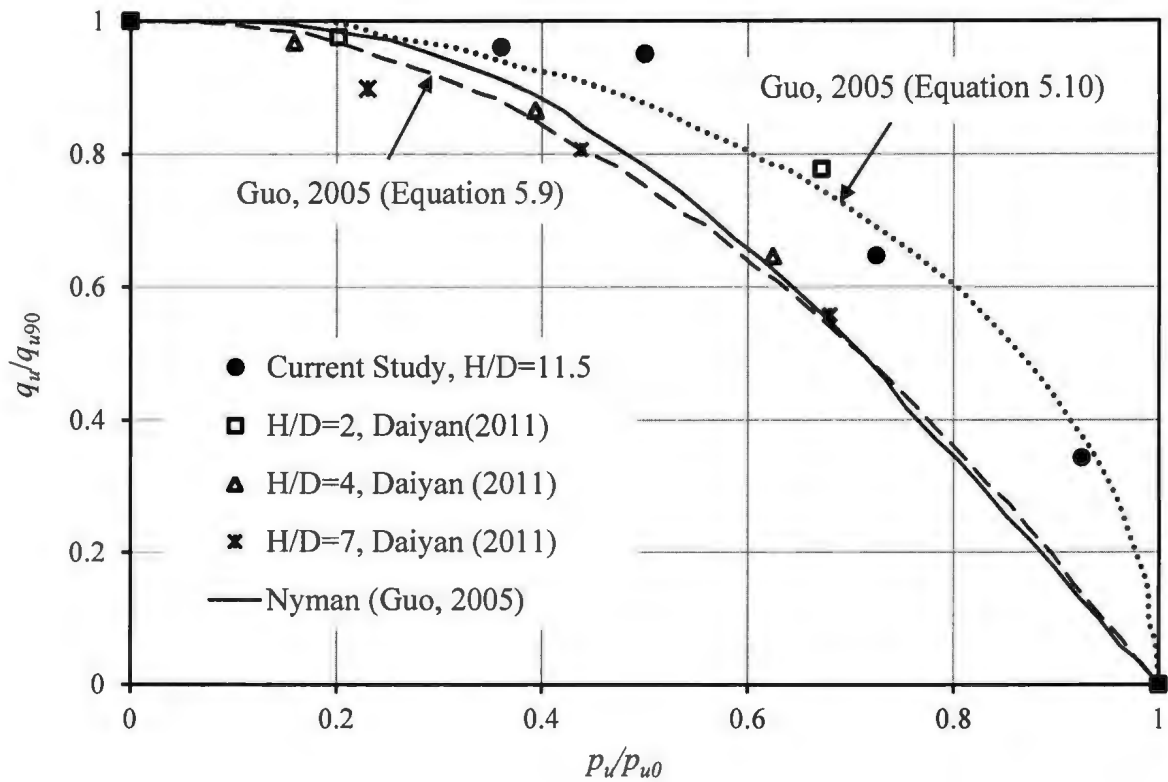


Figure 5-23: Comparison of different representations of failure envelope

The theoretical analyses (Nyman, 1984 and Meyerhof and Hanna, 1978) assume linear failure surfaces whereas the present research show that the failure zone to be more complex. The shear strain in the soil around the pipe at a post-peak displacement is shown in Figure 5-25 for different oblique angles. As the pipe is at deep burial condition, the local failure mechanism of soil governs as shown by the shear strain contour. These figures also show that there is a transition from a surface heave type failure mechanism to lateral bearing failure with increasing oblique angle,  $\alpha$ .

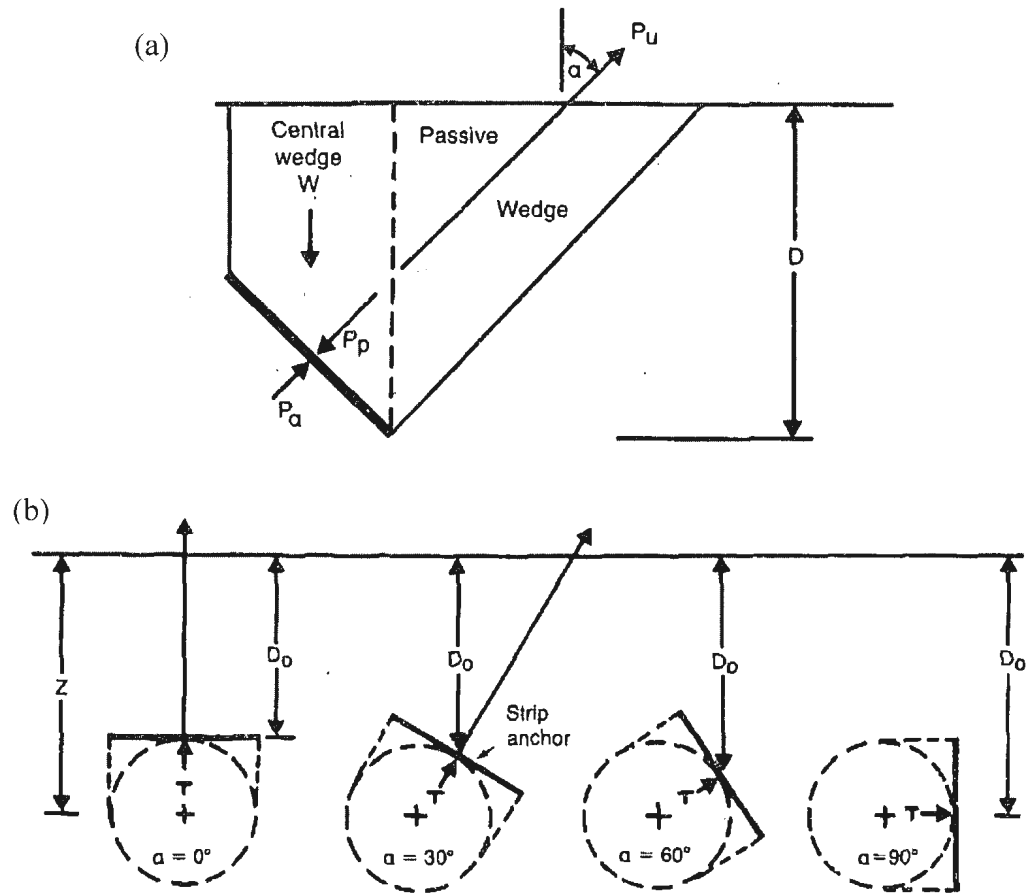


Figure 5-24: Oblique load capacity (a) Meyerhof model for inclined anchor, (b) anchor-buried pipe analogy (Nyman 1984)

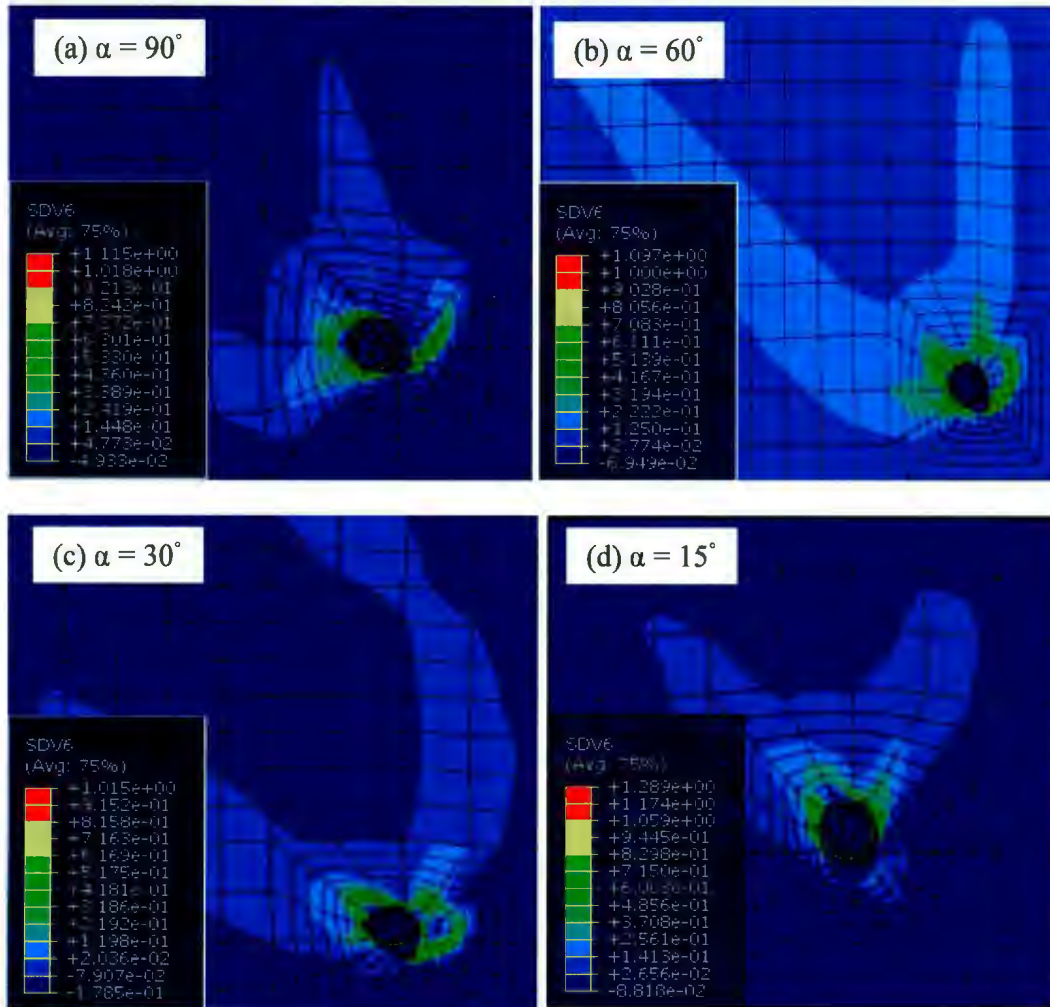


Figure 5-25: Typical plastic shear strain in oblique angle

## Chapter 6

### CONCLUSIONS AND FUTURE RECOMMENDATIONS

#### 6.1 Conclusions

In this thesis, finite element analyses of complex soil/pipeline interaction of buried pipelines are presented. The main focus of this study is to show the use of an advanced soil constitutive model to simulate the response of buried pipelines subjected to relative displacement between pipe and soil. Two soil constitutive models considered in this study are Mohr-Coulomb model and NorSand model. The Mohr-Coulomb model is a simple linear elastic-perfectly plastic model for geomaterials, which is a built-in model in ABAQUS finite element software, and is widely used in modeling of soil to simulate the response of buried structures under monotonic loading. However, this built-in model has an unrealistic constant dilation angle and is incapable of simulating the strain softening behaviour as observed in dense sands. The NorSand model is a generalised Cambridge-Type model for sand developed from the concept of critical state soil mechanics. The NorSand model adopts associated flow rule yet predicts realistic dilation of sand. However, this model is not available in ABAQUS FE software. In this study, FE element analyses have been performed using a user defined subroutine UMAT where the NorSand model is implemented. Analyses are performed mainly in two-dimensional plane strain condition and some in three-dimensional conditions for pure lateral, vertical (upward), and oblique pipe movements.

The first series of analyses presented in Chapter 4 is with the built-in Mohr-Coulomb model in ABAQUS. The auto generated mesh sometimes gives numerical difficulties, which could be overcome by using structured mesh that is also computationally efficient. The Mohr-Coulomb model can simulate some of the model test results if the geotechnical parameters are properly refined. However, the Mohr-Coulomb model cannot simulate some experimental observations, such as post-peak softening and some force-displacement response.

In Chapter 5 the implementation of NorSand model is presented. The performance of the simulation is improved when the control parameters in ABAQUS are properly adjusted. A series of triaxial compression tests are simulated. The NorSand UMAT can simulate triaxial tests for a wide range of initial conditions. The dilation behaviour observed in laboratory tests is simulated correctly using the UMAT for very loose to very dense sands and also at overconsolidated states.

The force-displacement behaviour for pure lateral and pure vertical (upward) loading obtained with the NorSand UMAT shows a very similar trend as observed in model experiments with post-peak softening behaviour.

The response under lateral-vertical (upward) oblique loading is successfully simulated using the NorSand UMAT for a deep burial pipeline in dense sand. For this condition, the lateral component of force gradually increases with lateral displacement without showing any strain softening response, except for an oblique angle very close to the vertical.

However, the vertical component of force with vertical displacement shows a softening behaviour for all oblique angles with a clear peak. The variation of peak force with oblique angle is different from the prediction reported by previous authors for clay and also for sands using built-in Mohr-Coulomb model. The vertical component of force increases rapidly with oblique angle from horizontal. The peak force components obtained with NorSand UMAT are compared with failure envelopes developed by previous authors. The failure envelope obtained from this study is considerably far from Nyman's (1984) analytical solution for sand.

## **6.2 Recommendations for Future Work**

The developed UMAT for NorSand soil constitutive model can successfully simulate the response of sand under monotonic loading and many important features of soil/pipeline interaction behaviour of buried pipelines in sand. The author spent a significant amount of his time for M.Eng. study to understand the constitutive models of sand especially NorSand and its implementation in ABAQUS. Therefore, a comprehensive parametric study for various conditions could not be performed in this study. The following are the recommendations for future studies.

- The soil/pipeline interaction analyses using NorSand UMAT are performed mainly for dense sand in deep burial condition. Further analyses are required for different soil density and burial conditions.

- Analyses for oblique loading are performed only for lateral vertical condition. The axial lateral and axial vertical oblique loading are equally important and should be analyzed.
- More comparison between NorSand UMAT and Mohr-Coulomb model for different pipe/soil interaction events is required. Simplified methods or some design guidelines for buried pipelines in sand would be useful.
- The developed UMAT could be also used for other buried structures in sand such as pile foundations.
- The implemented NorSand model in ABAQUS in this study was originally developed by Jefferies in 1993. But subsequent development has been done in the recent versions of NorSand. So the recent version of the NorSand should be implemented in ABAQUS.

## Bibliography

American Lifeline Alliance (ALA) (2002). Guidelines for the design of buried pipe. ([www.americanlifelinealliance.org](http://www.americanlifelinealliance.org)).

Anderson, C., Wijewickreme, D., Ventura, C., and Mitchell, A. (2004). "Full-Scale Laboratory Testing of Soil-Pipe Interaction in Branched Polyethylene Pipelines.", *Experimental Techniques*, Vol. 29, No. 2, pp.33-37.

Audibert, J. M. E., and Nyman, K. J. (1977). "Soil restraint against horizontal motion of pipes.", *J. Geotech. Eng. Div., Am. Soc. Civ. Eng.*, 103(10), 1119–1142.

Banerjee, P. K., Stipo, A. S., and Yousif, N. B. (1985). "A theoretical and experimental investigation of the behaviour of anisotropically consolidated clay." *Developments in soil mechanics and foundation engineering-2*, Elsevier Science, New York.

Been, K., Jefferies, M., and Hachey, J., (1991), "Critical state of sands", *Geotechnique*, Vol. 41, No. 3, pp. 365-38

Bolton, M. D. (1986). "The strength and dilatancy of sands.", *Geotechnique*, 36(1), 65–78.

Cathie, D.N., Jaeck, C., Ballard, J-C. and Wintgens, J-F., (2005), "Pipeline Geotechnics- State of the Art", *Int. Symp. Frontiers in Offshore Geotechnics*, Perth, Australia.

C-CORE report (2003), Extended Model for Pipe Soil interaction. Reports for Pipelines Research Council International, Inc. Contract Report Series 113, Contract PR-271-0184.

Cocchetti, G., Prisco, C., Galli, A. (2009b). "Soil-pipeline interaction along unstable slopes: a coupled three-dimensional approach. Part 2: Numerical analyses". Canadian Geotechnical Journal, 46: 1305-1321.

Cocchetti, G., Prisco, C., Galli, A. and Nova, R. (2009a). "Soil-pipeline interaction along unstable slopes: a coupled three-dimensional approach. Part 1: Theoretical formulation." Canadian Geotechnical Journal, 46: 1289-1304

Conte, J.P., Elgamal, A., Yang, Z., Zhang, Y., Acero, G., and Seible, F. (2002). "Nonlinear Seismic Analysis of a Bridge Ground System.", Proceedings, 15th ASCE Engineering Mechanics Conference, Columbia University, New York, NY.

Daiyan, N., Kenny, S., Phillips, R. and Popescu, R. (2009). "Parametric Study of Lateral-Vertical Pipeline/Soil Interaction in Clay.", Proceedings, 1<sup>st</sup> International/1<sup>st</sup> Engineering Mechanics and Materials Speciality Conference, St. John's, Newfoundland and Labrador, Canada.

Daiyan, N., Kenny, S., Phillips, R. and Popescu, R. (2010a). "Investigation of axial/lateral interaction of pipes in dense sand.", ICPMG 2010, Int. Conf. on Physical Modeling in Geotechnics, Zurich, Switzerland.

Daiyan, N., Kenny, S., Phillips, R. and Popescu, R. (2010b). "Numerical investigation of oblique pipeline/soil interaction in sand.", IPC 2010, Int. Pipeline Conf., Calgary, Canada.

Daiyan, N., Kenny, S., Phillips, R. and Popescu, R. (2011). "Numerical investigation of axial-vertical and lateral-vertical pipeline/soil interaction in sand.", 2011 Pan-Am CGS Geotechnical Conference, Canada.

Das, B.M. (2008). "Advanced Soil Mechanics", Taylor & Francis, New York, USA.

Dasari, G.R. and Soga, K. "A Guide Book for Soil Models and Soil-Pipe Analysis Using Abaqus", Report submitted to Tokyo Gas Ltd., Tokyo, Japan.

Eidinger, J., M. O'Rourke, and J. Bachhuber, (2002). "Performance of Pipelines at Fault Crossings", Proceedings, 7th U.S. National Conference on Earthquake Engineering, EERI, Boston, MA, July.

Eskandari F., Phillips R, & Hawlader B. (2011). "Ice Gouging Analysis Using NorSand Critical State Soil Model.", Proceedings, 14th Pan-American Conference on Soil Mechanics and Geotechnical Engineering, Toronto, Canada

Giovanazi, S., and Cubrinovski, M. (2007). "Liquefaction Hazards for Seismic Risk Analysis.", New Zealand Society of Earthquake Engineering 2007 Conference (NZSEE 2007). Proceedings. 2007 Annual NZSEE Technical Conference, Paper 06. Palmerston North, New Zealand, Apr 2007.

Guo, P. (2005). "Numerical modeling of pipe-soil interaction under oblique loading", *Journal of Geotechnical and Geoenvironmental Engineering*, ASCE, 131(2), pp. 260-268.

Ha, D., Abdoun, T.H., and O'Rourke, M.J. (2008a). "Soil-Pipeline Interaction Behavior under Strike-Slip Faulting.", *Proceedings, Geotechnical Earthquake Engineering and Soil Dynamics IV*, ASCE, Sacramento, CA, May 2008.

Ha, D., Abdoun, T.H., O'Rourke, M.J., Symans, M.D., O'Rourke, T.D., Palmer M.C., and Stewart H.E. (2008b). "Centrifuge Modeling of Earthquake Effects on Buried High-Density Polyethylene (HDPE) Pipelines Crossing Fault Zones.", *Journal of Geotechnical and Geoenvironmental Engineering*, Vol. 134, No. 10, pp. 1501-1515.

Hamada, M. and O'Rourke, T.D. Eds. (1992). "Case Studies of Liquefaction and Lifeline Performance During Past Earthquakes." NCEER-92-0001, Vol.1, National Center for Earthquake Engineering Research, Buffalo, NY, April

Hansen, J. B. (1961). "The ultimate resistance of rigid piles against transversal forces.", *Bulletin No. 12*, Danish Geotechnical Institute, Copenhagen, Denmark, 5-9.

Hardin, B.O. and Black, W.L. [1966]. "Sand stiffness under various triaxial stresses", *Journal of the Soil Mechanics and Foundations Division*, ASCE, Vol. 92, No. SM2, pp. 27-42.

Honegger, D. and D.J. Nyman, (2004). "Guidelines for the Seismic Design and Assessment of Natural Gas and Liquid Hydrocarbon Pipelines," Pipeline Research Council International, Catalog No. L51927, October.

Houlsby, G.T. (1991) "How the Dilatancy of Soils Affects Their Behaviour", Invited Theme Lecture, Proceedings of the Tenth European Conference on Soil Mechanics and Foundation Engineering, Florence, May 27-30, Vol. 4, pp 1189-1202, ISBN 90-5410-005-2

Hsu, T.W., Chen, Y.J. and Hung, W.Y. (2006). "Soil Restraint to Oblique Movement of Buried Pipes in Dense Sand.", Journal of transportation engineering, ASCE, 132(2): 175-181.

Janbu, N. (1963). "Soil compressibility as determined by oedometer and triaxial tests." Proc. Euro. Conf Oil Soil Mech. 111/1.1 FUUIld. Ic·llgrg., German Society for Soil Mechanics and Foundation Engineering, Wissbaden, Germany, Vol I, 1925.

Jefferies, M. and Been, K (2006). "Soil liquefaction: A critical state approach.", Taylor & Francis, London; New York.

Jefferies, M., 1993, 'NorSand; a simple critical state model for sand' Géotechnique, Vol. 43, No. "pp. 91-103.

Jefferies, M., 1997, "Plastic work and isotropic softening in unloading" Geotechnique, Vol. 47, No. 5, pp. 1037-1042.

Jefferies, M., and Been, K., 2000, "Implications for critical state theory from isotropic compression of sand" *Geotechnique*, Vol. 50, No. 4, pp. 419-429.

Jefferies, M., and Shuttle, D., 2002, "Dilatancy in general Cambridge-type models" *Géotechnique*, Vol. 52, No. 9, pp. 625-638.

Jefferies, M., and Shuttle, D., 2005, "NorSand: Features, calibration and use", Geotechnical special publication No. 128, American Society of Civil Engineers, United States, pp. 204-236.

Kennedy, R.P., Chow, A.W., and Williamson, R. A. (1977). "Fault Movement Effects on Buried Oil Pipeline.", *Journal of the Transportation Engineering Division, ASCE*, Vol. 103, No. TE5, Sept., pp. 617-633.

Lade, P. V. and Duncan, J. M. (1975), "Elasto-plastic stress-strain theory for cohesionless soil", *J. Geotech. Eng. Div., ASCE*, 1975.

Matsuoka, H. and Nakai, T. (1974), "Stress-deformation and strength characteristics of soil under three different principal stresses", *Proceeding of Japan Society Civil Engineering*, Vol. 232, pp. 59-70.

Meyerhof, G.G., and Hanna, A.M. (1978). "Ultimate bearing capacity of foundation on layered soil under inclined load" *Can. Geotech. J.*, 15(4):565-572.

Mitchell, J.K. (1993). "Fundamentals of soil behavior", John Wiley & Sons.

Neely, W. J., Stuart, J. G., and Graham, J. (1973). "Failure loads of vertical anchor plates in sand." *J. Soil Mech. Found. Div.*, 99(9), 669-685.

Nobahar, A., Kenny, S., and Phillips, R. (2007). "Buried Pipelines Subject to Subgouge Deformations.", *International Journal of Geomechanics*, Vol. 7, No. 3, pp. 206-216.

Nova, R. (1982). "A constitutive model for soil under monotonic and cyclic loading". *Soil mechanics - transient and cyclic loads*. (eds G. N. Pande and O. C. Zienkiewicz), pp. 343-373. Chichester: Wiley.

Nyman, K.J. (1984). "Soil response against oblique motion of pipes". *Journal of Transportation Engineering*, 110(2), pp. 190-202.

O'Rourke T.D., and Liu, X. (1999). "Response of Buried Pipelines Subject to Earthquake Effects.", *Multidisciplinary Center for Earthquake Engineering Research, Monograph Series No. 3*, MECCR, Buffalo, New York.

O'Rourke, M.J., Symans, M.D., Masek, J.P. (2008). "Wave Propagation Effects on Buried Pipe at Treatment Plants.", *Earthquake Spectra*, Vol. 24, No. 3, pp. 725- 749.

O'Rourke, T.D. (1998). "An Overview of Geotechnical and Lifeline Earthquake Engineering.", *Geotechnical Special Publication No. 75*, ASCE, Reston, VA, *Proceedings of Geotechnical Earthquake Engineering and Soil Dynamics Conference*, Seattle, WA, August 1998, Vol. 2, pp. 1392-1426.

O'Rourke, T.D. (2010). "Geohazards and Large, Geographically Distributed Systems.", *Rankine Lecture, Geotechnique*, 60(7), pp. 505-543.

O'Rourke, T.D. and C. Trautmann, (1981). "Earthquake Ground Rupture Effects on Jointed Pipe," Proceedings, Second Specialty Conference of the Technical Council on Lifeline Earthquake Engineering, ASCE, Aug., p. 65-80.

O'Rourke, T.D., and Bonneau, A.L. (2007). "Lifeline Performance Under Extreme Loading During Earthquakes." Earthquake Geotechnical Engineering, Pitilakis, K.D. Eds., Springer, Dordrecht, Netherlands, June, pp. 407-432.

O'Rourke, T.D., Jezerski, J.M., Olson, N.A., Bonneau, A.L., Palmer, M.C., Stewart, H.E., O'Rourke, M.J., and Abdoun, T. (2008). "Geotechnics of Pipeline System Response to Earthquakes.," Proceedings, eotechnical Earthquake Engineering and Soil Dynamics IV, ASCE, Sacramento, CA, May 2008.

Oliveira, J.R.M.S., Almeida, M.S.S., Almeida, M.C.F., and Borges, R.G. (2010). "Physical Modeling of Lateral Clay-Pipe Interaction.," Journal of Geotechnical and Geoenvironmental Engineering, Vol. 136, No. 7, pp. 950-956.

Olson, N.A. (2009). "Soil Performance for Large Scale Soil-Pipeline Tests." Ph.D. Thesis, Cornell University, Ithaca, New York.

Ovesen, N. K. (1964). "Anchor slabs, calculation methods and model tests." Bulletin No. 16, The Danish Geotechnical Institute, Copenhagen, Denmark.

Ovesen, N.K. and Stromann, H. (1972), "Design Methods for Vertical Anchor Slabs in Sand", Proceedings, Speciality Conference on Performance of Earth and earth-Supported Structures. ASCE, Vol. 2.1, pp.1481-1500.

Paulin, M. J. (1998). "An investigation into pipelines subjected to lateral soil loading." PhD thesis, Memorial University of Newfoundland, St. John's, Canada.

Phillips, R., Nobahar, A. and Zhou, J. (2004). "Combined axial and lateral pipe-soil interaction relationships.", Proceedings of IPC2004, International pipeline Conference, Calgary, Canada.

Pike, K. and Kenny, S. (2011). "Advancement of CEL procedures to analyze large deformation pipeline/soil interaction events.", Proceedings of OTC 2011, Offshore Technology Conference, Houston, Texas, USA.

Popescu, R., Phillips, R., Konuk, I., Guo, P. and Nobahar, A. (2002). "Pipe-Soil Interaction: Large Scale Tests and Numerical Modelling.", Proceedings of the International Conference on Physical Modelling in Geotechnics, St. John's, Newfoundland, Canada.

Ranjan, G., and Aurora, V. B. (1980). "Model studies on anchors under horizontal pull in clay." Proc., 3rd Australia, New Zealand Conf. on Geomechanics, Vol. 1, 65-70.

Rizkalla, M., Poorooshab, F., and Clark, J. I. (1992). "Centrifuge modelling of lateral pipeline/soil interaction." Proceedings, 11th Offshore Mechanics and Arctic Engineering Symposium.

Roscoe, K., Schofield, A., and Wroth, C., 1958, "On yielding of soils", Géotechnique, Vol. 8, No. 1, PP. 22-53.

Rowe, P. W., 1962, "The stress-dilatancy relation for static equilibrium of an assembly of particles in contact", Proc. of the Royal Society, A269, 500-527.

Rowe, R. K., and Davis, E. H. (1982). "The behaviour of anchor plates in sand." Geotechnique, 32(1), 25-41.

Scarpelli, G., Sakellariadi, E., and Furlani, G. (1999). "Longitudinal pipeline-soil interaction: results from field full scale and laboratory testing." Panel Contribution in the Proc. of 12th ECSMGE, Balkema, Rotterdam, The Netherlands.

Shuttle, D. and Jefferies, M. (2010). "NorSand: Description, calibration, validation and application" invited lecture note.

Taiebat, M. and Dafalias, Y.F. (2007). "SANISAND: Simple anisotropic sand plasticity model." International Journal for Numerical and Analytical Methods in Geomechanics, 32(8): 915-948.

Tatsuoka, F., and Ishihara, K., 1974, "Yielding of sand in triaxial compression", Soils and Foundations, Vol. 14, pp. 63-76.

Trautmann, C.H., AND O'Rourke, T.D., (1983). "Behavior of Pipe in Dry Sand Under Lateral and Uplift Loading", Geotechnical Engineering Report 83-7, Cornell University, Ithaca, New York

Trautmann, C. H., O'Rourke, T. D., and Kulhawy, F. H. (1985). "Uplift force-displacement response of buried pipe." J. Geotech. Eng., 111(9), 1061-1076.

Trautmann, C.H. (1983). "Behavior of pipe in dry sand under lateral and uplift loading.", PhD thesis, Cornell University, Ithaca, New York

Turner, J. P., and Kulhawy, F. H. (1987). "Experimental analysis of drilled shaft foundations subjected to repeated axial loads under drained conditions.", Rep. to Electric Power Research Institute, Cornell University, Ithaca, N.Y.

Vesic, A. S. (1971). "Breakout resistance of objects embedded in ocean bottom." J. Soil Mech. Found. Div., 97(9), 1183–1205.

Wantland, G.P., O'Neil, M.B., Coelogyne, E.H. and Reese, L.C. (1982). Pipeline lateral stability in soft clay. Journal of petroleum technology, 34(1), 217-220.

Wijewickreme, D., Karimian, H. and Honegger, D. (2009). "Response of buried steel pipelines subjected to relative axial soil movement." Canadian Geotechnical Journal, 46: 735-752.

Winkler, E. (1867). "Die lehre von elastizitat und festigkeit (teaching on elasticity and stiffness)." Prague, Czechoslov.

Wood, D. M., 1990, "Soil behaviour and critical state soil mechanics", Cambridge University Press, Cambridge, UK.

Yeh, C-H., Shih, B-J., Chang, C-H., Walter Chen, W.Y., Liu, G-Y., and Hung H-Y. (2006). "Seismic Damage Assessment of Potable Water Pipelines.", 267 Proceedings, 4th International Conference on Earthquake Engineering, Taipei, Taiwan, Oct., 2006.

Yimsiri, S. (2001). "Pre-failure deformation characteristics of soils: anisotropy and soil fabric," Ph.D. Dissertation, University of Cambridge, Cambridge, England.

Yimsiri, S., Soga, K., Yoshizaki, K., Dasari, G.R. and O'Rourke, T.D. (2004) "Lateral and upward soil-pipeline interactions in sand for deep embedment conditions". Journal of geotechnical and geoenvironmental engineering, 130(8): 830-84

